HIGH ASPECT RATIO MICROFILLING FOR MEMS USING METAL NANOPOWDER

FATIN SYAZANA BINTI JAMALUDIN

DISSERTATION SUBMITTED IN FULFILMENT OF THE REQUIREMENTS FOR THE DEGREE OF MASTER OF ENGINEERING AND SCIENCE

FACULTY OF ENGINEERING

UNIVERSITY OF MALAYA

KUALA LUMPUR

2013

UNIVERSITI MALAYA

ORIGINAL LITERARY WORK DECLARATION

Name of Candidate: **FATIN SYAZANA BINTI JAMALUDIN**

Registration/Matric No: **KGA100056**

Name of Degree: **MASTER OF ENGINEERING SCIENCE**

Title of Project Paper/Research Report/Dissertation/Thesis ("this Work"):

HIGH ASPECT RATIO MICROFILLING FOR MEMS USING METAL NANOPOWDER

Field of Study: **MECHANICS AND METAL WORK**

I do solemnly and sincerely declare that:

1) I am the sole author/writer of this Work;

2) This Work is original;

3) Any use of any work in which copyright exists was done by way of fair dealing and for permitted purposes and any excerpt or extract from, or reference to or reproduction of any copyright work has been disclosed expressly and sufficiently and the title of the Work and its authorship have been acknowledged in this Work;

4) I do not have any actual knowledge nor do I ought reasonably to know that the making of this work constitutes an infringement of any copyright work;

5) I hereby assign all and every rights in the copyright to this Work to the University of Malaya ("UM"), who henceforth shall be owner of the copyright in this Work and that any reproduction or use in any form or by any means whatsoever is prohibited without the written consent of UM having been first had and obtained;

6) I am fully aware that if in the course of making this Work I have infringed any copyright whether intentionally or otherwise, I may be subject to legal action or any other action as may be determined by UM.

Candidate's Signature……. Date: 00/05/2013

Subscribed and solemnly declared before,

Witness's Signature…… Date: 00/05/2013

Name:

ABSTRACT

High aspect ratio microstructures (HARMS) are sought in MEMS devices, as they fulfil several criteria such as low driving voltage, increased structural rigidity, higher sensitivity in sensor systems, bigger displacement and greater actuation force in actuator applications, and larger magnetic forces for magnetic MEMS. However, the fabrication of HARMS requires advanced equipment and complicated fabrication procedures, which increase the production cost. Thus, the objective of this project is to explore a fabrication method to produce HARMS, which considers the best compromise between simple production techniques and high device performance. In this research, focused ion beam (FIB) milling was introduced to fabricate high aspect ratio microholes. Nickel nanopowder was chosen as a candidate of metal structural filling for HARMS due to its intrinsic net shaping characteristics and its superior mechanical properties, such as high fracture toughness. Microholes (2.0µm x 17.5µm) with a maximum aspect ratio 8 were achieved using the FIB direct milling technique. The parameters used to obtain this aspect ratio were 500pA for beam current and 100µm for initial milling depth. Milling was done using a beam current of 500pA, which formed the most precise microhole structure with low milling time and an aspect ratio close to 1, compared to the other holes. The aspect ratio of microholes increased with increase of the initial milling depth, D_i. The actual depth, D_f gained was 17.5µm at D_i = 100µm, which is five times less than the initial milling depth. Although FIB milling is less useful in mass production, it is an excellent choice for producing highly precise microholes. However, it is limited by the effects of amorphisation and re-deposition. For the filling process, two different methods were used; magnetic assembly and ultrasonic dispersion followed by annealing at 500°C. The magnetic assembly technique provided better filling behaviour compared to the ultrasonic dispersion method due to the occurrence of agglomeration at the entire sidewall using the magnetic assembly technique. This agglomeration was induced by

the magnetic field, which attracted the ferromagnetic nickel into the holes. The filling structure formed after annealing at 900°C is of higher quality with fewer voids than the filling structure formed at 500°C. Only small agglomerations were formed at the entire sidewall, no voids occurred and a higher average thickness of filling structure of 526nm was achieved. Furthermore, the annealing process created bonding between the nickel nanopowder and silicon substrate thus forming a nickel silicide (NiSi) layer. The composition of nickel was higher at 900°C (14.78%) rather than 500°C (4.36%), where in the former case; more nickel nanopowder diffused into the silicon and formed two phases of nickel silicide layer, NiSi and $NiSi_2$. Although the agglomeration occurred at the sidewall of holes, a good formation of microfilling was achieved without cavitations. Thus, from this research, the magnetic assembly technique with annealing temperature of 900°C provides optimal conditions of microfilling using Ni nanopowder.

ABSTRAK

Mikrostruktur dengan nisbah aspek tinggi (HARMS – High Aspect Ratio Microstructure) telah menjadi keutamaan dalam peranti sistem mikroelektromekanik (MEMS – MicroElectroMechanical Systems). HARMS menawarkan beberapa kelebihan termasuk voltan gerakan yang rendah, peningkatan ketegaran struktur, gerakan yang lebih besar dan daya anjakan yang lebih tinggi dalam sistem penggerak, kepekaan yang tinggi dalam aplikasi penderia atau sensor, dan daya magnet yang lebih besar untuk MEMS bermagnet. Walau bagaimanapun, fabrikasi untuk HARMS memerlukan peralatan canggih dan prosedur fabrikasi yang rumit, menyebabkan peningkatan kos pengeluaran. Oleh itu, objektif penyelidikan ini adalah untuk meneroka kaedah fabrikasi untuk menghasilkan HARMS, yang menjadi kompromi terbaik antara teknik pengeluaran yang mudah dan prestasi peranti yang tinggi. Dalam kajian ini, penggerudian menggunakan sinaran ion tertumpu (FIB - Focus Ion Beam) telah digunakan untuk menghasilkan lubang mickro nisbah aspek yang tinggi. Serbuk nano nikel telah dipilih sebagai logam pengisi untuk HARMS berdasarkan oleh ciri-ciri pembentukan sempurna dan sifat mekanikal nikel yang baik seperti mempunyai kekuatan yang tinggi untuk dieksploitasi dalam bidang MEMS. Lubang mikro nisbah aspek 8 telah dicapai dengan menggunakan teknik penggerudian FIB. Parameter yang digunakan untuk mendapatkan nilai nisbah aspek ini ialah arus sinaran 500pA dan kedalaman penggerudian awal 100µm. Penggerudian menggunakan arus sinaran 500pA menghasilkan struktur lubang yang berketepatan tinggi dengan masa penggerudian yang singkat dan nisbah aspek menghampiri 1 berbanding lubang lain. Nisbah aspek lubang mikro bertambah dengan pertambahan kedalaman penggerudian awal, D_i. Kedalaman sebenar, D_f yang diperoleh ialah 17µm pada D_i = 100µm, berkurang lima kali ganda berbanding kedalaman penggerudian awal. Walaupun penggerudian FIB kurang digunakan dalam pengeluaran besar-besaran, FIB adalah pilihan yang baik untuk

menghasilkan lubang mikro berketepatan tinggi. Namun, kelemahannya adalah kesan pembentukan amorf dan pemendapan semula. Dalam proses pengisian, dua kaedah berbeza telah digunakan; pemasangan magnet dan sebaran ultrasonik dan dipanaskan pada suhu 500°C. Pada dasarnya, kedua-dua kaedah ini tidak menjadikan serbuk nikel mengisi sepenuhnya lubang mikro. Namun, teknik pemasangan magnet lebih baik dalam mengisi nikel berbanding kaedah sebaran ultrasonik melalui kehadiran penggumpalan di keseluruhan dinding lubang. Hal ini berlaku kerana daya magnet yang dihasilkan menarik nikel yang bersifat feromagnetik ke dalam lubang. Struktur pengisi yang terbentuk selepas pemanasan pada suhu 900°C mempunyai kualiti yang tinggi berbanding struktur yang terbentuk pada suhu 500°C. Hanya gumpalan kecil terbentuk di seluruh dinding lubang, tiada kaviti berlaku dan purata ketebalan yang tinggi, 526nm. Proses pemanasan membentuk ikatan antara nikel dan silicon menyebabkan pembentukan lapisan nikel silisid (NiSi). Komposisi nikel adalah tinggi pada suhu 900°C (14.78%) berbanding 500°C (4.36%). Ini bermaksud lebih banyak serbuk nikel menyerap ke dalam silicon dan membentuk dua fasa lapisan nikel silisid, NiSi dan $NiSi_2$. Walaupun penggumpalan berlaku pada dinding lubang, pembentukan pengisi mikro yang baik telah diperoleh tanpa kaviti. Dari penyelidikan ini, dapat disumpulkan bahawa teknik magnetic dengan pemanasan 900°C memberikan kondisi yang lebih baik bagi pengisi logam untuk HARMS menggunakan serbuk nano nikel.

ACKNOWLEDGEMENTS

Alhamdulillah, thank Allah for His blessings that I have successfully completed this dissertation. I would like to express my wholehearted appreciation to my research supervisor, **Dr Mohd Faizul Mohd Sabri** on the encouragement and ideas that he has given. My gratitude to Dr. Suhana Mohd Said on her guidance and unwavering support towards me throughout the course of this study. Grateful thanks to Mr. Mohd Nazarul Zaman Bin Mohd Nazir, Assistant Science officer of the FESEM lab for his full cooperation and tireless assistance operating the FIB/SEM system for fabricating the high aspect ratio of micro holes. Not forgetting my grateful thanks to all the lecturers and lab assistants for cooperation and guidance throughout this research.

Appreciation also goes to the staff members of the Faculty of Engineering and Faculty of Science for the provision of all instruments and apparatus used throughout the duration this research study. Thanks also to the University of Malaya for funding support (UMRG and PPP grant). I would like to give my heartfelt appreciation and gratitude to the lab members of the NanoMicro Engineering Laboratory, Department of Mechanical Engineering and Solid state Nanoengineering Laboratory, Department of Electrical Engineering, for their guidance and cooperation in this study. I would like to express my appreciation to Mrs Nurul Hajar Mohd Fuad, from Faculty of Engineering, IIUM on her willingness to share ideas and provide support for this research.

I finally express my sincere thanks to my lovely parents, En. Jamaludin and Puan Enon, family members and colleagues on every encouragement, advice, guidance and assistance throughout the challenges in this study to succeed. All support is greatly appreciated.

TABLE OF CONTENT

LIST OF FIGURES

LIST OF TABLES

LIST OF SYMBOLS AND ABBREVIATIONS

PIM	Powder Injection Moulding
RF	Radio Frequency
IC	Integrated Circuit
Nd:YAG	Neodymium-Doped Yttrium Aluminum Garnet
.XBM	X BitMap
PDMS	Polydimethylsiloxane
EDM	Electrical Discharge Machining
kHz	Kilohertz
BMP	Bitmap Image File
DXF CAD	Drawing Exchange Format

CHAPTER 1 INTRODUCTION

1.1 Background

Micro-electromechanical Systems (MEMS) stands for a combination of mechanical elements, sensors, actuators and electronics that are integrated in a device through micro-fabrication technology (Bleris & Kothara, 2005). MEMS devices consist of three dimensional structures, with important features including small sizes, high performances, and low costs. In order to reduce the size of a MEMS device, fabrication of microstructures with a consistent dimension and high aspect ratio are the key challenges in the MEMS industry (Lü, et al., 2007). The aspect ratio of the microstructures is the proportion of the ratio of the length of the microstructure to the aperture diameter of the microstructure (Fu, et al., 2007).

Today, high aspect ratio microstructures (HARMS) are frequently utilised in MEMS for enhanced mechanical strength, decreased out-of-plane movement of flexures, and enhanced surface region for capacitive actuation and detection (Hutchison, et al., 2010). HARMS are preferable especially in sensors and actuators as this type of microstructure provide advantages such as low driving voltage, enhanced structural toughness, higher sensitivity in sensor applications; advanced actuation force and greater displacement in actuator systems; and larger magnetic forces for magnetic MEMS (Fu, et al., 2007). Furthermore, HARMS allow the realization of sophisticated mechanical devices with high capacity and strength, for example; high-efficiency micro heat exchangers as well as heat tackled mechanical seals (Cao, et al., 2003). The common fabrication techniques for HARMS include LIGA (Lithographie Galvanoformung, Abformung) and DRIE (Deep Reactive Ion Etching), are the best choices for commercial scale production (Lohmann, et al., 2003). However, correspondingly, these advanced equipment and complicated fabrication procedures

require high production costs, specifically in cases of greater need for sophisticated microstructure design. Therefore, the two-fold need lower production costs and greater device performance is a key issue to be resolved in the development of devices in the MEMS field.

The use of nanopowder filling to produce microstructures has garnered keen interest as the request for these structures increased, due to their ability to achieve net-shaping (Fu, et al., 2007). Nanopowders used in the micro-powder injection moulding process (μPIM) was identified to be more advanced compared to traditional PIM powders, which provide good dimensional control and flow-ability (Kasanov & Dvilis, 2008). In this research, metal is used as the candidate material to replace silicon or polymers, which have dominated the production of microstructures. Metals provide more attractive characteristics, such as superior mechanical properties and thermal conductivity (Fu, et al., 2007). Metals inherently possess larger fracture rigidity compared to more brittle semiconductor materials, such as silicon which consequently provide higher reliability and shock-resistance (Fu, et al., 2007).

The focused ion beam (FIB) is similar to a scanning electron microscope (SEM) in many ways. The FIB technique uses a focused beam of ions to scan the surface of a specimen, analogous to the way electrons are used in SEM. The difference is FIB uses gallium ions instead of electrons as the focusing beam. The gallium ion beam can then be manipulated (in terms of focus and acceleration) by an electric field. Ions possess relatively high mass compared to subatomic particles which allow them to be used to induce the milling and deposition effects. FIB direct milling is a process of transferring patterns by direct impingement of the ion beam on the substrates (Urbanek, et al., 2010). The typical ion source for FIB is the Liquid Metal Ion Source (LMIS), such as Ga, Al, Be, Fe, Li, Pb, Pd, Zn and Au. However, gallium (Ga) is commonly used as an

ion source in FIB system as it has a high surface tension, which is able to maintain stability of the liquid surface against the electric field. FIB direct milling has many advantages over other high energy particle beams, including maskless etching on various materials (Fu & Ngoi, 2001). The pattern desired can be milled directly on metal, silicon, glass and carbon substrate. In terms of the achieved surface quality, FIB direct milling is more suitable for hard brittle materials rather than metals (Youn, et al., 2006).

In order to fill metal nanopowders into the high aspect ratio micro holes, two methods are introduced in this research. Magnetic assembly or magnetic self-assembly is an immediate filling technique that magnetically assembles conductive material into holes (Youn, et al., 2008). The magnetic field provides non-contact force that enables a highly directional control of ferromagnetic materials over long distances, whilst is concurrently insensitive to the surrounding non-magnetic medium and is independent of details of the surface chemistry. Fischer et al. (2012) has presented the concept of the fabrication of TSVs (Through Silicon Via) with an aspect ratio of 8 using manual magnetic assembly which enables high aspect ratio vias with an inherently void-free metal core. Another filling method is ultrasonic dispersion. Generally, this method is required to disperse materials with nano-meter sizes in a liquid because of the scale of action of the ultrasonic waves as well as approximately large surface area-to-volume ratios. None of the previous research ultrasonic filling has employed dry metal in nanopowder form. However, this technique is able to eliminate or substantially reduce voids formed at the bottom of high aspect ratio holes.

1.2 Objectives

This study embarks on the following objectives, with regards to the fundamental investigation of metal nanopowder properties:

i) To study the methodology of fabricating high aspect ratio micro structures. This includes the FIB parameters used to fabricate microholes for the microfilling technique to be tackled in this thesis.

ii) To achieve microfilling of HARMS using the magnetic assembly and ultrasonic dispersion method. Evaluate the criteria include the compacting ability of metal nanopowders in high aspect ratio microstructures, as well as occurrences of voids.

iii) To analyse the surface bonding in fabricated HARMS, including identification of metal-silicon bonding structures, the phase transformation upon annealing and the composition of the elements in filling structures.

1.3 Scope of Study

The study examines the microfilling of HARMS structures using metal nanopowders. FIB was selected as the fabrication method to produce the HARMS, whilst Ni nanopowder was chosen for its superior mechanical and net-shaping properties. The magnetic assembly and ultrasonic dispersion methods were compared for the microfilling process. The filling process was followed by annealing of the filled structures. Evaluation of the structure was done in term of cavitations and compaction behaviour, and surface bonding and elemental analysis of the resulting microfilled structures.

1.4 Organisation

This dissertation is organised as follows:

Chapter 1 Introduction

A brief background of the research, the research objectives as well as the scope of study is presented in Chapter 1.

Chapter 2 Literature Review

This session reviews the state of art in this study field. A large number of references were critically reviewed based on MEMS, HARMS, microfabrication and metal filling topics. Some of the major methods in MEMS fabrication and their limitations are presented. The parameters used in FIB milling and the applications of magnetic assembly and ultrasonic dispersion techniques are discussed in detail.

Chapter 3 Research Methodology

This chapter describes materials selection and explains the experimental procedures of fabricating micro holes with aspect ratio more than 5 using FIB direct milling. Next, the formation of microfilling structures by magnetic assembly and ultrasonic dispersion with metal nanopowder approaches were elaborated, and finally, the annealing.

Chapter 4 Result and Discussion

This chapter presents the analysis results and detail discussion of fabrication process and the outcome gained.

Chapter 5 Conclusion and Recommendation

This chapter concludes the results and discussion from the analysis conducted, according to the objectives of this research. A few suggestions are recommended for future study of this research, based on the knowledge gained in literature review and experimental investigation.

CHAPTER 2 LITERATURE REVIEW

2.1 Micro Electromechanical Systems (MEMS)

Micro-Electro Mechanical Systems (MEMS) is a remarkable technology that has achieved great transformation in semiconductor technology and application, which drives the next technological revolution of smart devices. The phrase MEMS was originally coined in the United States, whereas in Japan, the term called Micromachines is more generally known and in Europe it is known as Microsystem Technology (MST) (van Heeren & Solomon, 2007). In the broadest sense, MEMS is described as minuscule mechanical and electronic mechanical devices that are produced by microfabrication techniques. MEMS are developed from components in the range of 1 to 100 micrometers in size (0.001 to 0.1mm) whilst MEMS devices usually range in dimensions from 20μm to few millimetres. The MEMS devices or systems can sense, control, and actuate on the micro-scale, and produce tasks to promote impacts on the macro-scale either individually or in arrays (Baloglu, 2011) such as accelerometers and micro positioning.

MEMS products were first developed in the 1960s when accurate hydraulic pressure sensors were required for aircraft operation. In the early 90's, MEMS accelerometers for car airbags were promoted as an accurate replacement for a conventional crash sensors which coupled high reliability with low cost. Some example of commercialized MEMS devices are listed in Table 2.1 (Prime Faraday Technology Watch, 2002):

Table 2.1: Commercialisation of selected MEMS devices

Product	Discovery	Evolution	Cost Reduction/ Application Expansion	Full Commercialisation
Pressure sensor	1954-1960	1960-1975	1975-1990	1990-present
Accelerometer	1974-1985	1985-1990	1990-1998	1998
Gas Sensor	1986-1994	1994-1998	1998-2005	2005
Valve	1980-1988	1988-1996	1996-2002	2002
Nozzle	1972-1984	1984-1990	1990-1998	1998
Photonics/ Displays	1980-1986	1986-1998	1998-2004	2004
Bio/Chemical sensors	1980-1994	1994-1999	1999-2004	2004
RF (Radio frequency) switches	1994-1998	1998-2001	2001-2005	2005
Rotation rate sensors	1982-1990	1990-1996	1996-2002	2002
Micro relays	1977-1982	1993-1998	1998-2006	2006

(Prime Faraday Technology Watch, 2002).

The following considerations are integral to the design and application of MEMS systems: Materials selection, device geometry and dimension, aspect ratio, accuracy of device structure and precision of device operation. Generally, these parameters cannot be fulfilled easily by mainstream silicon-based micro fabrication technologies. Manufacturing a successful MEMS device requires a deep understanding of basic physics and operating principles, including scaling laws at both the macro and micro level (Prime Faraday Technology Watch, 2002). Therefore, new and improved techniques of fabrication are desired based on the specific applications and designs. The requirement of high aspect ratio microstructures (HARMS) in MEMS and the interest of metal nanopowders as a new technology in microfilling are reviewed in this chapter. Also, several methods of fabricating MEMS are discussed with their advantages and limitations.

2.2 High Aspect Ratio Micrstructures (HARMS)

High aspect ratio microstructures (HARMS) are today of great importance in microelectronics and MEMS technology. They are essential when deep structures or thick layer are required in addition to maintain the microscopic lateral dimensions of the structures. Normally, HARMS are hundreds of micrometres in height; whilst their diameter range from 1 to 10μm, and they can be manufactured from a variety of materials such as metals, polymers and ceramics (Marques, et al., 1997).

There is an increasing demand for MEMS products containing higher aspect ratio and larger spatial resolution such as the dies for creating an IC lead frame, the fabrication of miniature thin films used in the semiconductor industry and medical devices and microelectronic medical implants in the biotechnology industry (Liao, et al., 2005). HARMS are required in various implementations of electrostatic transduction mechanisms, including in-plane, out of plane and torsional oscillations with high force density (Monajemi & Ayazi, 2005). HARMS are often desirable in MEMS technology as they offer a number of benefits including:

1. Increase in mechanical flexibility and robustness of MEMS devices, reduction of out-of plane motion of flexures, and increase in surface area for capacitive actuation and detection (Hutchison, et al., 2010)

2. Achievement of high actuation force at low driving voltage due to the large surface area of the sidewalls.

3. Structural rigidity and high torque in actuator systems due to thick structures.

4. Higher sensitivity in sensor applications due to structural integrity (Kim, et al., 2002)

5. Larger magnetic forces for magnetic MEMS due to the larger volume of HARMS (Kim, et al., 2002).

Furthermore, HARMS which are covered on wide surface areas ranging from $10cm^2$ to several square meters, have potential applications in a variety of fields, including heat transfer, fluid mechanics, composite materials, bearings, and catalytic systems (Morales, 2006). Thus, several fabrication techniques have been established to maximize the aspect ratio of microstructures needed in the MEMS industry.

2.3 Major Fabrication of HARMS

Microfabrication is the category of fabrication processes employed in manufacturing of micro and nano scale components with high precision and reproducibility. Moreover, microfabrication is a technology that enables to fabricate very small three dimensional (3D) structures. There are a few differences between microfabrication and IC fabrication such as (Mei, 2009):

- The aspect ratio in microfabrication is greater than IC fabrication.
- The device sizes in microfabrication are larger than in IC processing.
- The structures produced in microfabrication usually include cantilevers and bridge connections, also other shapes requiring gaps between layers.

Many academic and industrial institutions have anchored a concerted research effort in the field of microfabrication technologies. Example of fabrication technologies that have been developed and put into practice successfully are the LIGA technique, photolithography and Excimer laser micromachining. The broadening interest in MEMS devices and consequently microfabrication techniques has been driving a variety of MEMS applications. The major MEMS microfabrication methods will be discussed next.

2.3.1 LIGA

The acronym LIGA derives from the German terms (Lithographie, Galvanoformung, Abformung) which means lithography, electroforming and moulding methods that are used to produce microscale structures (Mei, 2009). LIGA represents a fundamental approach towards producing metal-based HARMS. In X-ray LIGA, an X-ray sensitive polymer, such as poly-methyl methacrylate (PMMA) is deposited on an electrically conductive substrate (Hruby, 2001). PMMA photoresist is then exposed to aligned beams of high-energy X-rays from a synchrotron emission source. A mask covered with a strong X-ray absorbing material is used during the exposition to obtain a desired pattern (Mei, 2009). The process is then followed by chemical dissolution of the exposed portion of PMMA photoresist, and the cavities are filled by the electrodeposition of metal. The remaining resist is chemically removed to produce a metal mould insert which is generally used to fabricate parts in polymers or ceramics through injection moulding (Chiu, et al., 2011). Fig 2.1 shows the flow steps of LIGA process:

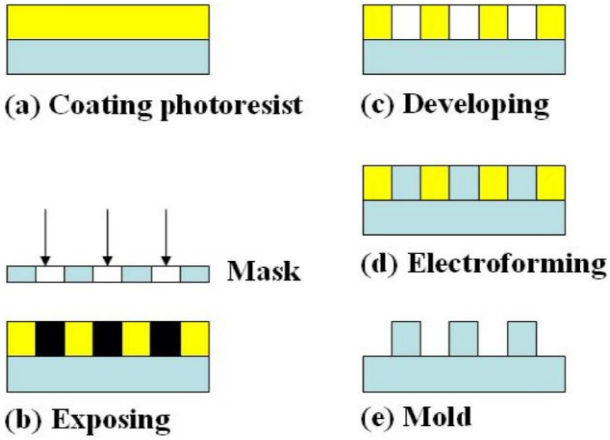

Fig 2.1: The flow steps of LIGA process

(Chiu, et al., 2011)

LIGA is a popular method to develop HARMS with aspect ratios up to 100:1 with a few millimetres in height (Kim, et al., 2002). However, LIGA has limitations which only can be formed with the materials that can be electroplated such as gold, copper, nickel and a few nickel alloys. Furthermore, LIGA requires a synchrotron facility and X-ray radiation source to fabricate HARMS. Thus, the operational cost is highly increased.

2.3.2 Laser Micromachining

Laser micromachining is a material elimination process carried out through laser and target material interactions. In the laser micromachining process, photon energy is transferred into the target material in the mode of thermal energy or photochemical energy. These energies will eliminate material by melting, and blowing away, or by direct vaporization/ablation (Kibria, et al., 2010). Fig 2.2 shows the schematic diagram of laser micromachining.

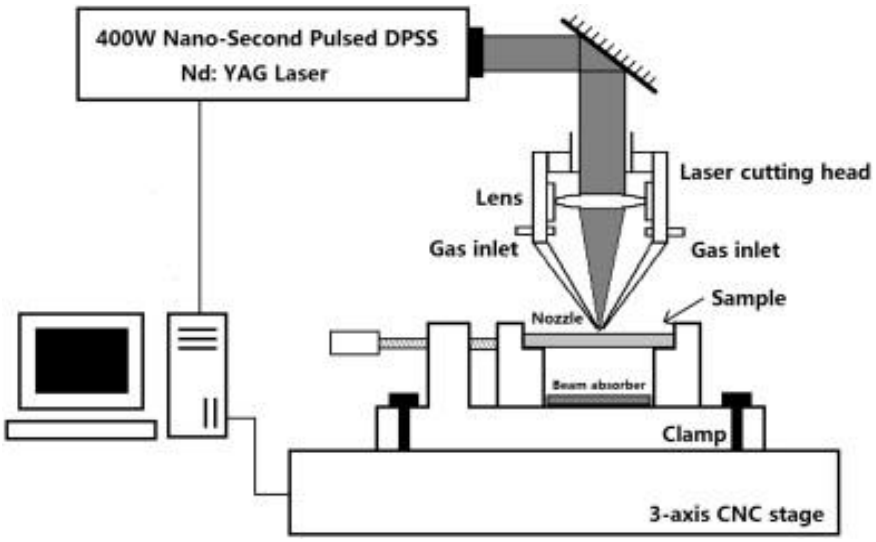

Fig 2.2: A schematic diagram of laser micromachining

(Yan, et al., 2012)

Laser etching is a precise materials fabrication process, which allows precise and accurate formation of geometries through tuning of a wide range of wavelength and

pulse widths, to match the target material properties. It also allows a single step direct machining and locally restricted structural modification. Pulsed lasers with wavelengths in different regions of the electromagnetic spectrum have been used for material removal in a non-contact fashion, including excimer lasers operating in the ultraviolet (UV) radiation and femtosecond pulsed Nd:YAG laser operating in the near infrared (IR) (Mei, 2009). Molecular dynamics (MD) simulations have been used to study and predict the non-thermal and thermal mechanisms of material removal by interaction with a fast laser pulse (Mei, 2009).

Recent studies include the use of nanosecond laser for nanoscale ablation of thin metal films and, nanoscale patterning of Au nanoparticle films (Hwang, et al., 2006). For microscale machining of metals, the material removal rates are observed to be of the order of 1μm per pulse, with the laser beam diameter in the range of 10μm (Semak, et al., 2006). Serial scanning of the laser beam is therefore necessary to form extended microscale features in silicon and metals with depths of the order of a few hundred microns.

At typical pulse repetition rates of 1 kHz or less, the production of microscale structures of typical MEMS (several micrometers) dimensions will be time consuming (Mei, 2009). The formation of surface roughness during high aspect ratio holes drilling is another limitation of laser micromachining that requires surface finish treatments by picoseconds lasers. Laser micromachining is also highly dependent on the incident laser intensity and average laser power. The maximum depth of holes drilling with focused spot sizes less than 100μm requires a higher intensity beam greater than 10^{14} W/cm^2 , and a laser power greater than 10^{10} W. These complications will increase the production costs and time.

2.3.3 Photolithography

Photolithography is a UV standard method employed to define the shape of microstructures by transferring the copy of a master pattern onto the surface of a substrate, such as a silicon wafer (Prime Faraday Technology Watch, 2002). Photolithography is also known as optical lithography or ultra-violet (UV) lithography and is the basis for most microfabrication methods. Before the commencement of the photolithography processes, a mask, typically a chromium pattern on a glass plate needs to be produced.

The photolithography process is begun by coating the silicon substrate with a thin film of other material, such as silicon dioxide (SiO_2) (Prime Faraday Technology Watch, 2002). An organic polymer called the photoresist is deposited on the substrate to form a thin layer. There are two types of photoresist, a positive and a negative resist and both are sensitive to ultra-violet light. The positive resist is weakened by UV emission whilst in the negative resist the polymer linkage is strengthened. After that, the designed mask is placed in contact with the photoresist coated surface (Prime Faraday Technology Watch, 2002). Exposure of substrate to the UV emission; enables transfer of the pattern on the mask to the photoresist. The emission causes a chemical reaction in the exposed areas of photoresist to either weaker or strengthen the polymer bonds, depending on the type of resist coated on the substrate.

Finally, the exposed oxide is stripped away from the uncovered areas of photoresist using hydrochloric acid, whilst excess photoresist is subsequently cleaned away using hot sulphuric acid. The sulphuric acid attacks the photoresist, but not the oxide layer that formed a pattern of oxide on the substrate. In MEMS fabrication, the oxide pattern serves as a mask for additional chemical etching in creating 3D microstructures with high aspect ratio.

2.4 Fabrication of Microholes Using Focused Ion Beam (FIB) Milling

Silicon micromilling by focused ion beam (FIB) is a favourable technology used in MEMS especially when rapid fabrication of the critical dimensions is demanded (Krueger, 1999). Comprehensive knowledge of the fundamental mechanisms required in the milling process is compulsory to enable full exploitation of the FIB technique. The Focused ion beam (FIB) method applies a focused beam of ions to scan the surface of a sample, comparable to the way electrons are used in a scanning electron microscope (SEM) (McPhail, et al., 2008). The difference is that FIB uses gallium ions instead of electrons. An ion is a charged particle by changed formed either by gaining or losing electrons. Ions can be accelerated, controlled or focused by electrostatic fields and possess an approximately higher mass than subatomic particles, which allow them to be utilised in the milling processes (Fu & Ngoi, 2005).

The typical ion source for FIB is the liquid metal ion source (LMIS), such as Ga, Al, Be, Fe, Li, Pb, Pd, Zn and Au. However, gallium (Ga) is usually used as an ion source in FIB system due to its high surface tension, which is able to control stability of the liquid surface against the electric field (Fu & Ngoi, 2005). Ga also possesses low vapour pressure, which allow high ionization of the Ga atom. The melting point of gallium is also slightly above the room temperature, which simplifies the operations of the FIB. When Ga^+ ions hit the surface of a solid sample, they lose energy to the electrons of the solid as well as to its atoms (Raffa, et al., 2006).

The most significant physical effects of incident ions on the substrate are: 1) removal of the material by sputtering/milling, 2) deposition through chemical reactions such as breaking of chemical bonds, by the scattered molecules), 3) ion implantation either by displacement of atoms in the solid or emission of photons, and 4) imaging through the secondary electron emission effect (Kim, et al., 2012). Based on these

complex contributions the FIB process is divided into four categories: a) FIB milling (sputtering and etching), b) FIB deposition, c) FIB implantation, and d) FIB imaging as shown in Fig 2.3. The FIB system is able to perform cross-section on devices and provide a high resolution image of the internal structure of a semiconductor device (Krueger, 1999).

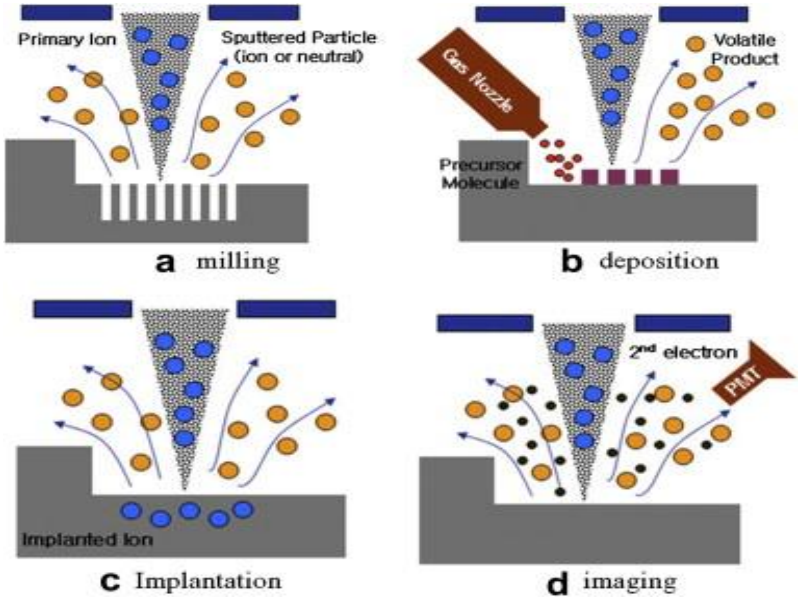

Fig 2.3: Working principle of FIB; a) milling, b) deposition, c) implantation, d) imaging (Kim, et al., 2012).

The FIB direct milling method, which is also known as FIB direct writing, is interesting owing to the high flexibility in performing direct patterning, where dimensions of structures ranging from 1nm to 100µm can be fabricated on a wide range of materials (Youn, et al., 2007). FIB has the ability to direct mill the structures with features sizes at or below 1µm because of the short wavelength and large density. As a result, FIB is presently recognised as a favoured technique in fabrication of high-quality microdevices containing highly precise microstructures (Tseng, 2004).

2.4.1 Advantages and Limitations of FIB Milling

Several benefits of FIB milling have been recognized by recent findings, such as high flexibility in the direct patterns, precise dimensions of structures and wide applicability to materials (Youn, et al., 2006). The pattern desired can be milled precisely on metal, silicon, glass, carbon substrate without any pattern exchange (Youn, et al., 2006). The lateral scattering of FIB is relatively low due to the high mass of the atom (Tseng, 2004). Therefore, FIB is able to strike only the intended regions. The density of patterns can be controlled with FIB-assisted gas injection system and produce a hole geometry of high aspect ratio up to 15 (Jamaludin, et al., 2013a).

In terms of dry etching, the FIB process is faster than the electron beam. The FIB is able to cut out as well as deposit the target materials in the nano-scale using focused Ga^{+} ion beam, instead of the electron beam (Reyntjens & Puers, 2001). Secondary ions that are forced out from the sample are detected so that a high resolution image can be obtained (Kim, et al., 2008). The pattern transfer process using masks and resists is complicated and has related defect; this can be mitigated through complementary use of FIB milling (Tseng, 2004). Moreover, FIB can work at room temperature and does not have any impact upon the performance of the substrate material.

The FIB milling process also possesses a few limitations, such as slow mass production due to the low milling rate. Thus, some improvement in the FIB milling rate is needed in order to enhance the throughput and enable the possibilities of mass production (Tseng, 2004). During the imaging process in FIB, the ion beam is gradually strikes out the material from the sample and destructs the crystal structure of the sample. This destruction can be reduced by monitoring the change of the current signal during ion milling (Tseng, 2005).

A noise or disturbance from the side walls of the milled structure that occur during analysis also has the effect of preventing the accuracy of depth measured by atomic force microscopy (AFM) and profilometer. Both the AFM and profilometer cannot access the bottom of the high aspect ratio structure. Moreover, the formation of the amorphous layer on the surface of the crystalline sample has become a common limitation due to knock-on damage of the crystalline structure during the milling process.

2.4.2 FIB Milling using FIB-SEM System

The effect of the imaging process which involves continuous removal of the material from sample using the ion beam can cause damage to the crystal structure of the sample. However, the FIB-SEM system has been designed to optimize the ion beam's milling and deposition capabilities with the high resolution electron beams for non-destructive imaging, without compromising the performance (Krueger, 1999). The FIB-SEM system is an integration of a focused ion beam, an electron beam and secondary ion and/or secondary electron detectors on the same platform (Drobne, et al., 2005). Ga^+ ions at higher beam currents are used for sputtering or milling, and lower beam currents are used for imaging. A significant amount of time can be saved by incorporating these applications because there is no necessity to move the sample from one system to another (Krueger, 1999).

Furthermore, the FIB-SEM system is able to give specific control of FIB performance through the SEM by applying the slice-and-view method (Bushby, et al., 2011). In this method, typically the FIB exposes a cross section by milling perpendicularly to the top of the surface of the sample having a hidden feature to be viewed. A portion of the sample in front of the face is preferably removed because the SEM beam axis is typically at an acute angle relative to the FIB beam axis, in order for

the SEM beam to gain access to image the face. The two beams are co-focused at the coincidence point at 5mm working distance (WD), which maximize the efficiency for the majority of processes taking place within the machine (van Tendeloo, et al., 2012). The stage also can be monitored to tilt so that adjustments in the sample beam orientation can be made (Yao, 2005). In order to ensure better performance, the ion beam is adjusted at a range of tilt angles between 45° to 54° from the electron beam. This adjustment can allow SEM imaging and FIB sample modification without having to transfer the sample (van Tendeloo, et al., 2012). The signals from the sputtered secondary ions or secondary electrons are collected to form an image (Drobne, et al., 2005). Fig. 2.6 shows the schematic diagram of slice and view technique using FIB-SEM system.

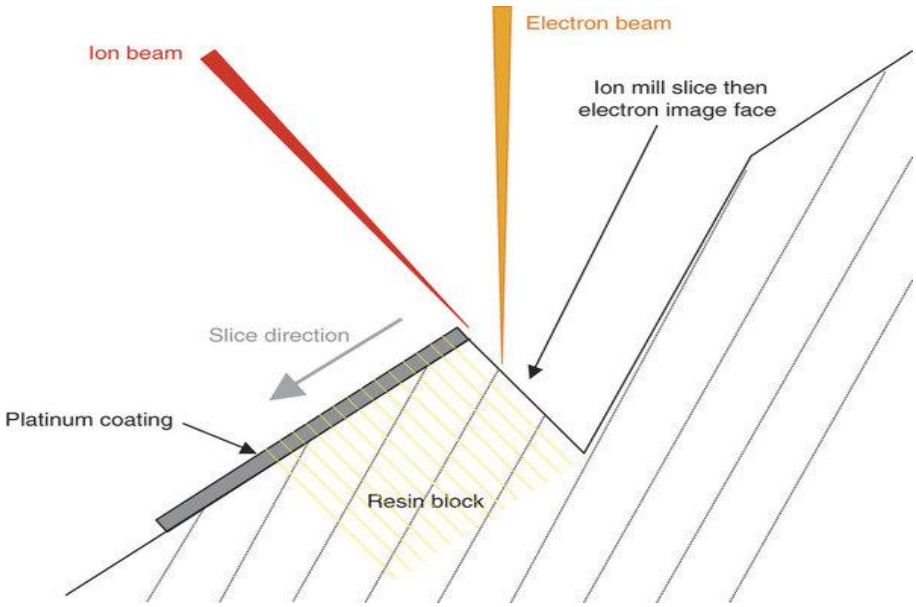

Fig. 2.4: Side view schematic of slice face in relation to the electron and ion beam, using slice and view technique

(Bushby, et al., 2011)

2.5 Parameters of FIB Milling

The FIB milling process is commonly used to accomplish precise milled patterns by cutting out a desired amount of material from a scanned area. The essential parameters of the FIB should be controlled with the appropriate beam size, shape, current and acceleration voltage, plus the secondary parameters of dwell time, pattern size, scan mode, and pixel spacing (Kim, et al., 2008). The diverse impacts of physical sputtering, material re-deposition and pattern geometry are the goal of the milling process by controlling the FIB parameters. The efforts to achieve the precision high aspect ratio micro holes milling will be revised in these following subsections; 1. Sputter yield, 2. Acceleration voltage, 3. Beam current, 4. Dwell time, 5. Scan mode, 6. Pixel spacing, 7. Pattern size, and 8. Milling mode.

2.5.1 Sputter Yield

Physical sputtering is the major mechanism to remove material and its effectiveness is generally represented by the sputter yield, described as the number of atoms derived from the target surface per incident ion at given ion beam parameters (atoms/ion) (Youn, et al., 2007). Sputter yield is a quantification of the effectiveness of material removal (Ali, et al., 2010). The yield is generally in the range of 1-50 atoms per ion and is influenced by various variables, involving the accumulation of ions and target atoms, ion energy, direction of incidence to the target surface, target temperature and ion flux (Tseng, 2004). In the beginning, when the ion energy increases, the sputter yield increases. However, the sputter yield begins to decrease with increasing energy above the optimised level of depth for ion penetration into the substrate (Benawra, et al., 2008). At this point, the ions become trapped into the substrate as their energy is expended. The trapping of ions can cause the implantation of the atoms of material to

take place. This implantation or doping is called the re-deposition effect and can decrease the aspect ratio of microstructures.

Typical sputter yield varies for various materials, incident angle and energy. However, these values are not valid for direct counting of the etch rate (Kim, et al., 2008). The reason for this is the dependable of the etch rate on the scanning style and the formation of re-deposition which intensely decreases the efficiency of etch rate. The sputtering yield approximately increases with $1/\cos(\theta)$, where θ is the angle between the surface normal and the ion beam direction (Kim, et al., 2008). The changes in the sputtering yield can be evaluated by changing the dwell time (the time the ion beam remains fixed on one pixel position) at the pixels during the milling process (Raffa, et al., 2006). Table 2.2 shows the sputtering yields of various materials for 30keV Ga^+ ions (Reyntjens & Puers 2001).

Table 2.2: The sputtering yield of various materials for 30keV Ga^+ ions

Material	Range (nm)	Sputter Yield (atom/ion)
Silicon	27	2.6
Aluminium	24	4.4
Copper	10	11.0
Silver	11	14.0

(Reyntjens & Puers, 2001)

2.5.2 Acceleration Voltage

Acceleration voltage is the acceleration of energetic Ga^+ ion source held at a positive potential relative to ground (Fu & Ngoi 2005). The gallium source is heated up and gallium liquid flows down and wets a sharp tungsten needle. Then, the gallium liquid is pulled into an extremely sharp "Taylor-Gilbert" cone when an extraction voltage is used between an extraction aperture and the metal source. Ga^+ ions are extracted from the tip of this cone by field emission (Lindquist, et al., 2012). The balanced electrostatic potential created by the extraction voltage and the liquid surface

tension forces causes Ga^+ ions to accelerate through the column to reach its ground potential (Ali, et al., 2010).

The ions are able to travel very fast by increasing the acceleration voltage as they exit the column and impact onto the specimen with a great energy (Fu & Ngoi, 2005). Fig. 2.5 shows the schematic diagram of FIB system and the gallium liquid-metal source. Higher acceleration voltage is more beneficial as it does not affect the probe current (Raffa, et al., 2006). With acceleration voltage of more than 30keV, the probe size decrease to 1nm but the milling time increases for a feature milled at a fixed area.

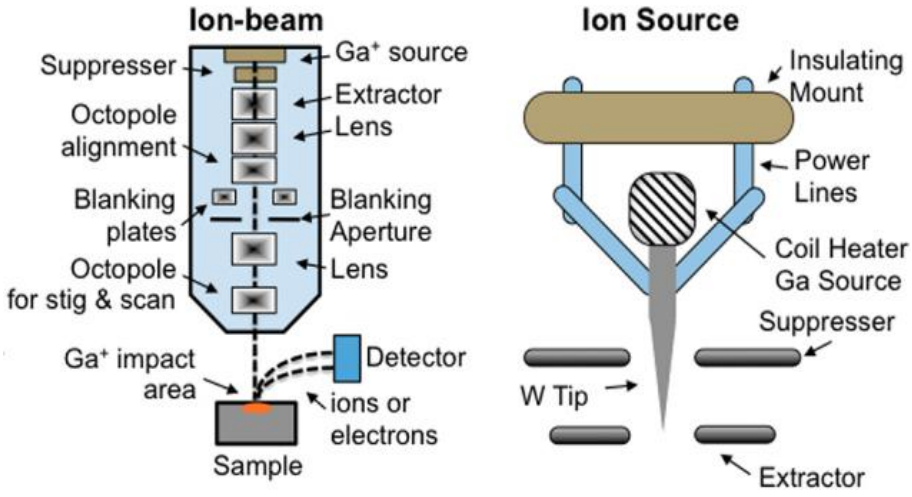

Fig. 2.5: The schematic diagram of FIB system and the gallium liquid-metal source (Lindquist, et al., 2012).

Typically, an acceleration voltage of approximately 30keV is selected in order to achieve the minimum lateral resolution with high sputtering yield. Re-deposition may form in this point of interaction due to the trapped ions in the substrate as their energy is expended (Fu & Wang, 2010). As a result, the typical acceleration voltage required for sputtering is between 10 and 100keV for most of the ion species used for milling (Tseng, 2004). Rajsiri et al. (2002) found that FIB milling with Ga^+ ion at energy of 30keV results in amorphisation damage on the silicon surface, consequently

demonstrating low sputtering yield and implantation of Ga^+ ions within the damaged region. However, the amorphisation damage and the implantation of Ga^+ ions can be reduced by milling at a low acceleration voltage.

2.5.3 Beam Current

Beam current is one of the major factors for the aspect ratio. Various beam currents determine various beam spot sizes. Generally, the measurement of the real spot size is difficult in practice. Hence, beam current is typically used as a main parameter to show the effect of the spot size (Fu & Ngoi, 2005). The beam current represents the spot size of the beam, which in turn describes resolution and feature size (Malek, et al., 2003). Table 2.3 shows different beam currents and corresponding milling spot sizes of the FIB-SEM Auriga Crossbeam.

Table 2.3: Different beam currents and corresponding milling spot sizes (at 30keV).

Beam current (pA)	Milling spot size (nm)
1	3
2	7
5	9
10	13
20	13
50	22
120	25
240	40
600	59
1000	200
4000	300
16000	900
20000	1100

(Langford & Petford-Long, 2001)

Normally, a material can be sputtered rapidly from the surface when using a high beam current. Therefore, a low current beam is used if only a high magnification imaging is required (Mei, 2009). For the milling process, high beam current is applied for sputtering or removing material from the surface, whilst a lower beam current is used for fine polishing (van Tendeloo, et al., 2012). The sputtering rate can be easily

and accurately monitored by adjusting the beam current or using smaller spot sizes. Lower beam currents with the number of repetitive passes are able to produce channels with a finer quality, which in turn, can extremely reduce the productivity (Tseng, 2004).

2.5.4 Dwell Time

Dwell time is the period of time where the beam stays at a particular position, and it is also defined as the duration of ion beam stops at each pixel (t_d) (Raffa, et al., 2008). The unit of dwell time is usually represented by μs and ms. The dwell time needs to be optimised for a particular material and a particular application. The dwell time normally influences the sputtering depth in silicon milling. At the time of line by line scanning, the ion beam stays at a specific point (dwell point or pixel point) for a particular time (dwell time) and then turns to the next pixel point (Ali, et al., 2010). With fast scanning, the dwell time at any pixel point is short, during which time the ion beam converts any material on the surface to a deposited product. Long dwell time is suitable for small structures such as vias, and it may be possible to achieve a depth more than 10μm or even higher.

Tseng (2004) also concluded that the aspect ratio can be increased by increasing the dwell time. However, the dimension of micro holes is continuously reduced as the dwell time increases although the whole feature sizes increases with the dwell time, which vary from 5 to 50ms. This may imply that a large amount of sputtered materials is deposited into the ridge (outside the channel) and inside the channel. There is also reported that a long dwell time can lead to the formation of structures with inclined bottoms (Urbánek, et al., 2010). On the other hand, Tseng (2004) have found that the detection accuracy for FIB milling can be significantly improved by reducing the dwell time.

2.5.5 Scan Mode

Two types of scanning modes, raster and serpentine scans are generally used to drive the FIB movement (Tseng, 2004). They are performed in a sequential action, one scan line after another. In raster scanning, the beam returns to the initial point of the next scanning line after finishing any line (retracing), or in simple words, the scan moves in the same direction (Ali, et al., 2010). The raster scan is widely applied in computer graphics and each series of the lateral pixels is called a raster line or scan line (Tseng, 2004). In a raster scan, sputtered materials are continuously re-deposited into the region milled earlier and the re-deposited materials accumulate more on the regions milled earlier in the pass, resulting in the inclined bottom of the milled surface (Youn, et al., 2007). Hence, the raster scan is an effective process to fabricate V-shaped channels or cavities with inclined bottom surface (Tseng, 2004).

In the serpentine scanning mode, the beam moves in opposite directions from one row to the next which allow reduction in the scan time, by eliminating the retrace time between the last pixel of one row and the first pixel of the next (Ali, et al., 2010). The re-deposition is proportionally decreased in each pass and an amount of the re-deposition from each initial passes as eliminated by each successive milling (Youn, et al., 2006). By increasing the number of passes, the effects of re-deposition can be reduced. A sharply defined region with a uniform depth and smooth surface can be milled. The serpentine scan procedure is essential in order to form channels with longitudinal sidewalls as well as smooth channel bottom or producing any high aspect ratio or curved structure (Tseng, 2004). For best performance, a raster scan is used for the first beam pass to outline all the areas to be milled. Then, a serpentine scan is used following the scan milled previously (Tseng, 2004).

2.5.6 Pixel Spacing

Pixel spacing is the distance between the centres of two adjacent pixels (P_s) (Youn, et al., 2008). In order to mill a smooth profile at a constant milling rate, the pixel spacing must be sufficiently small to allow a suitable overlap between adjacent pixels. In addition, the pixel spacing between adjacent scan lines must be small enough to allow an appropriate overlap between adjacent pixels so that a smooth surface between scan lines can be milled (Tseng, 2004).

Moreover, Tseng (2004) has found that if the ion distribution of FIB along and across the scanning lines is considered as a Gaussian distribution, the scanning ion flux becomes stable and consistent when the normalized pixel spacing (Ps/α) is smaller than 1.5 as shown in Fig 2.6, where α is the standard deviation of the Gaussian distribution (Tseng, 2004). Hence, a uniform milling of the surface between scan lines can be obtained when the normalized pixel spacing is equal to or smaller than 1.5 (or $P_s/\alpha = 0.637$). On the other hand, the roughness on the milled surface is significantly influenced by pixel spacing due to a sufficient number of spots produced by digitally controlled pixel that promotes a superior milling surface (Kim, et al., 2008).

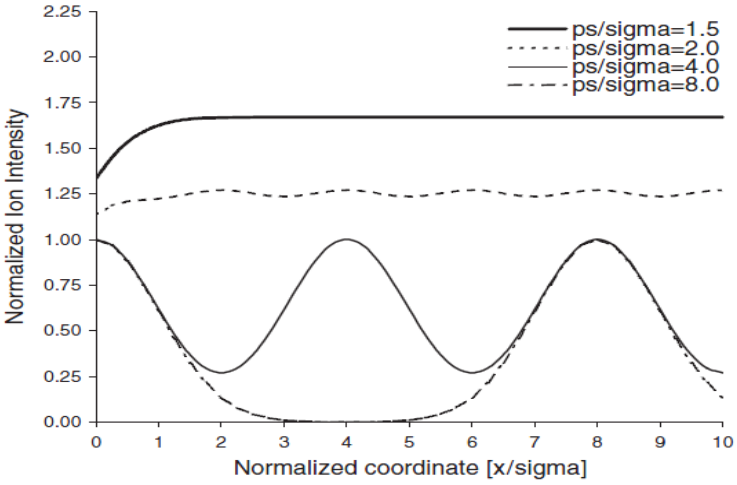

Fig.2.6: Overlap effect on ion flux distribution for Gaussian FIB Milling.

(Tseng, 2004).

2.5.7 Pattern Size

Pattern size is the other key parameter which determines sputtering depth. This is due to the fact that the dwell time and pixel spacing are dependent on the pattern size. Kim, et al. (2008) found that the reduction in the pattern size of the milled hole resulted in rough edges in the silicon samples, and non-uniform diameter of the hole, as shown in Fig.2.7. Thus, each device required adjustments in the pattern size before fabrication. Langford & Petford-Long (2001) suggested changing the raster pattern and the dwell time to improve pattern fidelity. Different profiles are dependent on the increase or decrease of the radius(r) of the profiles milled, and the holes with the most vertical sidewalls are obtained if the dwell time is proportional to (r) (Langford, et al., 2007).

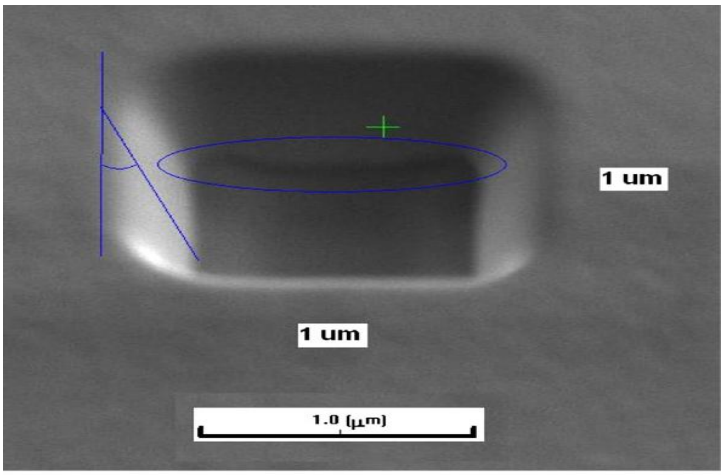

Fig. 2.7: A milled hole with pattern size of 1x1m^2. The hole's width is not uniform and rough damage occurs at the bottom edge of hole.

(Kim, et al., 2008)

2.5.8 Milling Mode

There are two types of milling modes, the bitmap function and pixel space mode. For bitmap function, the first step is preparing a designed pattern with bitmap format of *.XBM (Fu & Ngoi, 2005). Then, this pattern file can be transferred from the folder to a selected area to be milled. After the commencement of milling, the FIB can directly write the pattern by deflecting of the beam according to the location of holes defined by the bitmap file. Micro-holes can be directly milled by this type of milling mode. For the pixel space mode, the pixel spaces in both lateral and vertical directions are set to be wide enough that centre distance is more than twice of the holes diameter (Fu & Ngoi, 2005).

The vibration of the stage which occurs during the milling process is the main limitation for both bitmap function and pixel space mode (Atiqah, et al., 2012). Moreover, it is difficult to mill the micro-hole array with sizes below 100nm using the bitmap function in sample larger than 100µm square. This problem occurs because of a limitation of beam deflection for a large area, which subsequently influences the

resolution. The large area of microhole patterning can only be realized by using the pixel space mode with large pixel spaces in both horizontal and vertical scanning directions (Fu & Ngoi 2005).

2.6 Effects of FIB Milling on Microholes

The understanding of FIB damages is important to ensure that the region being milled is indeed representative of the hole pattern, and is not due to a specimen preparation artefact. The interaction between the incident ions (Ga^+ ions) and the target material during FIB milling may lead to surface damage and consequently limit the ability to achieve a high quality of the milled holes.

2.6.1 Re-Deposition

For FIB milling, the aspect ratio is decreased by the re-deposition of sputtered material on the surfaces of the holes, thus cause difficulty to correctly estimate the depth of the holes (Malek, et al., 2003). A collision cascade of substrate atoms at the regions bombarded by sputtering occurs when energy is transferred from the Ga^+ ions to the target substrate (Tseng, 2004). The sputtered atoms are not in their thermodynamic equilibrium state and have a tendency to solidify with nearby surfaces after collision. Sputtered atoms are re-deposited at the walls of patterns and they then distort the pattern profiles (Raffa, et al., 2006). The quantity of re-deposited material can be depending on the geometry of the structure being milled, and the process of re-deposition is nonlinear with time (Raffa, et al., 2006).

In a normal FIB milling, it is found that re-deposition on the sidewall is controllable by adjusting the FIB scan speed (dwell time) and direction (Yao, 2005). During FIB milling, a small step-like slope is formed in the bombarded slope, as shown in Fig. 2.8. Sputtered atoms are re-deposited more on the sidewall facing the slope

having the gradient (Θ) than on the sidewall at the back of the slope (Malek, et al., 2003). By varying the scan speed and the gradient (Θ), re-deposition can be controlled (Latif, 2000).

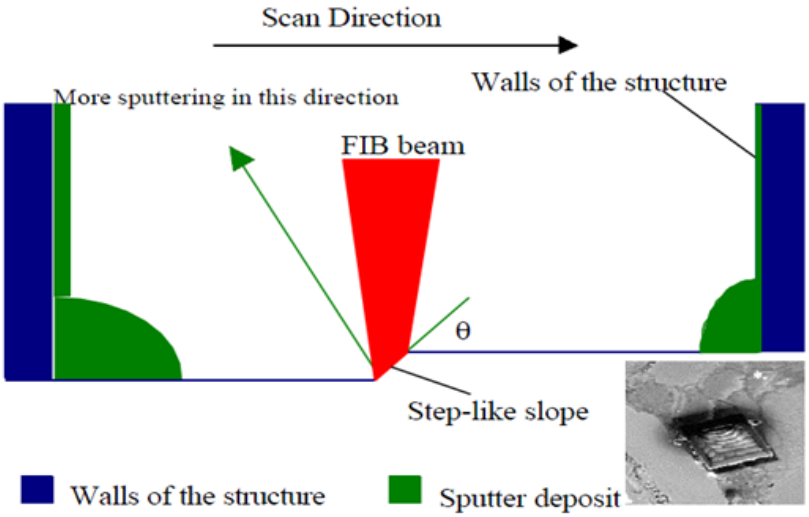

Fig. 2.8: Schematic diagram of FIB milling at the slow speed.

(Latif, 2000)

More than half of the sputtered atoms from the bottom surface will redeposit back at the bottom and adhere to the sidewall for milling a 3D structure with an aspect ratio (>1). Re-deposition also occurs on the bottom at aspect ratio below 1, causing a variation of milling depths. Hence, the actual milling depth is less than the designed value owing to the accumulated material at the bottom (Fu, et al., 2000). Re-deposited material accumulated on the convex surface is increased with increasing of the aspect ratio. The reason is that the sputtering yield from the sidewalls increases when the ion beam is nearer to the edge and leads to increase in the milling depth (Fu, et al., 2000). According to Tseng (2004), re-deposited material tends to accumulate at the same region during early milling. Thus, the region which is desired for a greater milling depth should be milled last in the scanning sequence.

High aspect ratio holes cannot be produced unless the material removed is volatile and does not deposit on the walls of the holes, which often limits the obtainable aspect ratio of a micro machined feature to 10 (Stevie, et al., 2005). The holes grow deeper but also narrower because of re-deposition. The flux density of material sputtered from the bottom of the hole and deposited to the sidewall of the hole, *F(h)*, can be represented by:

$$F(h) = \frac{F_0 h}{2} \int_0^d \frac{x dx}{r^3}$$

where F_0 is the total number of atoms sputtered per unit length, d is the hole diameter, and h is the depth of the processed hole, $r=(x^2+h^2)^{1/2}$ (Fu & Ngoi, 2005).

The FIB attained aspect ratio of the micro-hole reduces exponentially with normalized re-deposition, $F(h)/F_0$, as shown in Fig. 2.9 (Fu & Ngoi, 2005). At an aspect ratio below than 1, more than 50% of the sputtered atoms from the bottom surface redeposit on the sidewall (Fu, et al., 2007). The ratio of $F(h)/F_0$ will degrade for material with higher sputter yield. Hence, the aspect ratio can be upgraded further by choosing the substrate material with high sputter yield.

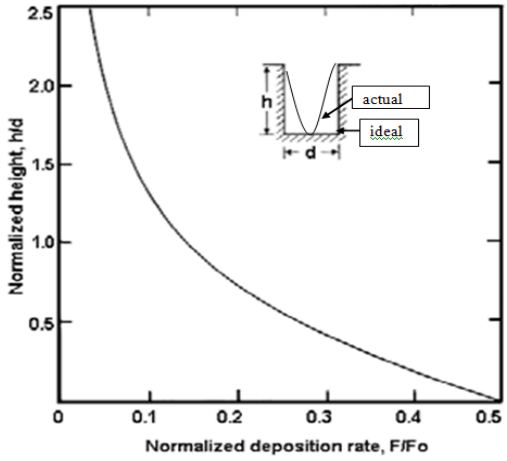

Fig. 2.9: Aspect ratio *vs.* normalized re-deposition rate, F/F_0.

(Fu, et al., 2000).

2.6.2 Amorphisation

Amorphisation of a FIB milled crystalline surface may occur due to sufficient atom displacement during the collision cascade, thus reducing the resulting in long range order when the density of point defects reaches a critical stage. Low intensity levels of milling ions create amorphisation in the bombarded area of a crystalline substrate and induce the substrate to swell (Tseng, 2004). For a crystallized Si substrate penetrated by Ga^+ ions, the dose level to cause amorphisation is of the order of 10^{15} ions cm^{-2}, whilst the effective milling dose should be at least two orders of magnitude higher than the amorphisation dose as suggested by Tseng (2004).

Since the majority of the FIB ion distributions are roughly similar to the Gaussian ion distribution, the intensity at the fringe (tail) of the beam is slightly smaller than at the core (centre region). FIB ion distributions possess a minimum strength to sputter materials but are enough to form amorphisation that cause substrate swelling. Rajsiri et al. (2002) has found that FIB milling with Ga^+ ions at energy of 30keV will produce amorphisation damage along a Si sidewall that is ~28nm thick and up to 20wt% Ga^+ ions may be present within the damaged region. Deposition of a layer of platinum

or other metals using an FIB instrument prior to the beginning of any milling by using low energy ions can be applied to prevent top surface damage (Reyntjens & Puers, 2001). The coating also ensures that the microstructures are milled evenly and remain parallel to the direction of ion beam. Fig. 2.10 shows the re-deposition and amorphisation on FIB milled holes (Rajsiri, et al., 2002).

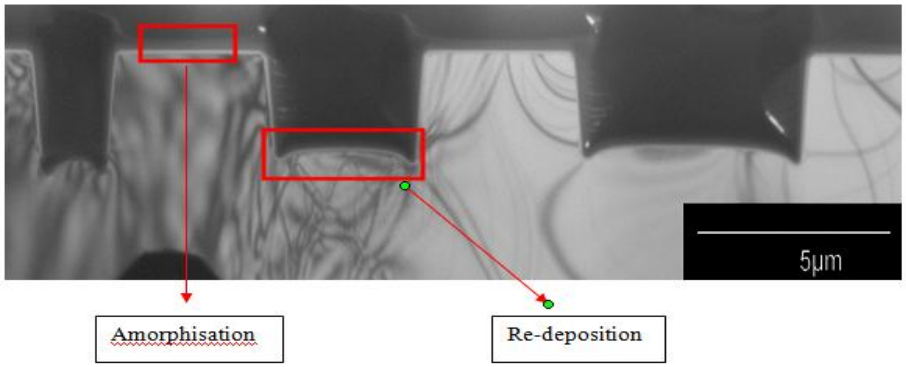

Fig. 2.10: Effect of FIB milling, re-deposition and amorphisation on FIB milled holes (Rajsiri, et al., 2002).

The FIB parameters to be controlled and the effects that possibly occur during milling using these parameters are summarized in Table 2.4.

Table 2.4: The FIB parameters and the possible effects occur on milled structures

Parameter	Effect	
	Increase	Decrease
Sputter yield	Milling depth increases, low re-deposition effect (Fu, et al., 2000).	Milling depth decreases, high re-deposition effect.
Acceleration voltage	Fast milling, damages occur (amorphisation, implantation) (Rajsiri, et al., 2002).	Slow milling, reduced damage (Einsle, et al., 2011).
Beam current	Fast milling but the quality of milling is low (Yao, 2005).	Slow milling, good for fine polishing, produce finer quality of channels with increasing the number of serpentine scan (Tseng,

		2004).
Dwell time	Suitable for small structures (vias), high aspect ratio, re-deposition occurs.	Requires long milling time, low aspect ratio, reduce re-deposition and improved detection accuracy (Kim, et al., 2008).
Pixel spacing	Aspect ratio larger than 8.0 can be milled (Tseng, 2004).	Smaller values than 1.5 for smooth profile.
Pattern size	Long dwell time required (dwell time α radius (r)) (Kim, et al., 2008).	Surface roughness, holes are not uniform in width.
Scan mode	• Raster – continuously re-deposited, suitable for V-shaped channels (Tseng, 2004). • Serpentine – reduce re-deposition, suitable for high aspect ratio structures.	
Milling mode	• Bitmap – direct write, difficult to fabricate holes below than 100nm in large area (Fu & Bryan, 2005). • Pixel space – mill one by one, able to fabricate holes below than 100nm in large area (Atiqah, et al., 2012).	

2.7 Enhancement of FIB Milling Depth

The effect of re-deposition in FIB milling has been a major limitation to achieve higher aspect ratio microstructures with accurate geometry of structures as similar as designed patterns. However, this inevitable phenomenon can be improved by introducing appropriate gases through the gas injection system (GIS) on the sample during sputtering or by further wet chemical etching using TMAH (Kim, et al., 2012). These two methods are discussed in the following sub-sections.

2.7.1 Gas Injection System (GIS)

Most FIB systems are provided with a gas injection system (GIS) which is able to deliver different type of gases used for metal or insulator deposition and gas chemical etching. The system is also known as gas-assisted etching (GAE) (Raffa, et al., 2006).

Generally this system operates by injecting an appropriate gas on the substrate and forms volatile by-products that are removed by ultra-high vacuum (Malek, et al., 2003). Typically a needle is used to deliver gas and allow gas fluxes in the range of 1015 molecules $cm^{-2}s^{-1}$ to 1017 molecules $cm^{-2}s^{-1}$ whilst maintaining the high vacuum conditions for operating a focused ion beam column (Orloff, 2008). The gas molecules absorbed at the surface are decomposed by excited surface atoms and the etching process can be initiated (Kim, et al., 2012).

There are various types of etching gases used in this system to enhance the milling rate of microstructures during FIB milling. The common etching gases and the milling rate enhancement factors are shown in Table 2.5 (Reyntjens & Puers, 2001). The actual rate depends on the types of materials, the mass of the target atom, its binding energy to the atom matrix, and its matrix orientation with respect to the incident direction of the ion beam (Yao, 2005).

Table 2.5: Typical GIS/GAE gases and the etch rate enhancement factors on various materials.

GIS/GAE Gases	Aluminium (Al)	Tungsten (W)	Silicon (Si)	SiO_2, Si_3N_4	Photoresist, Polyimide
Cl_2	10-20	-	10	-	-
Br_2	10-20	-	6-10	-	-
ICI	8-10	2-6	4-5	-	-
XeF_2	-	10	10-100	6-10	3-5

(Reyntjens & Puers, 2001)

The FIB milling assisted by the gas injection system provides high removal efficiency (etch rate), high selectivity, reduced unwanted implantation and reduced re-deposition on the sidewall and bottom surface (Kim, et al., 2012). The enhancement in the etching rate is up to several hundred times higher than FIB convectional milling (Raffa, et al., 2006). This makes it possible to decrease the required dose of ion beam

for the milling process. The re-deposition is also significantly reduced and forms well defined grooves with aspect ratios of more than 10, which cannot be obtained by normal FIB milling (Raffa, et al., 2008). Moreover, Ga^+ ions are not detectable in sidewall channels when FIB milled using GIS. The GIS technique is more efficient in removing large volumes of material that would be too time-consuming otherwise (Malek, et al., 2003). GIS is also able to selectively etch one element or compound without affecting the others. For example, materials such as Si, Al and GaAs can have their removal rate increased 20 to 30 times through GIS, whilst oxides like SiO_2 and Al_2O_3 are not affected (Yao, 2005).

However, the GIS technique has its problems as well. The mechanism below GIS is a very complex phenomenon, because the material removal occurs due to the chemical action of the gas, the energetic ion motion, and the combined action of the gas and energetic ions (Ali, et al., 2010). Furthermore, the increase in removal rate decreases the amount of implanted gallium and resulting defects which form contamination (Yao, 2005). The use of etching compounds must be avoided, which may show spontaneous reaction with the sample material. GIS also does not possess the high precision that ion milling can achieve. Often, a combination of initial GIS followed by ion milling is used when an operation requires bulk volumes of material removal as well as high precision (Malek, et al., 2003).

2.7.2 TMAH Etching

Wet-chemical etching is a technique that utilizes liquid chemicals to remove material, in order to pattern a thin/thick film. The technique requires immersion of a substrate in a pure or mixture of chemicals. The immersion time is dependent on the composition and thickness of the layer to be etched, as well as the choice of etchant and temperature to be used (Elwenspoek, et al., 1994).

TMAH is widely used as a photoresist developer in large-scale integrated (LSI) circuits as it provides consistently high quality at a reasonable price (Sunami, et al., 2004). TMAH is preferred in the fabrication of MEMS devices due to its low toxicity compare to KOH and hydrazine. These two etching solutions are detrimental to MEMS device reliability and are toxic to human health (Sunami, et al., 2004). Typically silicon dioxide, SiO_2 and silicon nitride, SiN_4 are used as etch masks for TMAH etching on Si substrate due to lower etch rate compared to Si (Miney, et al., 2003). The Si substrate is immersed in aqueous TMAH solution with concentrations ranging from 20% to 25% at temperatures below 100°C. The duration of time needed for TMAH etching process is according to the etch rate of TMAH on the different orientation of silicon planes and the temperature of TMAH solution. The etching of the {100} Si plane can be completely etched after 8 hours, and smoothing the surface of Si requires about 16 hours.

In the TMAH etching process, the etch rate of Si is known to increase with increasing temperature. When immersed into 25% aqueous TMAH solution at 85°C, the etch rates of the {100} Si plane and {100} Si plane are about 0.6μm/min and 1.4μm/min (Sievilä, et al., 2010). However, the etch rate is decreased to approximately 0.15μm/min at a temperature of 60°C. The etch rate of TMAH for {111} Si plane is 100 times less than {100} and {110} Si planes. V-shaped grooves are significantly formed on {100} Si plane whilst straight grooves on {110} Si plane, as shown in Fig. 2.11 (Sunami, et al., 2004):

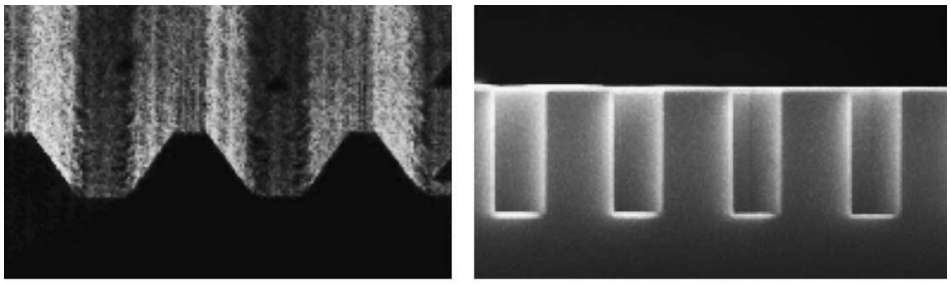

(a) {100} Si surface (b) {110} Si surface

Fig. 2.11: Grooves formed on (a) {100} and (b) {110} silicon surfaces with 25% TMAH aqueous solution at elevated temperature around 75°C.

(Sunami, et al., 2004)

The advantage of TMAH is that, since no alkali ions are present, it presents no danger to electrical circuits (Miney, et al., 2003). TMAH solution is low toxicity due to no metallic ions and can be handled easily. TMAH based solutions provide smooth surfaces, relatively high anisotropy and an interesting high silicon/silicon dioxide etching selectivity compared to KOH (Defforge, et al., 2011). TMAH is, therefore, increasingly recognized as a viable alternative for MEMS process applications (Miney, et al., 2003). An FIB-implanted Ga^+ layer acts as a mask with a high selectivity in TMAH wet etching enabling the fabrication of high resolution gratings, extremely narrow, long and thin freestanding elements, and vertical walls with very high aspect ratio (Sievilä, et al., 2010).

On the other hand, the etching conditions must be accurately defined to obtain smooth silicon sidewalls, especially at high temperature, otherwise the surface can roughen and micro-pyramids, also known as hillocks may develop. The origins of these hillocks remain unclear although they are assumed to be due to H_2 bubbles and/or waste micro-masking. The alkali species concentration is important to maintain a surface free of hillocks. The hydroxide content is well known to be a significant parameter regarding

micro-pyramids development. The low concentration of TMAH solution gives better quality of Si surface after etching (Defforge, et al., 2011).

2.8 Metal Nanopowder Filling

There are many filling materials that can be used to fill high aspect ratio micro holes/vias. The main characteristics of the filling material must be electrically conducting, corrosion resistant, feasibly adjustable to the available production system such as screen printable, low shrinkage after processing, high strength, good adhesion and yet, low cost (Kang, et. al., 2000).

The use of nanopowder filling to produce metallic/ceramic microstructures has great potential as the demand for such structures increased, due to the nature of nanopowder net-shaping in which complex machining is not required (Fu, et al., 2007). Nanopowders can create compact bulk nanostructure materials due to the excess of free surface energy that is related to a great number of the surface atoms, compared to the interior atom of nanopowder (Khasanov & Dvilis 2008). Moreover, nanopowder has a greater catalytic activity and higher sinterability compared with coarse grained bulk materials (Morales, 2006). The widely applied metals in MEMS devices are gold, copper, titanium, silver, aluminium, and nickel. These metals can be deposited by processes such as electroplating, sputtering, micro injection moulding and hot embossing (Fu, et al., 2005). A good example is the use of 316 stainless steel microgears, and microneedles for selective nerve stimulation, and micromolds made from hard metals for plastic micro injection moulding and hot embossing (Fu, et al., 2005).

Park et al. (2010) found that the photoluminescence (PL) intensity from a layer of quantum dots (QD) is increased by filling silver nanoparticles into photonic crystal

hole structure arrays. The enhancement was achieved due to hybrid effect of silver nanoarray-induced localized surface plasmon resonance (SPR) and outcoupling of wave-guided light in a two-dimensional nanopattern array. High aspect ratio microstructures of electrodeposited copper-γ-Al_2O_3 nanocomposites were successfully performed into deep recesses with uniform concentration of alumina nanoparticles along the length of the microposts (Hung, 2009). A gas bearing green part with tiny and complex structures was successfully produced by filling the 17-4 PH stainless steel nanopowders mixed with polymer binder into the PDMS soft mold.

There are several challenges in applying metal nanopowders to high aspect ratio microfilling. The particle size of the metal nanopowder is a very important parameter which limits the producible HARMS. The particles should be small enough to obtain a smooth filling surface with a fine filling topography. Furthermore, agglomeration becomes the critical issue during fabrication process. Highly agglomerating nanopowders leads to gas trapped in filling structures and cavitations may occur.

2.8.1 Nickel Nanopowder as Filling Material

In MEMS devices, the high aspect ratio microstructures should have high hardness and yield strength, good resistance against corrosion and low resistivity (Kim, et al., 2008). The metal also should be easily deposited or electroplated into hundreds of microns thickness on silicon wafer. Nickel and Ni based alloys have been found to have good mechanical properties that can be exploited to realize high aspect ratio structures in MEMS devices (Du, et al., 2004). Moreover the magnetic properties of Ni have been widely used in magnetic MEMS. Commonly, nickel is filled through holes by electroplating to form electrical contacts due to its good adhesion between the filling and the sidewall of holes, with the help of a seed layer (Inoue, et al., 2011). A fabrication technology of high density electrical feed-through in Pyrex glass wafers is

successfully fabricated by filling the through holes with electroplated nickel (Li, et al., 2002).

The decrease of grain size yields provides an optimal improvement of the mechanical properties. This is due to a simultaneously increase of strength and fracture toughness. Tensile tests on nickel with 30nm grains showed an improved ultimate tensile strength of 1.5GPa, and $\sigma_{0.2\%}$ of 1.0GPa which is a significant improvement to conventional nickel, which has 500MPa and 300MPa respectively (Larsen, et al., 2002). The melting point of nickel nanopowder also decreases to approximately 600°C, far below its bulk value, ~1450°C. The lower melting point of nickel nanopowder ensures that low energy is consumed during the fabrication process.

Nickel nanopowder has a face centered cubic (FCC) crystalline structure and categorized as a ferromagnetic material (Fischer, et al., 2012). Nickel nanopowders can be formed, which are of uniform size, monodispersed with a narrow size distribution and have low impurity contamination such as oxide layer (~1 nm). Although nickel has a slightly high resistivity than copper, the cost is affordable and best matches the volumetric coefficient of thermal expansion of silicon, as shown in Table 2.6 (Pecht, et. al., 1998). In addition of the large capabilities of nickel in nano-size has promise an alternative material of holes/vias filling.

Table 2.6: Comparison of cost, resistivity and volumetric coefficients of thermal expansion of copper, nickel and silicon.

Material	**Cost ($/lb)**	**Resistivity (Ω.cm) at 20°C**	**Volumetric coefficient of thermal expansion (3x linear coefficient),β at 20°C (β/°C)**
Copper	3.99	1.68×10^{-8}	5.1×10^{-5}
Nickel	3.33	6.844×10^{-8}	3.9×10^{-5}
Silicon	1.29	6.4×10^{2}	0.9×10^{-5}

(Pecht, et al., 1998)

2.9 Electroplating as a Commercial Filling Method

Plating method is generally uses for holes/vias filling in high density or through holes interconnection (HDI) technology. Due to the high deposition rates, comparatively less expensive and easiness in satisfying high aspect ratio features, plating deposition rates have been increased in the fields of semiconductors, especially in MEMS. Plating can be divided into electroplating, which requires a seed layer, and electroless plating which does not (Geissler, et al., 2003). Electroplating is more suitable than electroless plating since the method is simpler and provides good adhesion, in order to get an adhesive strength of plating with the holes wall and prevent the plating from being separated from the wall.

Electroplating of copper is preferred as filling material because of high electrical conductivity of copper and the high electrodeposition rate (Lühn, et al., 2009). Moreover, electroplating is amenable to process at close to room temperature, as well as a wide available tool vendor support and process maturity (Fischer, et al., 2012). However, it has some problems to be solved due to its complexity in terms of process controllability, reliability and throughput. In particular, high aspect ratios of holes/vias filling with void free metal cores are difficult to implement. The filling of holes/vias with high aspect ratio up to 15 is still lacking in detailed description of the mechanism of electroplating (Fischer, et al., 2012). In addition, Ramm et al. (2008) have found that electroplating takes too long to fill the holes/vias greater than 10μm without a void (~30 min). Alternative approaches to plating processes have therefore been investigated, such as filling with conductive metal pastes and solder (Fischer, et al., 2012).

2.9.1 New Filling Method using Magnetic Assembly

Magnetic assembly or magnetic self-assembly is an instant filling technique that magnetically assembles pre-formed conductive via cores into via holes (Fischer, et al., 2012). Magnetism as a non-contact force enables a controlled manipulation of ferromagnetic features over long-distances and is insensitive to the surrounding medium and independent of the details of the surface chemistry. Magnetic fields can have high energy densities and can influence feature sizes from the nanoscale to the macroscale. Magnetic interactions are being exploited in a wide range of micromechanic applications, including valve pumps, relays, micromirrors, actuators, RF switches, magnetic storage, magnetic field sensing and biomedical applications (Mastrangeli, et al., 2009)

The magnetic assembly of ferromagnetic nickel nanopowder is governed by particle-particle and particle-substrate interactions. Thus, when an external magnetic field is applied to a suspension of magnetic particles, they tend to assemble into linear aggregates, with their magnetic dipoles aligned in a head-to tail fashion and parallel to the magnetic field. Tanase et al. (2002) controlled the aggregation of Ni nanowires, permanently magnetized along their long axis, by applying a small external magnetic field to their suspension. The aligning effect of the field, coupled with the magnetic dipole–dipole interactions, because formation of the wires which extend in the form of head-to-tail chains aligned to the direction of the field (Mastrangeli, et al., 2009).

Fischer et al. (2012) presented the concept of the fabrication of TSVs with an aspect ratio of 8 by manual magnetic assembly, which enables high aspect ratio vias with inherently void-free metal core. The magnetic assembly process that utilizes the ferromagnetic properties of nickel has been developed by randomly placing an excess amount of nickel nanowire on the front side of a wafer and assembled into etched via

holes. By applying a magnetic field which is induced by a permanent magnet from the back side of the wafer, the nickel wires align themselves along the field lines and erect themselves perpendicular to the wafer surface, as shown in Fig. 2.12. This effect allows the nickel wires to be steered around on the wafer surface by simply moving the permanent magnet laterally underneath the wafer. The assembly of the nickel cores is achieved by magnetically moving the wires over via holes. The upright position of the wires allows them to be pulled into the holes by the magnet.

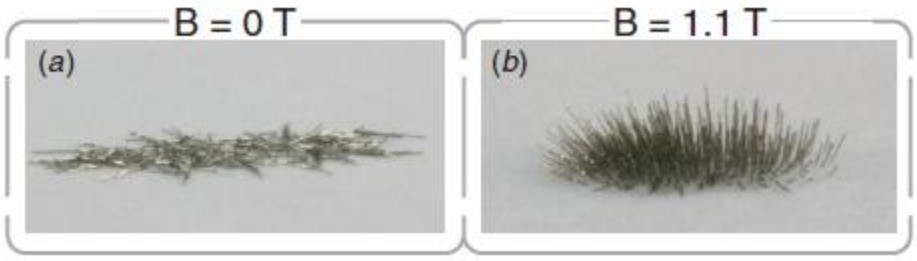

Fig. 2.12: Behaviour of nickel wires in a magnetic field. (*a*) About 300 straight nickel wires (35 μm diameter, 350 μm length) without an applied field. (*b*) A magnetic field of 1.1 T is generated by a cylindrical permanent magnet. It aligns the nickel wires along the field lines perpendicular to the ground plane.

(Fischer, et al., 2012).

Although this procedure possesses a low magnetic field and requires further modification for electro/ mechanical connections, magnetic interactions can be both attractive and repulsive depending on polarization, and can be tailored by magnet geometry and materials. In addition, magnetic assembly has several potential advantages such as a non-contact, long-distance action; insensitivity to the surrounding medium; independence on the details of surface chemistry; high energy density and their favourable downscaling properties (Mastrangeli, et al., 2009). All these remarkable features make magnetic forces very interesting as a new filling method of high aspect via holes for MEMS.

2.9.2 Ultrasonic Dispersion as a Filling Method

Ultrasonication is a technology which applies highly oscillating sound waves to agitate particles in an aqueous or organic medium, which in turn acts on particles which adhere to the substrate. The ultrasonic frequency is ranging from 20 to 40 kHz and generally used with other methods such as electrodeposition and EDM. Manu et al. (2011) has presented the application of ultrasonication for liquid manipulation during copper deposition into high aspect ratio via features. The filling process was achieved at a reduced plating time and at low concentration of copper sulphate (0.1M) compared to normal concentration, 0.8 – 0.9M which is generally employed in acidic copper plating bath. Ultrasonic vibration is also used in drilling high aspect ratio micro-holes by EDM, which provides an unevenly distributed gap for the debris and bubbles to escape from the discharge zone easily (Yu, et al., 2009).

Ultrasonication is the most widely used technique for dispersion of a range of nanoparticles. This technique usually disperses nanometer-sized materials in a liquid due to its relatively large surface area-to-volume ratios, as well as large scale of action of the ultrasonic waves. This technique can eliminate or substantially eliminate voids formed in the bottom of high aspect ratio holes. For example, ultrasonication was chosen as the best stirring method which affects the dispersion of the Fe_3O_4 nanopowder in the bath. Uniform dispersion allowed for greater contact area of the Fe_3O_4 nanoparticles in the bath (Li, et al., 2002). Ultrasonic vibration can damage the Coulomb and Van der Waals forces between the particles and render them homogeneously dispersed in the medium (Yinghong, et al., 2003). However, none of findings so far have used the ultrasonic dispersion technique in a dry form nanoparticles to fill via or holes. Thus, this technique is applied as a filling method in this research and its efficiency with the magnetic assembly filling method will be compared.

CHAPTER 3 METHODOLOGY

3.1 Overview of Fabrication Procedure

In the high aspect ratio microfilling technique developed, there are two steps of fabrication; i) formation of microholes and ii) filling of microholes with nickel nanopowder. Fig 3.1 and Table 3.1 illustrate the process flow and the summary of the processes involved in the fabrication and filling of high aspect ratio microstructures containing nickel nanopowder.

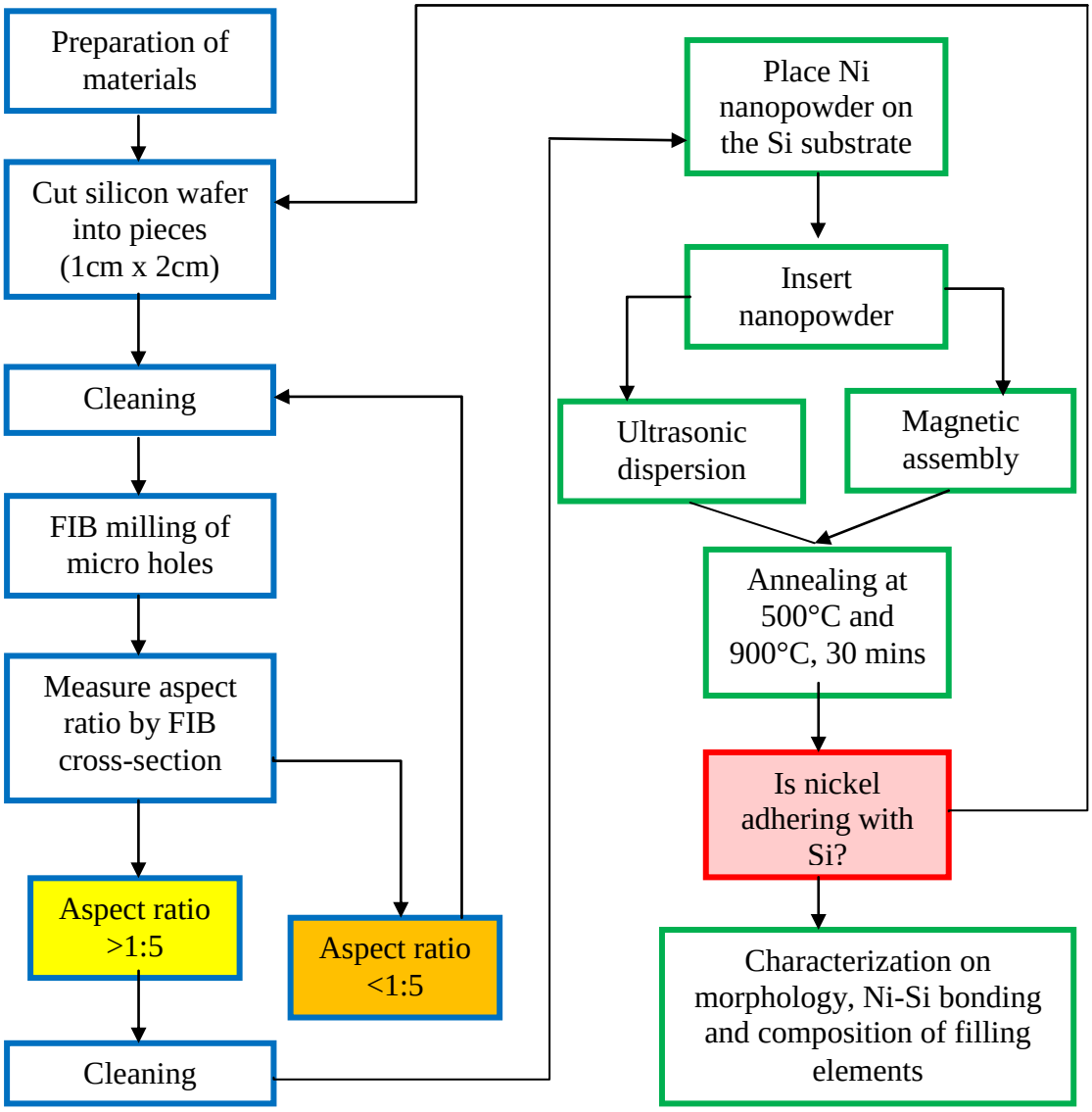

Fig. 3.1: The process flow for producing high aspect ratio microfilling using nickel nanopowder.

Table 3.1: The summary of fabrication process for high aspect ratio microfilling using nickel nanopowder

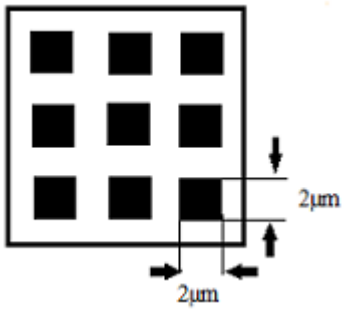	Pattern of micro holes; square shape, dimension (2µm x 2µm)
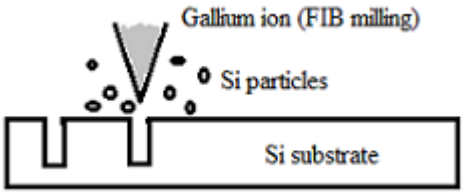	Vertical micro holes with high aspect ratio (>5) are fabricated by using Focused Ion Beam (FIB) direct milling
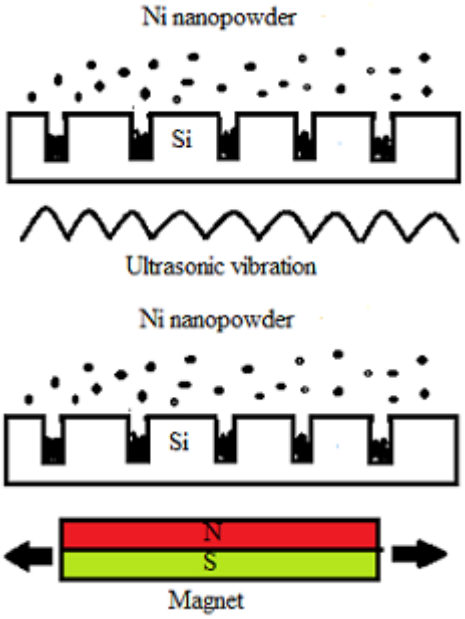	The micro holes are then filled with nickel nanopowder by ultrasonic dispersion/ magnetic assembly.
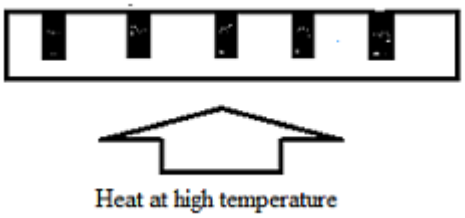	Once the nickel nanopowder is filled into the holes, they will be heated in high temperature to uniformly fill the micro holes and perform a bonding contact with Si (Annealing process).

3.2 Material Selection

3.2.1 The Substrate

The material for the substrate used in this research work is silicon, due to the fact that the fabrication technology for Si-based high-aspect-ratio microscale structures is the most mature and most widely available (Mei, 2009). The silicon wafer is supplied by Hamadatec Sdn Bhd. Because of limitations in supply, only p-type silicon wafers were available, of diameter 200mm and thickness 0.6mm, as shown in Fig 3.2. The orientation of silicon wafer is (100) with resistivity ranging from 1 to 50 Ω.cm.

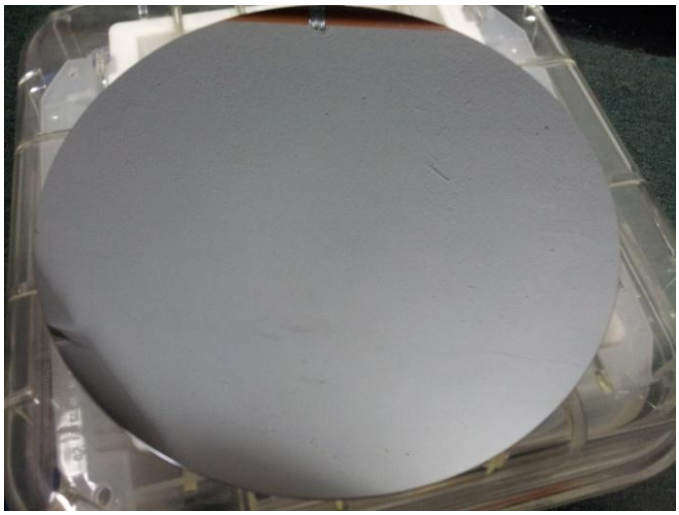

Fig. 3.2: P-type (100) silicon wafer, diameter 200mm and thickness 0.6mm.

3.2.2 Metal Nanopowder

Nickel (Ni) nanopowder is used in this research as the proposed metal filling for high aspect ratio micro holes. Nickel has desirable mechanical properties, such as high yield strength and high resistance to corrosion (Davis, 2001). Although nickel possesses a higher resistivity than copper as mentioned in Table 2.6, the thermal coefficient of expansion for nickel is much lower, which is compatible with silicon, as shown in Table 3.2:

Table 3.2: Comparison of the volumetric coefficients of thermal expansion for copper, nickel and silicon.

Material	Volumetric coefficient of thermal expansion (3x linear coefficient),β at 20°C (β/°C)
Copper (Cu)	$5.1x10^{-5}$
Nickel (Ni)	$3.9x10^{-5}$
Silicon (Si)	$0.9x10^{-5}$

(Davis, 2001)

In this research, the Ni nanopowder used is 99.9% pure nickel from Research Nanomaterials, Inc. (US). The average particle size is <70nm. The boiling and melting point are 2723°C and 1453°C whilst the density is 8.9g/cm^3 at 25°C, as stated in the Material Safety Data Sheet (MSDS) provided by the supplier. Fig.3.3 shows the Ni nanopowder in bulk form.

Fig 3.3: Nickel nanopowder from Research Nanomaterials, Inc. (US). The average particle size is <70nm.

3.3 Wafer Cutting and Cleaning

By using a diamond cutter, a silicon wafer was cut into pieces of 20mmx10mm in dimension, as shown in Fig. 3.4(a). The RCA (Radio Corporation of America) cleaning process was applied to clean the substrates. RCA cleaning is a standard set of wafer cleaning process to remove organic contaminants such as dust particles, grease or

silica gel from the wafer surface, followed by removal any oxide layer that may have built up, and finally removal of any ionic or heavy metal contaminants on the wafer surface (Han, 2012). For this research, the Si substrate was ultrasonically cleaned in soapy water and rinsed with acetone, isopropyl alcohol, distilled water, and hydrofluoric acid (HF). The purpose of each cleaning solvent is described as follows:

1. Soapy water was used to remove oil and grease on the surface of the Si substrate.
2. Acetone and isopropyl alcohol were used to remove all organic residues on the substrate.
3. Hydrofluoric acid solution HF:H_2O with a ratio of 1:20 was used to remove native oxide on the substrate (Nakahata, et al., 2004).
4. Distilled water was applied to clean the soap and ethanol and neutralize the surface of the substrate.

The RCA cleaning process was carried out by using an ultrasonic cleaning bath in a fume hood as shown in Fig. 3.4(b). The process began with immersion of the substrates in the soapy water for 5 min, which was then rinsed with distilled water. Then, the substrates were immersed in ethanol for 5 min, rinsed with distilled water and then was immersed in isopropyl alcohol for 5 min. After rinsing with distilled water, the substrates were then immersed in a Teflon container contained hydrofluoric acid solution (HF:H_2O) with a ratio of 1:20 for 40sec. Finally the substrates were rinsed and dried using an inert gas.

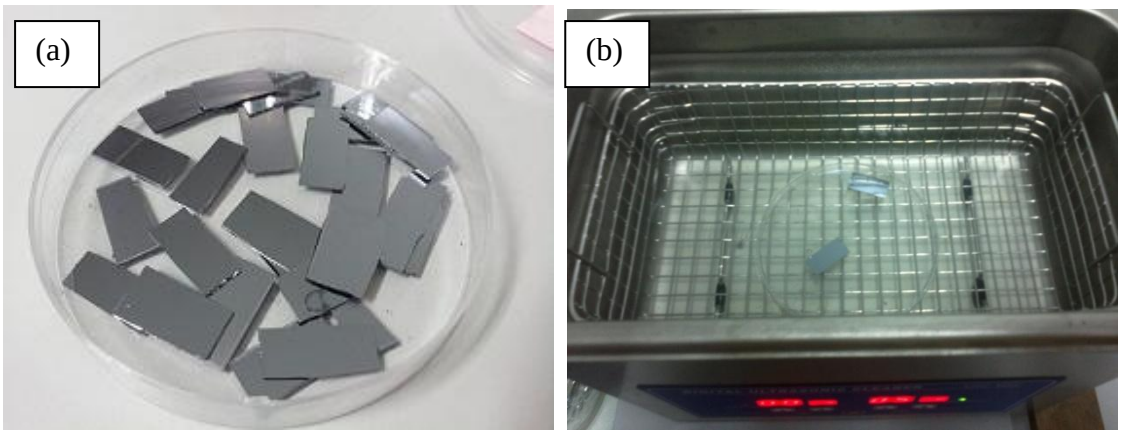

Fig.3.4: (a) The silicon wafer was cut into pieces of dimension 20mmx10mm. (b) The RCA cleaning process was carried out using an ultrasonic cleaning bath.

3.4 Formation of High Aspect Ratio Microholes

In this research, focused ion beam (FIB) direct milling was applied to form several microholes with a high aspect ratio of more than 5. FIB milling is an easy method to mill holes directly without any mask and produce a cross section in the same system with no external contamination. The milling process were carried out by the Zeiss Auriga FIB-SEM with an ion source of liquid gallium (Ga), integrated with scanning electron microscope (SEM), energy dispersion X-ray spectrometer (EDX) facilities and gas injection systems (GIS) functions. This machine uses a focused Ga^+ ion beam with energy of 30 keV, a probe current 1pA – 20nA and a beam limiting aperture size of 100µm. It is also capable of imaging up to 2.5nm resolution. For the smallest beam currents, the beam can be focused down to as small as 3nm in diameter (Fu & Ngoi 2005). The milling process was carried out, using a program which formed different relief depths by varying the probe current and initial milling depth. Fig. 3.5 shows the schematic diagram of the cross beam.

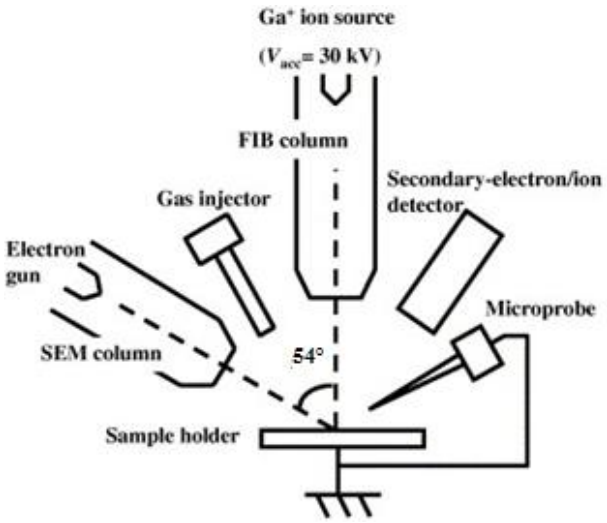

Fig. 3.5: Schematic diagram of the Zeiss Auriga Cross Beam.

(Fu & Ngoi, 2005)

For this work, the source was held at the maximum acceleration voltage, which is 30keV to form microholes. The mechanism of the milling process begins with the extraction of ions from the source. The difference in electrical potential exerts a force that causes ions to accelerate through the column to reach ground potential. By enhancing the acceleration voltage, the ions are travelling very fast as they exit the column and they impact on to the specimen at the highest energy (Fu & Ngoi 2005). The flow of milling process is shown in Fig. 3.6:

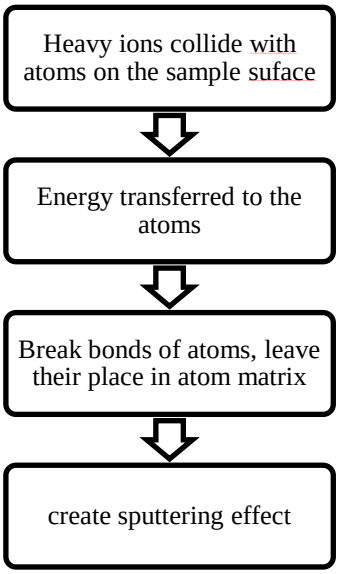

Fig. 3.6: The mechanism of focused ion beam (FIB) milling

(Fu & Ngoi, 2005).

Before the FIB milling process started, the pattern of microholes was realised using a FIB function called the feature mill function which is usually used for complex milling objects. The pattern can be designed by using geometric design shapes provided in the FIB system (pixel function) or by importing the BMP or DXF CAD file (bitmap function) of the desired pattern. For this work, the pixel function is used to design square patterns of dimensions 2µmx2µm to form microholes. The scale of the pattern design can be defined by overlaying grid lines on the image of the Si surface with the required size, and then placing the square patterns on the grid lines, as shown in Appendix 1. The FIB cross-sectioning method was used to avoid contamination of the sample while measuring the actual depth.

The formation of microholes using FIB milling was done in two stages. The first stage was to identify the suitable value of beam current to be used in FIB milling. In order to do so, several microholes were milled with different values of beam currents and a constant initial depth. A beam current which formed the most accurate shape and dimension for the aperture hole will be selected as a constant value in FIB milling. The

second stage was to investigate the actual depth of holes obtained after milling by FIB. Several microholes were milled from a range of initial depths at a constant beam current, which was selected in the previous stage. Further etching using the TMAH solution was also conducted to investigate the ability of TMAH in eliminating re-deposition and enhancing the depth of microholes. The details for each stage are described in the following sections.

3.4.1 Selection on Beam Current for FIB Direct Milling

The shape and dimension of microholes milled by FIB are dependent on the beam current used during milling. Thus, a suitable value of beam current needs to be selected to form microholes with the most precise dimension and aperture hole shape according to the designed pattern. Various values of beam currents, ranging from 50pA to 4nA were used in order to identify the suitable value of beam current to be used for the FIB milling on silicon. One specific value of beam current was used to form a single hole. Grid lines were used to locate the pattern accurately on the same line, and a constant initial depth of each hole was set as 5µm. The details of parameters used are as shown in Table 3.3.

Table 3.3: Parameters used to mill microholes with different values of beam currents.

Parameter	**Value**
Acceleration voltage	30keV
Aperture size	120µm
Sputter yield of silicon	2.6 atom/ion
Width	2µmx2µm
Depth	5µm
Beam current	50pA, 100pA, 200pA, 500pA, 1nA, 2nA, 4nA

3.4.2 Mill with Different Initial Depth Setting, D_i

In the FIB milling process, the actual depth obtained is dependent upon the initial depth setting and influenced by the re-deposition effect. Thus, a range of values of initial depth were used to investigate the actual depth obtained after milling by FIB. Microholes milled with different initial depth settings were formed by selecting D_i values in a range from 10µm to 100µm. The initial depth, D_i was selected using the FIB software. The value of the exact depth (final depth, D_f) is expected to be as same as the value of D_i, or otherwise, the ratio of the value differences between both depths is known. A constant beam current was selected from the previous experiment, to be used as the fixed parameter. Milling time and dwell time were also investigated during the milling process. The details of parameters used as shown in Table 3.4.

Table 3.4: Parameters used to mill microholes with different values of initial depths.

Parameter	**Value**
Acceleration voltage	30keV
Aperture size	120µm
Sputter yield of silicon	2.6 atom/ion
Width	2µmx2µm
Beam current	*Selected from the experiment 3.4.1
Initial depth, D_i	10µm,20µm,30µm,40µm,50µm,60µm, 70µm,80µm,90µm,100µm

3.4.3 Enhancement of Hole Depth using TMAH Etching

The re-deposition effect is a main limitation in FIB direct milling. The actual depth after milled by FIB is expected to be less than initial depth setting, D_i. Thus, TMAH etching is applied after FIB direct milling to investigate the reaction of TMAH to the holes in terms of eliminating re-deposition and increasing the depth of holes. TMAH or tetramethyl ammonium hydroxide is an anisotropic etching solution that is able to penetrate silicon based on the pattern of the mask and the orientation of silicon. Ga^+ ions implanted on the surface of silicon during FIB direct milling acts as a mask for

TMAH etching. The formation of pyramidal hillocks is expected for {100}-oriented silicon.

For this experiment, two holes with dimensions (width x initial depth setting, D_i) of 2µmx10µm and 2µmx20µm were fabricated on two Si substrates by FIB direct milling. The beam current used was 500pA and acceleration voltage was 30keV. Both samples with their actual depths measured, were then immersed in 25% aqueous TMAH solution at 85°C, as successfully applied by Sievilä et al. (2010). Sample A was immersed for 10 mins and 100 mins for sample B so that the ratio of depth enhancement can be compared. The etch rate of the (100) Si crystal plane orientation was about 0.6µm/min (Sievilä, et al., 2010). The FIB cross-sectioned method was used to measure the depths of the holes. Table 3.5 shows the experimental parameters for TMAH etching.

Table 3.5: The experimental parameters for TMAH etching.

Sample	Initial Depth setting, D_i of FIB milling	Actual depth of holes after FIB milling	Concentration of TMAH etching, (%)	Temperature of TMAH solution, (°C)	Time of immersion, (min)
A	10µm	1.5µm	25	85	10
B	20µm	8.0µm	25	85	100

3.5 Microfilling using Nickel Nanopowder

Nickel nanopowder with an average particle size <70nm was used in this study, as depicted in Fig 3.3. Fig. 3.7 shows the flow of the microfilling process. Microfilling procedures were carried out in a glove box with a vacuum system to prevent contamination of the substrate and oxidization of the nickel nanopowder. For the filling process, ultrasonic dispersion and magnetic assembly techniques were applied to achieve complete filling. Then, the sample was annealed at high temperatures using a

high temperature furnace to form a strong bonding between nickel and silicon at the wall of microholes.

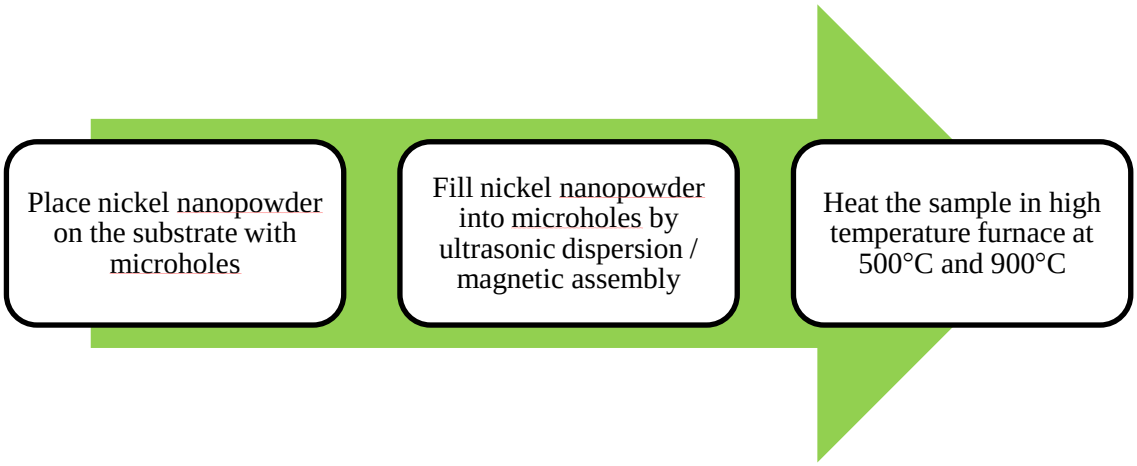

Fig. 3.7: Flow process of microfilling using nickel nanopowder

3.5.1 Filling Performance of Magnetic Assembly and Ultrasonic Dispersion Techniques

The investigation of the quality of filling structure was done to compare the effectiveness of two methods: ultrasonic dispersion and magnetic assembly. The ultrasonic dispersion technique is able to disperse nickel nanopowder on the silicon surface, in order to fill nickel nanopowder into the microholes. On the other hand, the magnetic assembly technique uses magnetic force to attract the ferromagnetic nickel nanopowder into the holes and increase the possibility of filling.

First, two samples of the Si substrate with micro holes of dimensions 2µmx17µm, sample A and sample B were cleaned in hydrofluoric acid (HF) solution (1:10) for 15s to remove the native oxide layer on the Si surface and hole walls. An excess amount of the nickel nanopowder was randomly placed on the top side of both substrates, as shown in Fig. 3.8. Then, sample A was placed on an inverted petri dish. The petri dish was then placed in the middle of two blocks. A small permanent magnet

bar (diameter: 2cm, thickness:1cm) with a magnetic field of 0.01T was placed under the petri dish as shown in the schematic diagram illustrated in Fig. 3.9. The magnetic field is measured using a Teslameter. The permanent magnet was oscillated laterally for 10 sec. This oscillating magnetic field served to align the nanopowder on the substrate, and transfer the nanopowder into the holes.

For the ultrasonic dispersion method, sample B was placed on a petri dish and floated on the water of the ultrasonic bath cleaner. By using ultrasonic vibration of 40 kHz, the dispersion process was carried out for 2 minutes to disperse the nanopowder and fill them into the microholes, as shown in Fig. 3.10. After the filling process, both samples A and B were annealed at 500°C for 30 mins. The annealing process was carried out in a high temperature furnace under vacuum conditions (-0.1MPa). The temperature of 500°C is the lowest temperature required to create Ni-Si bonding at 30 mins, according to Weber et al. (2006). Finally, both samples were analysed using the FIB cross-section technique to investigate the nickel filling structure.

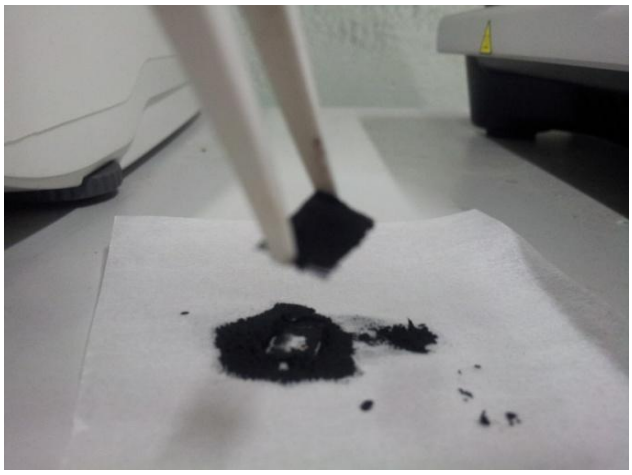

Fig. 3.8: An excess amount of Ni nanopowder was randomly placed on the top side of the substrate.

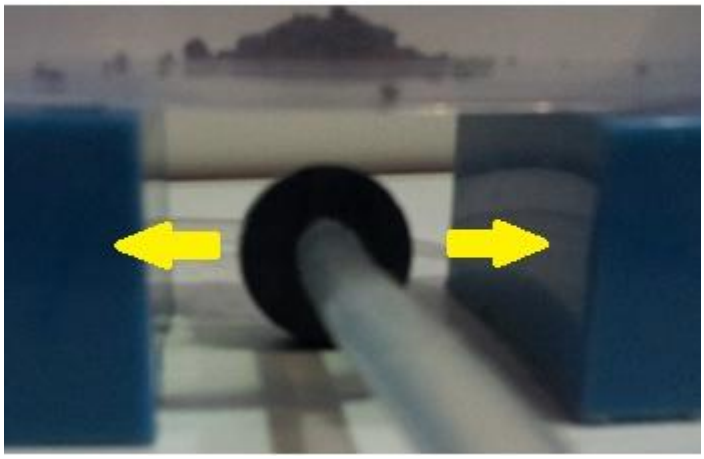

Fig. 3.9: A permanent magnet was placed under the substrate and moved laterally to attract Ni nanopowder into the holes

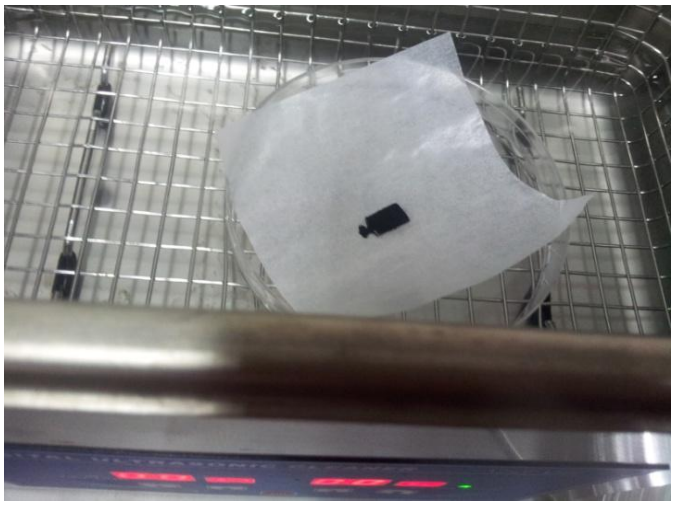

Fig. 3.10: The dispersion process using ultrasonic vibration in the ultrasonic bath cleaner.

3.5.2 Annealing Temperature Effects (500°C and 900°C)

Variation in annealing temperature was investigated in order to analyse the bonding between nickel and silicon. When nickel and silicon are annealed at high temperatures, Ni-Si bonding is formed with various phases. This experiment was conducted after the analysis of the nickel filling structure was formed using magnetic assembly and ultrasonic dispersion methods. The magnetic assembly technique was

chosen as a suitable method to fill nickel nanopowder into high aspect ratio holes, due to the ferromagnetic properties of nickel and ease of handling using this method.

In this experiment, two Si substrates, sample C and D, with 2µmx17µm of holes were cleaned in hydrofluoric acid (HF) solution and filled with nickel nanopowder by the magnetic assembly method, as explained in Section 3.5.1 above. Then, both samples were annealed at different temperatures; 500°C for sample C and 900°C for sample D. These two values of temperatures were chosen as the minimum and maximum temperatures needed to create Ni-Si bonding according to Weber et al. (2006). The duration of annealing process is 30 mins and the full annealing cycle for both temperatures is shown in Fig. 3.11.

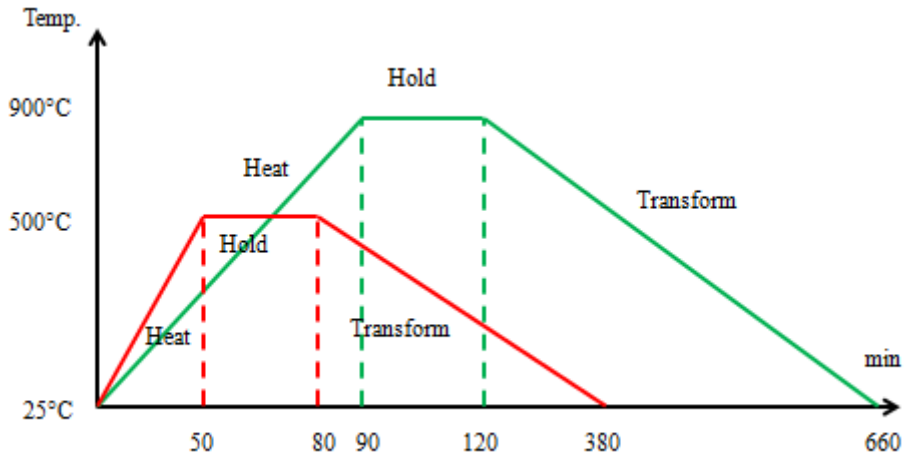

Fig. 3.11: Full annealing cycle for temperature 500°C and 900°C

3.6 Characterization of High Aspect Ratio Microholes and Filling of Nickel Nanopowder

Experimental characterization methods were used to study the structure in two stages;

(1) The quality of high aspect ratio micro holes structure after FIB milling, including the aspect ratio and the formation of defects (re-deposition and amorphisation)

(2) The filling of nickel nanopowder after the annealing process, including compaction of filling, presence of defects (voids and bubbles), Ni-Si bonding and phases, and percentage of elements in the filling structure.

The characterization techniques included both microscopic and spectroscopic methods, such as Scanning Electron Microscopy (SEM) and FIB cross section technique (FIB-SEM system), and also X-ray Diffraction (XRD). For the composition of filling, an Energy Dispersive X-Ray Spectroscopy (EDS) is used. In the proceeding sections, the characterization techniques utilized in this thesis are presented in detail.

3.6.1 Morphology Analysis using SEM and FIB Cross Section Technique

Scanning Electron Microscopy (SEM) and FIB cross section technique/ slice and view technique (Bushby, et al., 2011) are applied to investigate the structure of holes after:

1. Milling with various beam currents at a constant initial depth of 5µm
2. Milling with different initial depths at a constant beam current of 500pA
3. Etching with TMAH solution after FIB milling

Morphology analysis was also conducted to investigate the defects after:

1. Filling with nickel nanopowder using magnetic assembly and annealing at 500°C
2. Filling with nickel nanopowder using the ultrasonic dispersion method and annealing at 500°C

3. Annealing the nickel filling at 500°C and 900°C after filling using the magnetic assembly technique.

SEM was used in this research work for high magnification imaging of high aspect ratio microholes and filling structures. A combination system of FIB/SEM was employed to determine width, depth and shape of the milled cuts. By using the FIB cross section method, the hole structures were cross sectioned by FIB milling by tilting the beam at a tilt angle of 54°. A fine trapezium milling shape with beam currents ranging from 4nA to 500pA was used for precise cutting, as shown in Fig. 3.12. The micrographs of SEM were taken in a magnification range of 2000 and 4000 times, as shown in Fig. 3.13. This combination system can avoid contamination, save time and is able to monitor the cross section process accordingly.

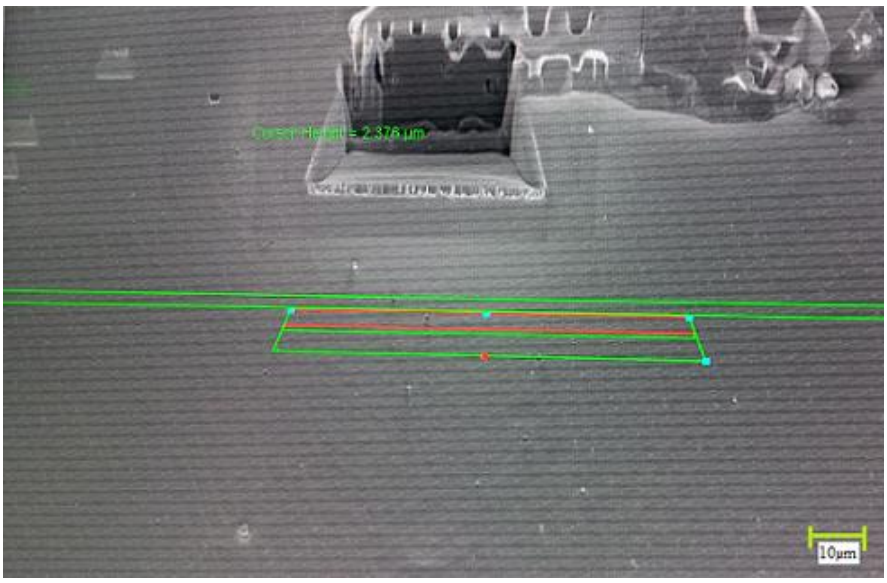

Fig. 3.12: A fine trapezium milling shape with beam currents range from 4nA to 500pA was used for cross section milling.

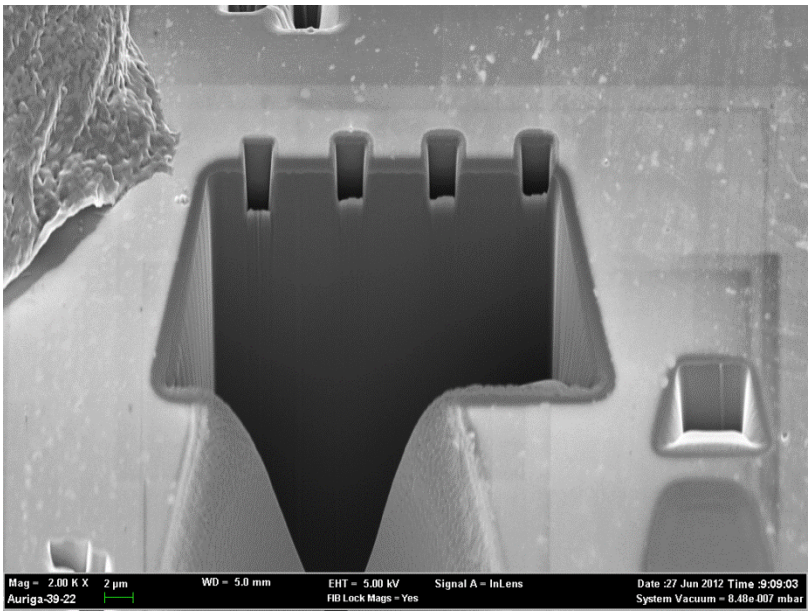

Fig. 3.13: The SEM micrograph of the cross section of holes using FIB at magnification of 2000 times.

3.6.2 Ni-Si Bonding Phases Analysis using XRD

X-Ray Diffraction (XRD) was used to investigate the Ni-Si bonding phases present in the sample and to determine the ageing-induced nickel-silicon phase transformations. This analysis is able to figure out the possibility of compact nickel filling in high aspect ratio microholes. X-rays are energetic enough to penetrate into the material and their wavelengths are of the same order of magnitude as interatomic distances in solids (Bassett & Brown, 1990). Thus, a collimated beam of X-rays is diffracted by the crystalline phases in the sample according to Bragg's Law:

$$n\lambda = 2d \sin\theta \qquad \text{(Eq. 3.1)}$$

where:

λ is the wavelength of the X-rays,

d is the distance between two atomic planes in the crystalline phase,

n is the order of the diffraction, and

θ is the incoming diffraction angle.

The XRD diffractograms presented in this study were recorded on a PANalytical X'pert PRO MRD (Material Research Diffractometer) as shown in Fig 3.14, employing Cu Kα radiation (λ = 1.5406 Å, 45 keV, 40 mA) at 0.020° intervals in the range $5° \leq 2\theta \leq 75°$ with 1s count accumulation per step directly from the silicon substrate. Diffraction patterns were assigned using the PDF database supplied by the International Centre for Diffraction Data (PDF2- Diffraction Database File).

3.6.3 Elemental Analysis of Filling Structure using EDX

The Energy Dispersive X-Ray Spectroscopy (EDX) system is able to supply atomic qualitative and quantitative information from the specimen. It relies on the investigation of a sample through interactions between electromagnetic radiation and matter. Analysis of the x-rays emitted by the sample in response to the bombardment of charged particles provides information of the elements in the sample (Lee, et al., 2004). Each element has a unique atomic structure allowing x-ray to identify and distinguish one element from another. For this work, EDX was used to quantify the percentage of nickel in the filling structure and to determine the percentage of other materials that can possibly form in the filling structure due to the filling process.

In this study, the Oxford Instruments INCA Energy – EDX was used for EDX analysis. The measurement was made at the cross section of microholes to investigate the actual phase growth of nickel on the side walls of the holes. The measurement was taken in a low electron image from SEM. Qualitative analysis is achieved through identification of the lines in the spectrum, where the line intensities for each element in the sample are recorded and compared against the same elements in calibration standards of known composition. The EDX analysis work for this project was focused

on the composition of nickel and silicon. Other compositions such as gallium and oxygen were also determined, in order to understand their contributions to the Ni-Si bond in the filled microhole structure.

CHAPTER 4 RESULT AND DISCUSSION

4.1 Introduction

In the present section, experimental findings of the formation of high aspect ratio microholes and filling of microholes with nickel nanopowder will be presented. The capability of FIB/SEM system for milling the micro holes with high aspect ratio will be discussed in detail, based on the experimental results. Furthermore, the filling performance of ultrasonic vibration method against the magnetic filling method, for filling the micro holes will be presented.

FIB milling parameters that have a significant impact on the fabrication of micro holes with high aspect ratio are investigated experimentally. Two main parameters, beam current and initial depth setting, D_i were used to obtain the best microholes in terms of aspect ratio, surface roughness and profile of micro holes. The other main parameters such as acceleration voltage and sputter yield are fixed for compatibility with the silicon substrate and the optimization of milling condition with the highest acceleration voltage, 30keV. Finally, the pixel space milling mode is used for comparing the quality of structures and the achievable aspect ratios of each holes milled by FIB.

The effects of using ultrasonic vibration and magnetic assembly for filling of micro holes by nickel nanopowder were investigated. In addition, the bonding between nickel nanopowder and silicon surface was characterized. The investigations and characterization for the mentioned items were conducted by using SEM imaging, FIB cross sectional views and elemental analysis of XRD and EDS.

4.2 Fabrication of Microholes by FIB Milling

A sequence of trials were executed in order to fabricate precise and accurate geometries of microholes with the highest aspect ratio by determining the optimal values of the beam current and the initial depth setting of milling, D_i. The ideal beam current can prevent the destruction of the aperture structure of holes during FIB milling. Furthermore, the initial depth setting, D_i was manipulated to measure the highest aspect ratio achieved by the FIB milling method with the occurrence of re-deposition effect as a major concern.

4.2.1 The Effect of Beam Current on the Holes Structure

In order to study the effect of beam current on the holes structure, seven end profiles of different beam currents were milled. This was achieved using the pixel function in milling the feature, (square shape) as shown in Fig. 4.1(a). The dimensions of square shape used was 2µm x 2µm. Grid lines were used to locate the pattern accurately on the same line, and the initial depth setting was set to 5µm. The resulting structure was analysed using SEM imaging and the FIB cross section technique, to measure the structure of holes and determine the hole depths obtained after milling.

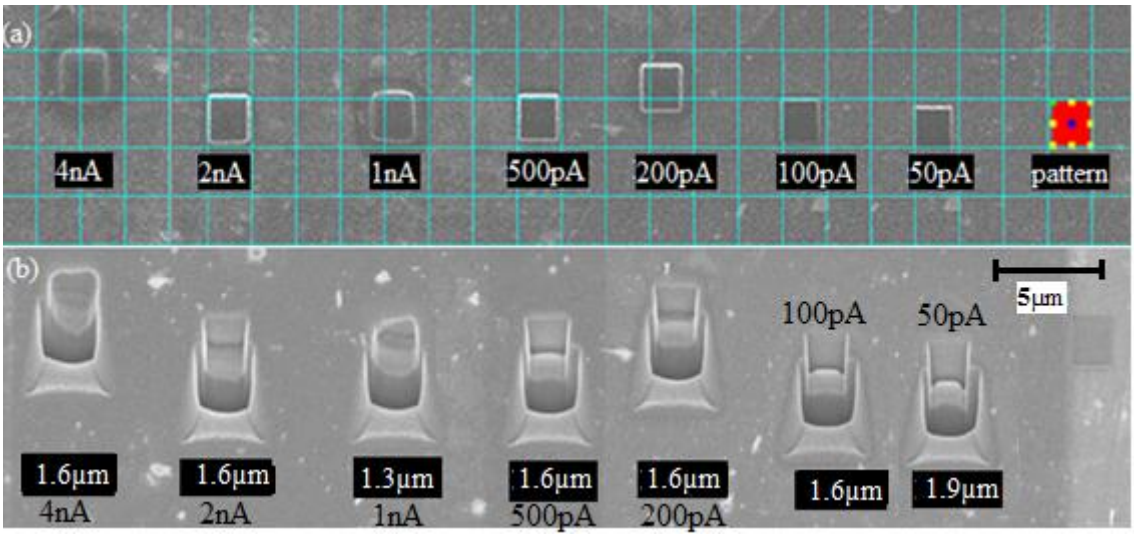

Fig 4.1: (a) SEM image of seven holes milled with various beam currents (50pA to 4nA). The pattern used is square in shape, with grid lines to locate the pattern for FIB milling. (b) Cross sectional view of holes milled with various beam currents.

Fig. 4.1(a) shows that the holes milled with beam current of 4nA, 1nA, and 200pA are out of the target line. This is due to beam deflection error and slight shifting of the sample holder stage caused by vibration during the FIB scanning process (Fu & Ngoi, 2001). The occurrence of vibration is influenced by several factors, including the stability of the working desk and external vibrations from building construction/ renovation. The aperture of these holes has also swelled due to amorphisation. For a crystallised Si substrate bombarded by Ga^+ ions, the dose level to cause amorphisation is of the order of 10^{15} ions/cm^2, whilst the effective milling dose should be at least two orders of magnitude higher than amorphisation dose. Fu & Bryan (2005) also stated that the critical value of the beginning of "net material removal" can be measured occurring at $3x10^{16}$ ions/cm^2, which is above the amorphisation dose.

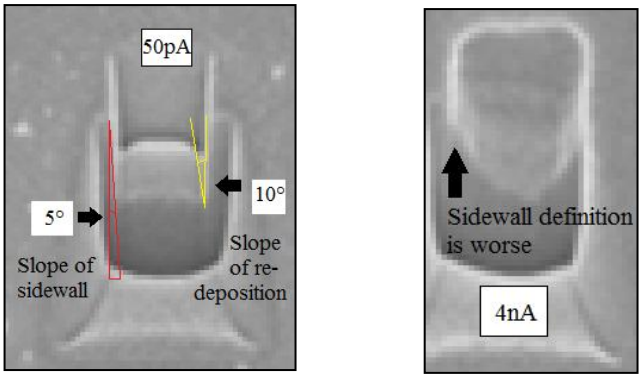

(a) (b)

Fig. 4.2: (a) Hole milled with 50pA, the slope of sidewall is 5°. (b) Hole milled with 4nA, the sidewall definition is worse.

From the cross sectional view in Fig 4.1(b), it can be seen that the slope of the sidewall increased at the holes milled with a lower beam current. For example, the hole milled with beam current 50pA had a slope of sidewall of 5° as shown in Fig. 4.2(a). For a higher beam current, the sidewall definition was worse, such as the structure of hole milled with beam current 4nA, as shown in Fig. 4.2(b). This phenomenon is due to the re-deposition effect. The higher the primary beam current, the faster the material can be sputtered from the Si surface (Fu & Ngoi, 2001). Therefore, the re-deposition effect increases and destructs the structure of holes. Furthermore, as the beam current decreased, the width of the tapered wall became smaller due to sputtered Si re-deposited at the sidewall, but a smooth surface was obtained, as shown by the SEM image in Fig. 4.1.

Table 4.1: The milling time, average width, depth and the aspect ratio of holes milled with various values of beam currents.

Beam Current	Milling time (s)	Upper width (μm)	Bottom width (μm)	Average width (μm)	Depth(f) (μm)	Aspect ratio
4nA	5.3	2.0	1.5	1.8	1.6	0.9
2nA	10.5	2.3	1.9	2.1	1.6	0.8
1nA	21.0	2.0	1.9	1.9	1.3	0.7
500pA	42.1	2.1	2.0	2.1	1.6	0.8
200pA	105.0	2.0	1.8	1.9	1.6	0.8
100pA	210.0	2.0	1.9	1.9	1.6	0.8
50pA	420.0	1.9	1.5	1.7	1.9	1.1

In Table 4.1, milling time is increased with decreasing beam current. A long milling time of 420s per hole was needed by using the lowest beam current 50pA, with the average width of 1.7μm and highest depth of 1.9μm. Low beam current has a low sputtering rate that can cause a longer time required to complete the milling process of a hole, especially for high aspect ratio structures (Adams, et al., 2003). Fig. 4.3 shows the milling time increased proportionally to the beam current. The higher beam current sputtered Si at a higher sputtering rate and reduced the milling time needed. Furthermore, Table 4.1 shows the aspect ratio of micro holes is 1:1 with lowest beam current 50pA. A low beam current reduces destruction on the sidewall, suppresses the surface relief significantly and improves the quality of the hole structure.

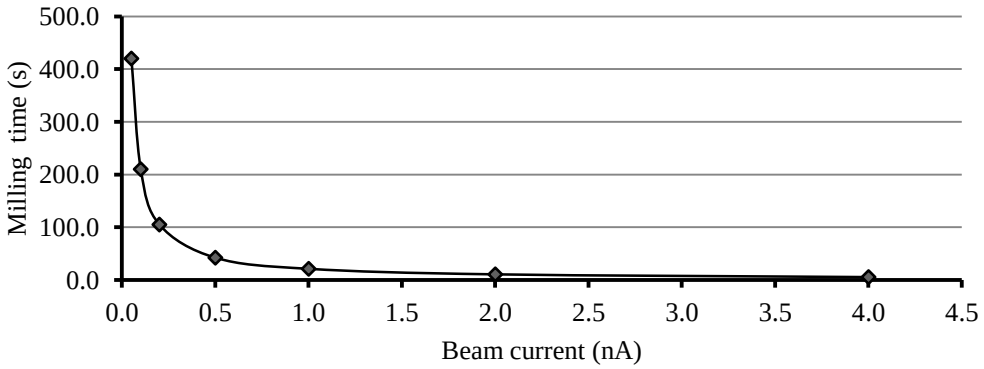

Fig. 4.3: Milling time of holes milled with different beam currents.

Based on Table 4.1, Fig. 4.1 and Fig.4.3, holes milled with beam currents of 500pA shows the most precise hole structure compared to the other holes. The aperture of this hole is not swollen which is a result of amorphisation, and has less re-deposition effect. The milling time is 42.1s per hole with dimensions of the upper and bottom widths are close to 2µm. A beam current of 500pA was chosen to be the constant value for milling process with different initial depth setting, D_i as it was able to provide short milling time and aspect ratio close to 1, with almost precise width.

4.2.2 The Effect of Initial Milling Depth Setting, D_i on Aspect Ratio of Microholes

Various values of initial milling depth setting, D_i were used to mill microholes in order to determine the actual depths and the aspect ratio of the holes. The microholes milled retained the dimensions of 2µmx2µm. A beam current of 500pA was used as a constant parameter due to the best structure formed at this value in the previous experiment.

Each hole was milled with different values of initial milling depth, ranging from 10µm to 100µm, and the total holes milled were 10. The values of dwell time and milling time are measured automatically in the FIB system, and were displayed automatically each time the initial milling depth was set at a certain value. After the

milling process, the holes were cross-sectioned to determine the actual depth and the aspect ratio was calculated. Table 4.2 shows the results obtained with different values of initial milling depth setting, D_i.

Table 4.2: Results of experiment using different values of initial milling depth setting, D_i

Initial Mill Depth, D_i (µm)	**Dwell time (s)**	**Mill time (s)**	**Average width, W_f (µm)**	**Actual Depth, D_f (µm)**	**Aspect ratio**
10	0.1	85	2.0	1.4	0.7
20	0.1	168	2.0	7.8	3.9
30	0.2	254	2.2	8.9	4.0
40	0.3	339	2.3	11.3	4.9
50	0.3	419	2.1	13.5	6.4
60	0.4	503	2.2	14.0	6.4
70	0.5	587	2.2	15.0	6.8
80	0.6	671	2.2	15.2	6.9
90	0.6	754	2.2	15.9	7.2
100	0.7	838	2.2	17.5	8.0

From Table 4.2, the dwell time and the milling time increased with increase in the initial milling depth, D_i. As discussed in detail in the previous chapter, both dwell time and milling time are the secondary parameters in FIB milling. Long dwell time and milling time lead to a deep milling depth due to slow single scans during the FIB milling process. In slow single scans, the ion beams needed to stop at each pixel for a long duration during line by line scanning in order to increase the milling depth (Ali, et al., 2010).

The average widths of aperture for each holes ranged from 2µm to 2.3µm (≥2µm), which were bigger than the aperture size in the previous experiment. By increasing the depth of mill, the width of holes also increased or expanded due to a long exposure time to Ga^+ ions which caused the sputtering effect. For the actual depths, the values are increased by increasing the initial milling depth, D_i. However, the values are almost five times less than the value of initial depth (1 to 5), as shown in Fig. 4.4. This

phenomenon proved that the milling depth is dependent on the sputtering yield of the material. By using 30keV of Ga^+, the sputter yield of silicon is 2.6 atoms/ion, which is much lower than the sputter yield of Al (4.4 atom/ion), Cu (11 atom/ion), and Ag (14 atom/ion). Lower sputter yield can cause the formation of re-deposition when the depth of hole exceeds the crater width (aspect ratio >1), and the milling depth became less than expected (Fu & Ngoi, 2001).

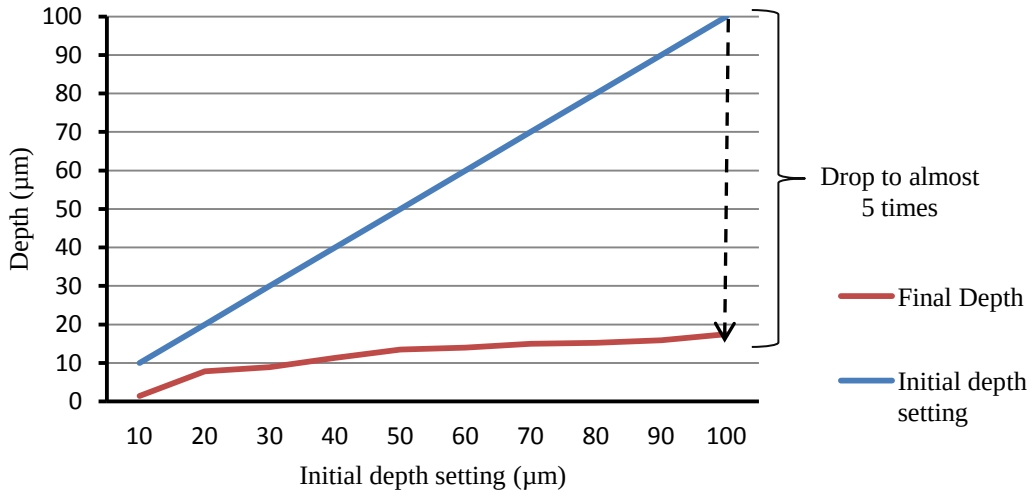

Fig. 4.4: The actual depth, D_f obtained after milling process are almost 5 times less than initial depth setting, D_i due to the re-deposition effect.

Fig. 4.5 shows that the aspect ratio of micro holes increased with increase of the initial milling depth, D_i. The highest aspect ratio of 1:8 was achieved in this milling process by using an initial milling depth of 100µm, as shown in Fig. 4.6. This value of aspect ratio has fulfilled the aim of this research, which is to achieve high aspect ratio for microholes which are higher than 1:5. Thus, a good result of FIB direct milling on the low sputter yield of silicon by using FIB/SEM system has been achieved successfully, without using the gas injection system (GIS).

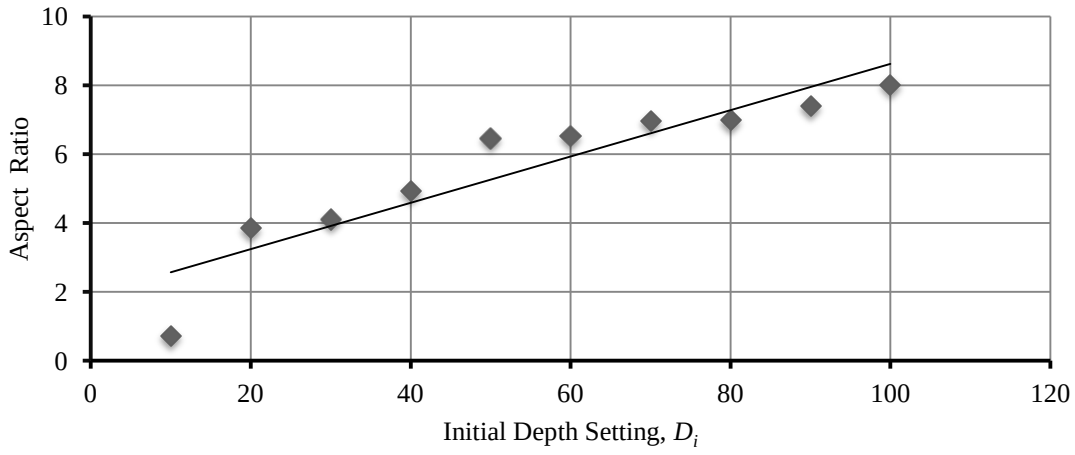

Fig. 4.5: Increased aspect ratio achieved with increase of initial depth setting of milling.

Fig. 4.6: The highest actual depth, D_f of micro holes (17.5µm) by FIB/SEM direct milling.

4.2.3 FIB Milling + TMAH Etching

In order to increase the depth of micro holes and eliminate re-deposition effect, two different depths of holes milled by FIB direct milling, Hole A (1.5µm) and Hole B (8.0µm) are immersed in 25% of Tetramethylammonium hydroxide (TMAH) solution at 85°C. Generally, TMAH solution is stocked in a 25% concentration by Aldrich. By enhanced TMAH concentration, the surface roughness is decreased and smooth surface

can be obtained (Zubel & Kramkowska, 2001). Hole A is immersed for 10 mins, and Hole B for 100 mins. The structure of holes was observed by FIB cross sectional view, done by using FIB/SEM system. Fig. 4.7 shows the structure of Hole A after being immersed in TMAH for 10mins.

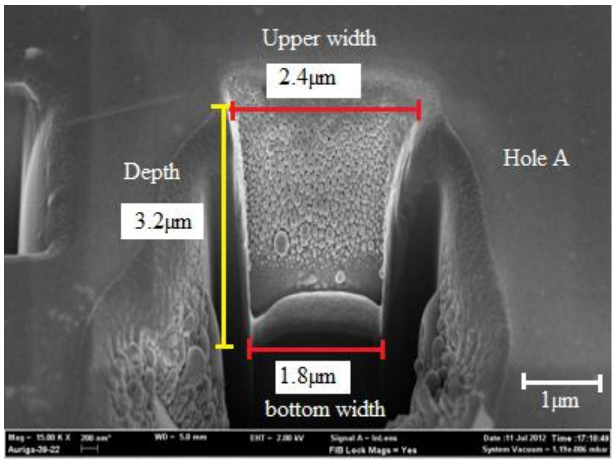

Fig. 4.7: The smaller depth hole's structure after immersed in TMAH for 10mins.

As can be observed in Fig. 4.7, the depth of Hole A was increased from 1.4µm to 3.2µm, due to etch process by TMAH solution. However, small egg-like structures were formed at the side wall of hole, as shown in Fig. 4.8. This kind of surface roughness is formed due to the formation of silicic acid. When silicon substrate immersed into the TMAH solution, the Si atoms reacted with hydroxide ions (OH^-) from TMAH. Then Si substrate started to dissolved slowly and forms a silicon hydroxide or silicic acid, $Si(OH)_4$. The reaction takes place according to Eq. 4.1 (Allongue, 1993):

$$Si + 4OH \rightarrow Si(OH)_4 \qquad \text{(Eq. 4.1)}$$

During TMAH etching process, the hydroxide ion (OH^-) will selectively etch along particular crystallographic planes depending on the wafer orientation, which is (100)-orientation for this research. The TMAH etch reaction is shown in Eq. 4.2 (Bressers, 1995):

$$Si + 4H_2O \rightarrow Si(OH)_4 + 2H_2 \qquad \text{(Eq. 4.2)}$$

According to the Eq. 4.2, the hydroxide ion does not appear definitely. However OH^- is important since it catalyzes the reaction and ensures the solubility of the $Si(OH)_4$ product.

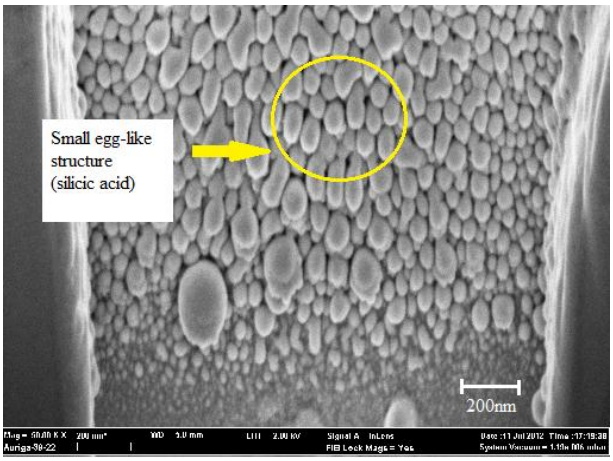

Fig. 4.8: The small egg-like structures of silicic acid form at the side wall of hole.

Another investigation was conducted on the structure of Hole B after being immersed in TMAH solution for 100mins. Fig. 4.9 shows the Si surface after immersion in TMAH solution. The surface area of Si where the holes B were milled was not etch by TMAH solution. This phenomena occurs due to Ga^+ ions implantaion during FIB direct milling. The ion energy of 30keV used in FIB direct milling produces a doped surface layer of Ga^+ ions in silicon with the thickness of 28nm and a standard deviation of 8nm (Sievilä, et al., 2010). Thus, this doped surface layer of Ga is act as a mask surrounding the holes.

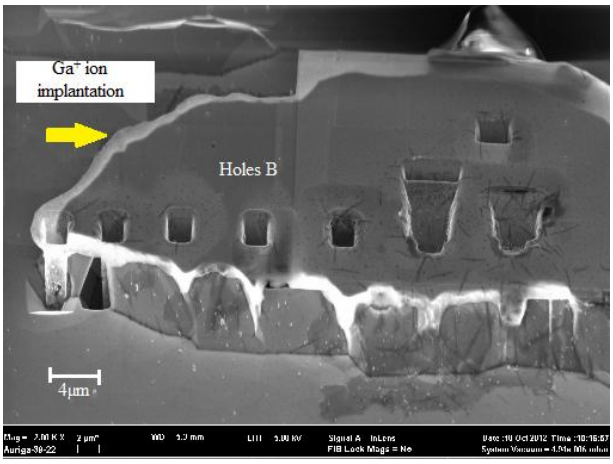

Fig. 4.9: Ga^+ ion implantation surrounding the holes B that prevent from TMAH etching for 100mins.

Holes B were cross sectioned to investigate the holes structure and measure the in depths. From Fig. 4.10, the depths of holes measured are ranging from 11.7µm to 16.6µm. This represent nearly two times increased of depth from 8.0µm, due to the etching by TMAH. However, the re-deposited Si at the bottom of the holes is not etched completely. This is due to the high concentration of TMAH solution that decreased the etch rate, thus a long time is needed to remove re-deposited Si completely (Miney, et al., 2003).

Moreover, the wall structure of holes is definitely not being etched by TMAH solution. The reason is that Ga^+ ion implantation occurred at the wall of holes, which has prevent the etch process at this area. Another interesting phenomenon is a pyramidal hillocks structure occurs beside the holes wall, which is the TMAH etching pattern of (100) silicon. This indicated that TMAH is also tends to etch Si substrate according to the orientation of Si on the surface that is not implanted with Ga^+ ion (Defforge, et al., 2011).

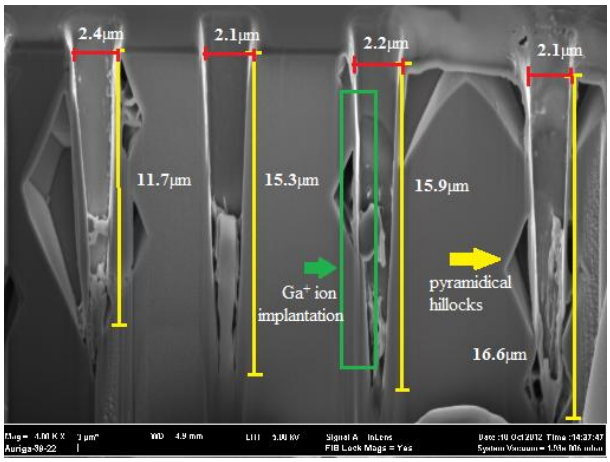

Fig. 4.10: The Holes B structures after immersed in TMAH solution for 100mins.

From Fig. 4.7 and Fig. 4.10, both Hole A and Holes B have enhanced depth almost twice of the depth of FIB direct milling. These are shown in Fig. 4.11, which is the comparison of depth after FIB direct milling and after further etching with TMAH solution. The depth of Hole A increases by 1.8µm and the average depth of Holes B increase by 6.9µm. Therefore the enhancement of depths of Hole A and Holes B is almost two times of previous depths milled by FIB. Based on the depth enhancement of both holes, the etch rate of TMAH is range from 0.07 to 0.18µm/min. The etch rate was below 0.6µm/min that obtained by Sievilä et al. (2010), due to short duration of TMAH etching process. The complete etching process of the {100} Si plane required more than 8 hours (Miney, et al., 2003).

In TMAH etch process, the etch rate depends on the temperature and the etchant composition of TMAH solution, and also on the crystallographic orientation of the surface. The reaction is only involves a chemical reaction, thus the etch rate is not affected by the potential charge of the silicon.

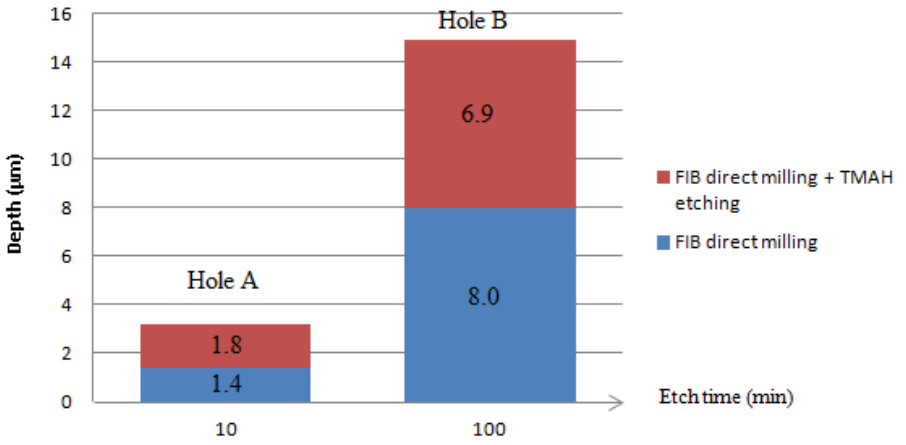

Fig. 4.11: The comparison of depth obtained using FIB direct milling and combination of FIB direct milling with TMAH etching.

4.3 Characteristics on Microfilling Structure of Nickel

Characterization of the nickel filled microstructure on silicon was done by taking images under SEM to evaluate the filling profile and the bonding contact between nickel and silicon substrate. The X-Ray Diffractometer (XRD) and Energy Dispersive Spectroscopy (EDS) are used to analyse the layer of nickel formed after annealing process and the composition of nickel bonded with silicon.

4.3.1 Grain Size Measurement of Nickel Nanopowder

A SEM image of nickel nanopowder was taken to measure the exact grain sizes before filling them into the micro holes. Fig. 4.12 shows the grain size of the nickel nanopowder. The sizes range from 50nm to 400nm, thus the average grain size is >70nm, slightly bigger than the grain size mentioned on the packaging (<70nm). This is due to oxidation formed during preparation for measurement itself, and at the moment of transferring nanopowder onto the surface of Si substrate. Fig 4.13 shows the composition of nickel and oxygen in nickel nanopowder analysed by EDX.

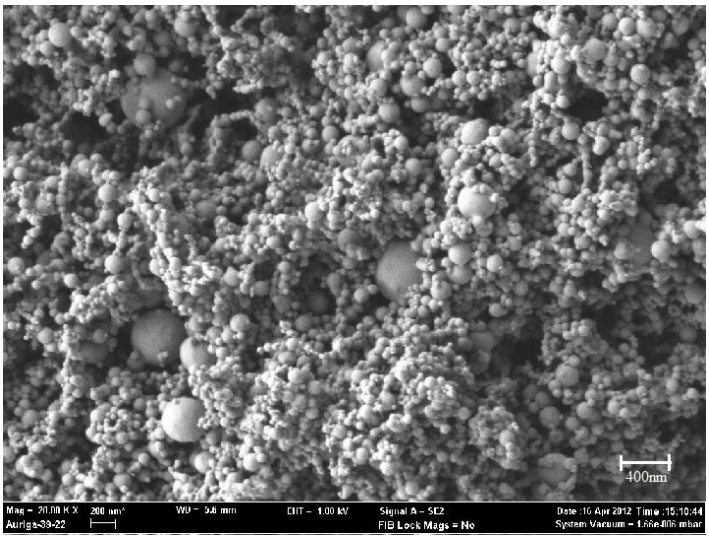

Fig. 4.12: The SEM image of nickel nanopowder. The average grain size is >70nm.

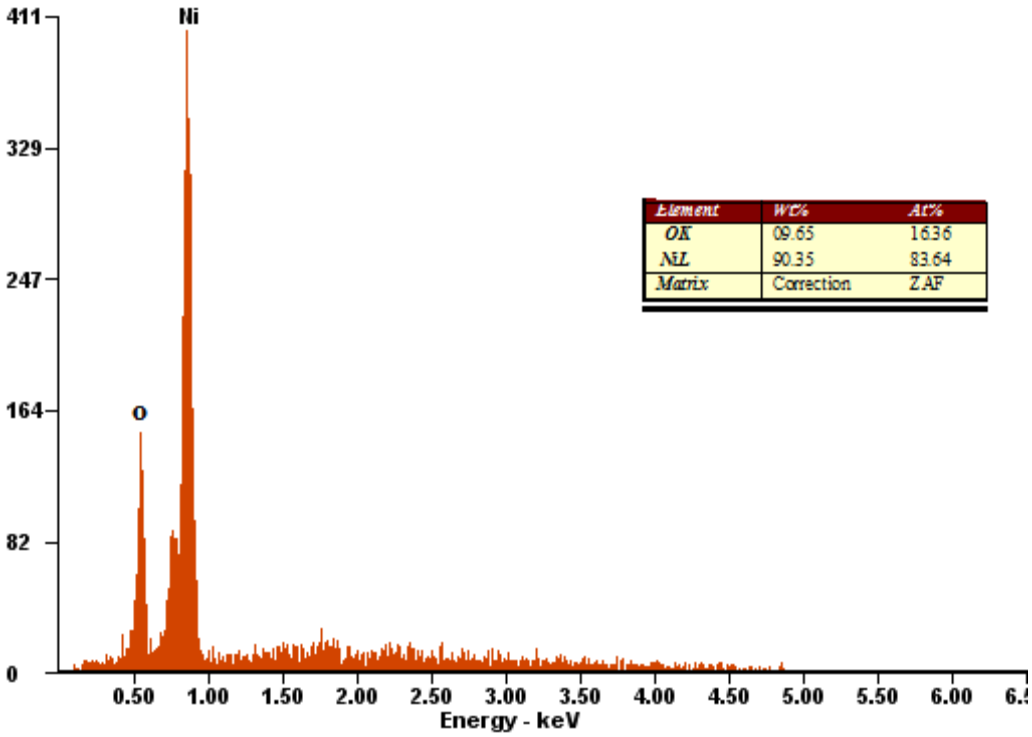

Fig. 4.13: The composition of nickel (90.35%) and oxygen (9.65%) in nickel nanopowder.

4.3.2 Comparison of Filling Methods after Annealing at 500°C

Nickel nanopowder was filled into the micro holes milled by FIB by using two different methods, ultrasonic dispersion and magnetic assembly. Mechanical filling of

high aspect ratio micro holes is difficult, due to very small hole sizes. It is difficult to detect the exact area of holes unless the filling process is done under a very high magnification microscope, which is not available in this research. The quality of filling using these two methods is compared to investigate the efficiency of both methods in microfilling after having been annealed at 500°C.

Fig. 4.14 and Fig. 4.15 show the surface of both samples, A (magnetic assembly) and B (ultrasonic dispersion) after annealing at 500°C for 30mins. The Ga^+ ion implantation from FIB milling process is clearly seen in both figures. Also observed are formations of nickel agglomerations at the surface of silicon substrate. However, the holes for Sample A and B are not fully filled by nickel nanopowder. This is because only a very thin Ni-Si layer is successfully formed. When the annealing temperature is below the melting point of nickel, which is 1455°C, most of the nickel nanoparticles remained in powder form and only a small portion have diffused into silicon or formed a bonding contact with silicon (Murakami, et al., 2003). Thus, the remaining nickel nanopowder which has not reacted was removed during cleaning after the annealing process is done.

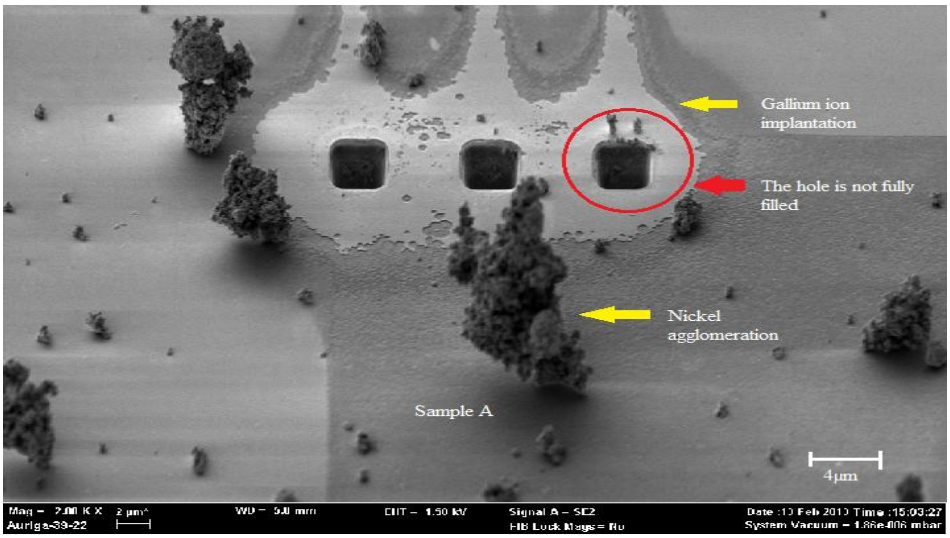

Fig. 4.14: The SEM image of Si surface for Sample A after filling by using magnetic assembly and annealed at 500°C (30mins).

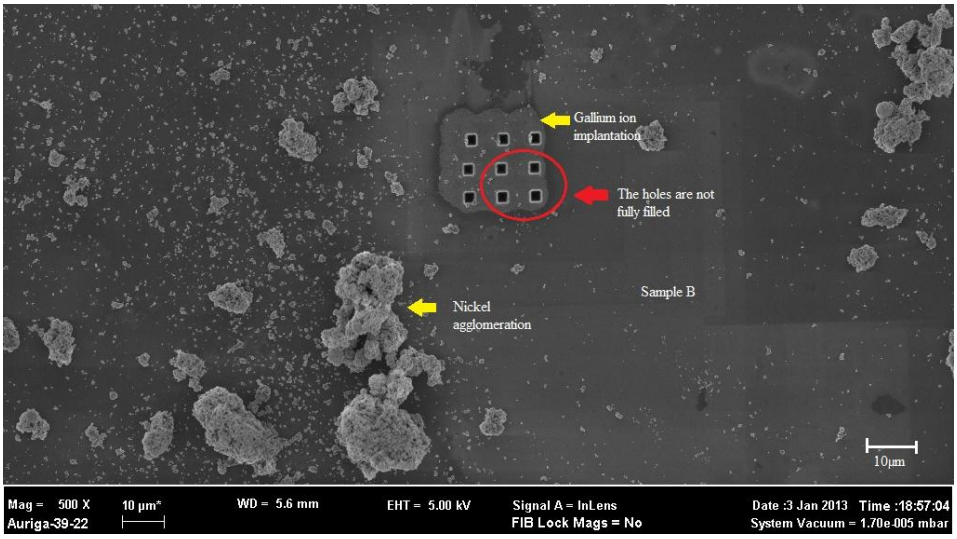

Fig. 4.15: The SEM image of Si surface for Sample B after filling by using ultrasonic dispersion and annealed at 500°C (30mins).

Fig. 4.16(a) and Fig. 4.16(b) show the SEM image of the nickel filling structure for Sample A and Sample B after cross-sectioned using FIB. Both figures show the formation of nickel agglomeration at the sidewall of holes. Agglomeration occurred due to weak thermal stability during the annealing process (Wei, 2005), also the process

impurity caused by oxidation during sample preparation and Ga^{+} ion implantation during FIB cross sectioning process.

There are a few differences in the characteristics of the filling structure inside the holes for Samples A and B. The filling structure of Sample A which was produced by magnetic assembly showed better filling compared to Sample B (ultrasonic dispersion). The nickel agglomeration formed at the entire sidewall of Si although the nickel nanopowder did not completely fill the holes. This happened due to the ferromagnetic characteristics of the nickel nanopowder itself (Fischer, et al., 2012). A permanent magnet at the back side of silicon substrate served as a magnetic field source that was able to assemble the ferromagnetic nickel nanopowder into the area where the microholes were located. The nickel nanopowder remained above the magnet and aligned themselves on the Si surface. Thus, the magnetic force can easily attract the nanopowder into the microholes.

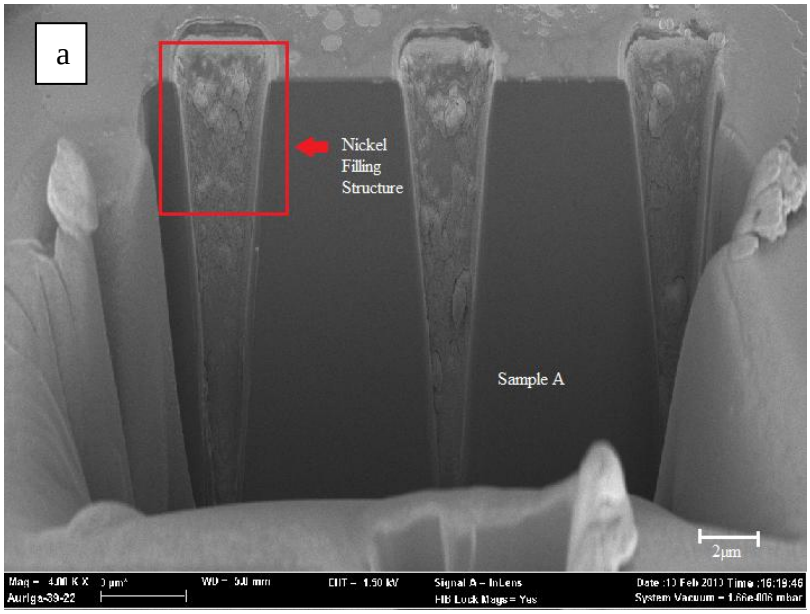

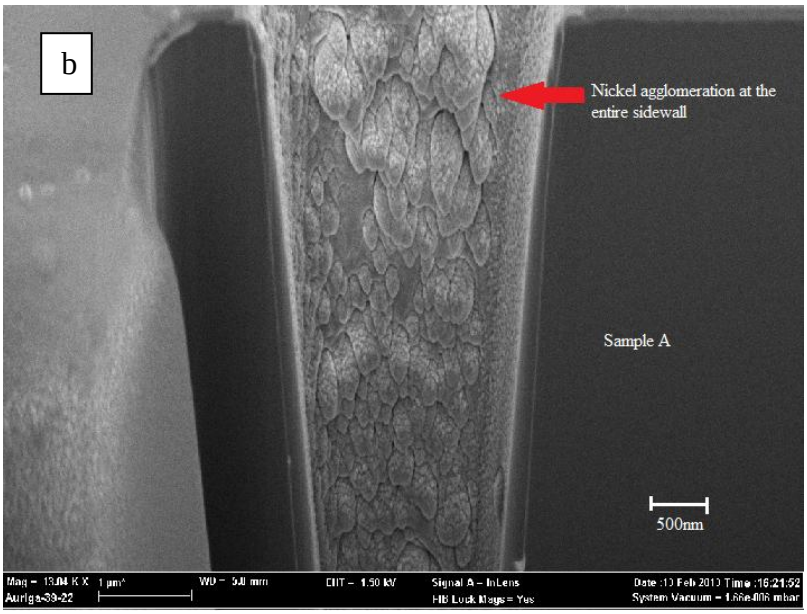

Fig. 4.16: (a) The SEM images of holes for Sample A (magnetic assembly) after cross sectioned by FIB. (b) Nickel agglomeration was formed at the entire sidewall of silicon.

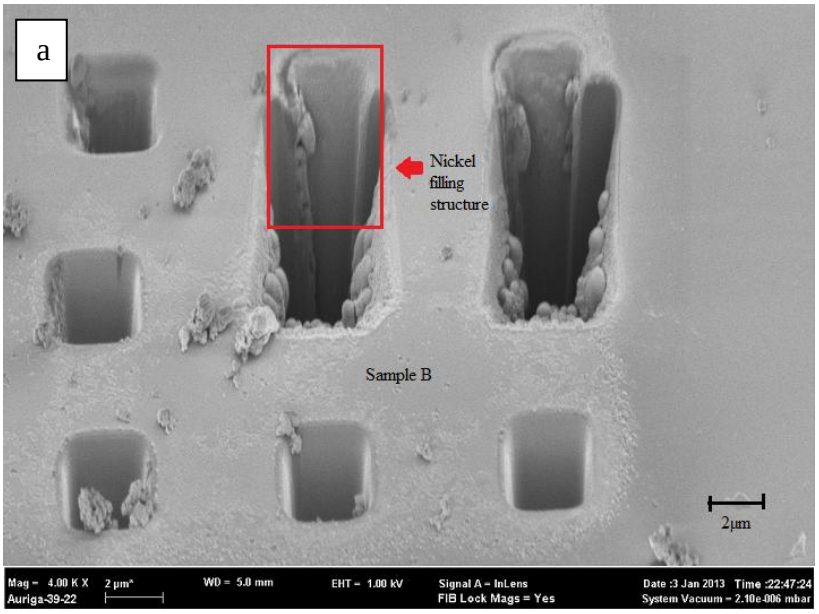

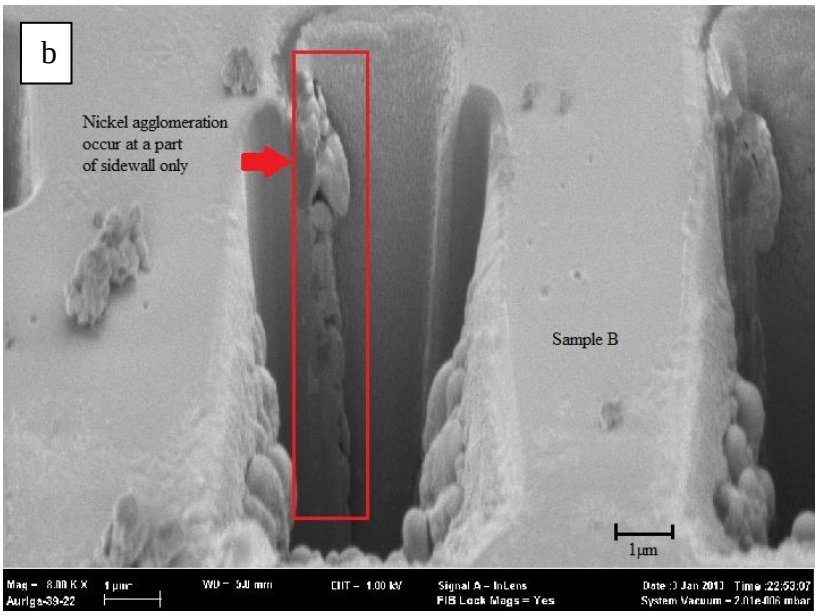

Fig. 4.17: (a) The SEM images of holes for Sample B (ultrasonic dispersion) after cross sectioned by FIB. (b) Nickel agglomeration formed only at a part of the Si sidewall.

The filling structure of Sample B produced by ultrasonic dispersion method has only created a large agglomeration at a part of the side wall. In this study, ultrasonic vibration acted as a dispersion source to disperse the nickel nanopowder on the whole surface. However, the dispersion mechanism cannot force or push the nanopowder to fill into the microholes. Thus, most of the nanoparticles are located on the silicon surface at the time of annealing process. Ultrasonic vibration requires a medium (generally liquid) to disperse the nickel nanopowder uniformly (Manu, et al., 2011). In this case, of no liquid medium was used due to the vacuum state, it is thus difficult to completely fill the nickel nanopowder into the holes.

4.3.3 Annealing at Different Temperatures (500°C and 900°C) after Filling using Magnetic Assembly

The annealing of nickel filling at different temperatures (500°C and 900°C) was studied to compare the existence of Ni-Si bonding between nickel nanopowder and the silicon substrate. Two samples, C and D with holes of dimensions 2µmx17µm were

filled with nickel nanopowder by using the magnetic assembly method, due to their ease of handling and also superior filling properties compared to the ultrasonic dispersion method. Fig. 4.18(a) and (b) show the nickel filling structure after annealing at temperature of 500°C (Sample C) and 900°C (Sample D). The filling structure was formed at the entire sidewall of holes due to the magnetic force applied by magnetic assembly method, during the nickel nanopowder filling process.

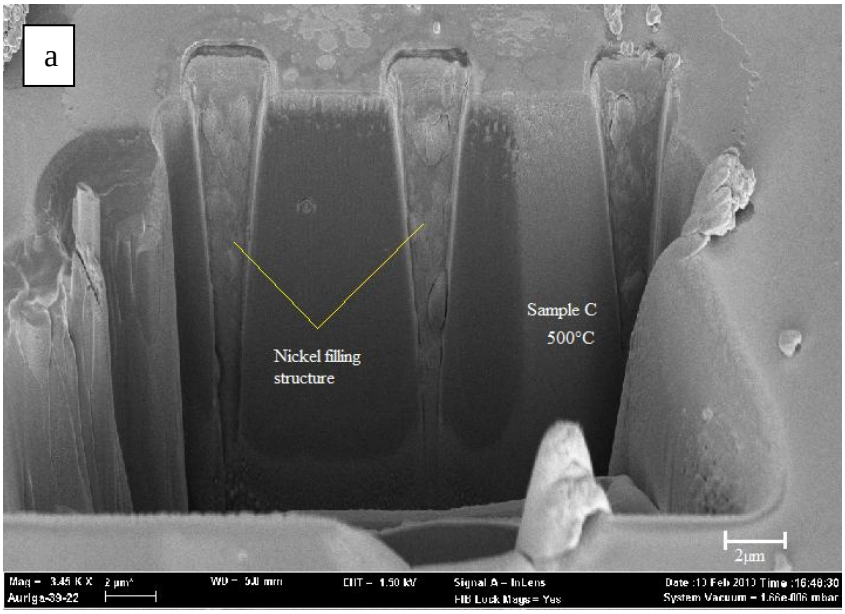

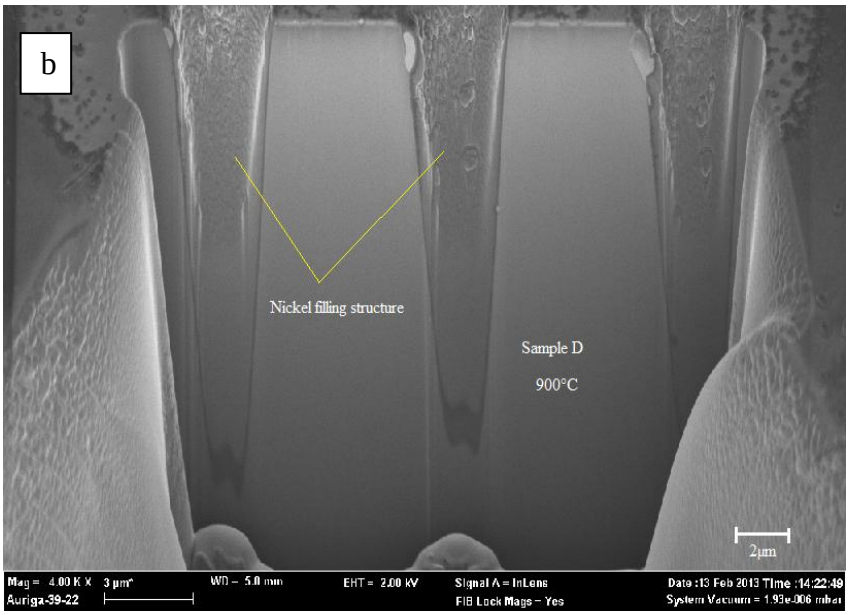

Fig. 4.18: The cross-section of the nickel filled structure for (a) Sample C after annealing at 500°C. (b) Sample D after annealing at 900°C.

In Fig. 4.19(a) Fig. 4.19(b), nickel agglomeration occurred at the sidewall of holes of both samples, C and D. However, the agglomeration can be seen clearly in Sample C that was annealed at a temperature of 500°C. Large agglomerations formed with the presence of voids between these agglomerations. On the other hand, the agglomeration was less for sample D after annealing at 900°C, without any voids formed. This phenomenon is due to the formation of various nickel silicide phases at different temperatures. During the annealing process, a proportion of nickel has diffused into the silicon substrate. The crystalline structure of pure NiSi phase was formed at 500°C, which explained the existence of agglomeration at the sidewall of holes as shown in Fig. 4.19(a). The agglomeration started again at 900°C which formed the crystalline structure of $NiSi_2$, as shown in Fig. 4.19(b). Further analysis using XRD was done to confirm the existence of nickel silicide layer.

There was also a difference in the thickness of the layer formed in both samples. The thickness was taken during SEM imaging process and measured the average of

three different points at the sidewall of the filling structure. In sample C (500°C), the three values taken are 257.0nm, 239.7nm, and 129.6nm. The average thickness of the Ni-Si layer formed is 208.8nm. The three points taken for sample D (900°C) are 466.3nm, 456.5nm and 655.5nm with the average thickness of 526.1nm. At the higher temperature, the thickness of Ni-Si layer was increased to form various types of Ni-Si phases. Thus, more than one type of Ni-Si phases was formed with increasing thickness of the layer at 900°C. The formation of Ni-Si phases can be determined by using XRD analysis.

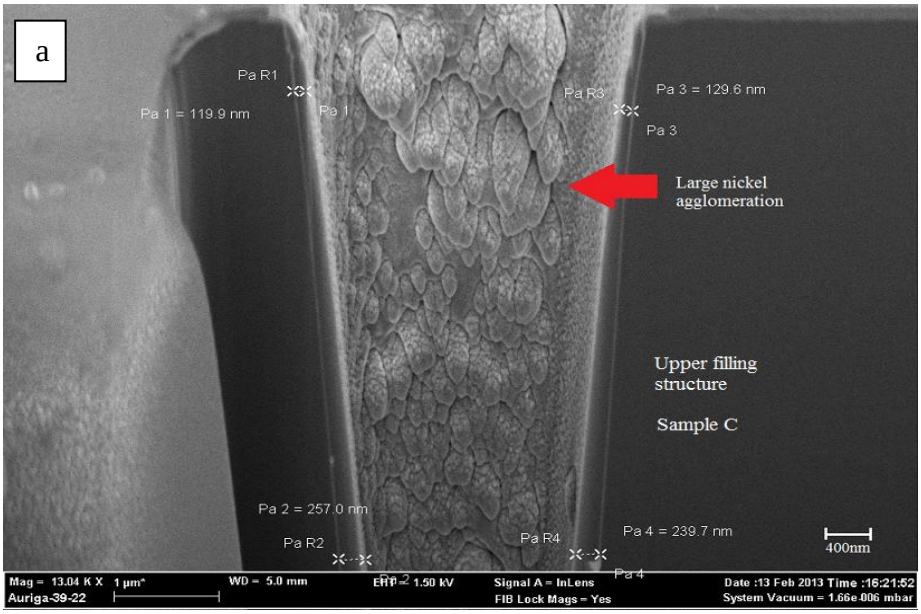

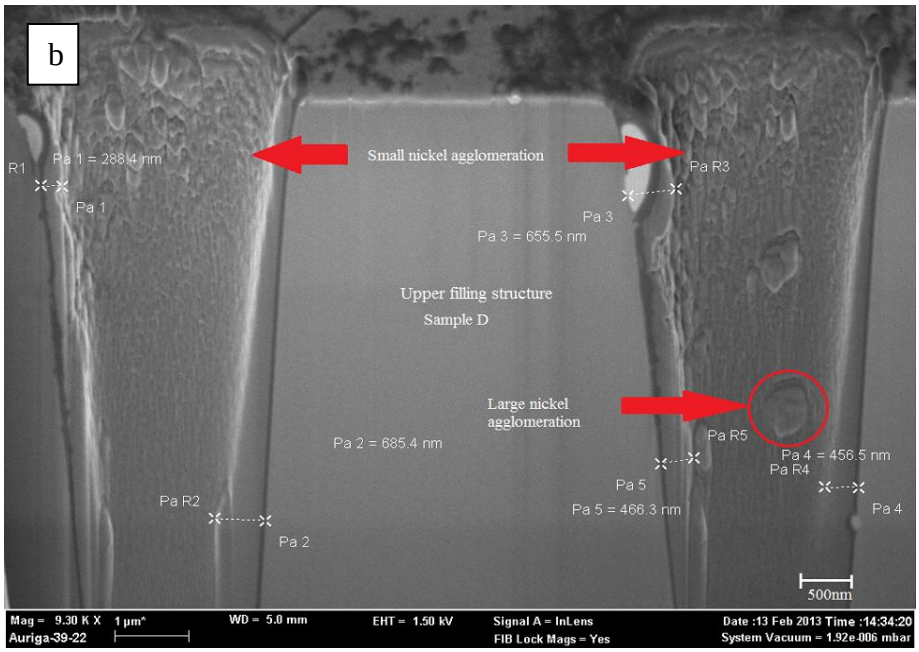

Fig. 4.19: (a) Large agglomerations occurred at the entire sidewall of hole in sample C (500°C). The average thickness is 208.8nm. (b) Small agglomerations formed at the entire sidewall of hole in sample D (900°C). The average thickness is 526.1nm.

Moreover, the SEM images of the filling structure annealed at 500°C (sample C) and 900°C (sample D) are slightly different especially at the bottom of holes, as shown in Fig. 4.20(a) and Fig. 4.20(b). The filling structure at temperature 500°C did not totally adhere on the sidewalls of the holes, as is clearly shown in Fig. 4.20(a). On the other hand, the filling structure at temperature 900°C showed a complete adherence to the sidewall of the holes, with the formation of different contrasts in surface layer can be identified clearly in Fig. 4.20(b). Generally the excess unreacted nickel nanopowder will not diffuse into the silicon substrate (Jang, et al., 1998), which is explained by the existence of voids at the bottom of filling structure annealed at 500°C. Due to the high temperature of 900°C and a narrow bottom of the resulting hole, the nickel nanopowder possessed enough energy to diffuse into Si and form a complete filling structure without incurring any void formation. Thus, an almost complete nickel filling structure was

achieved at the temperature of 900°C with small agglomerations and no presence of voids.

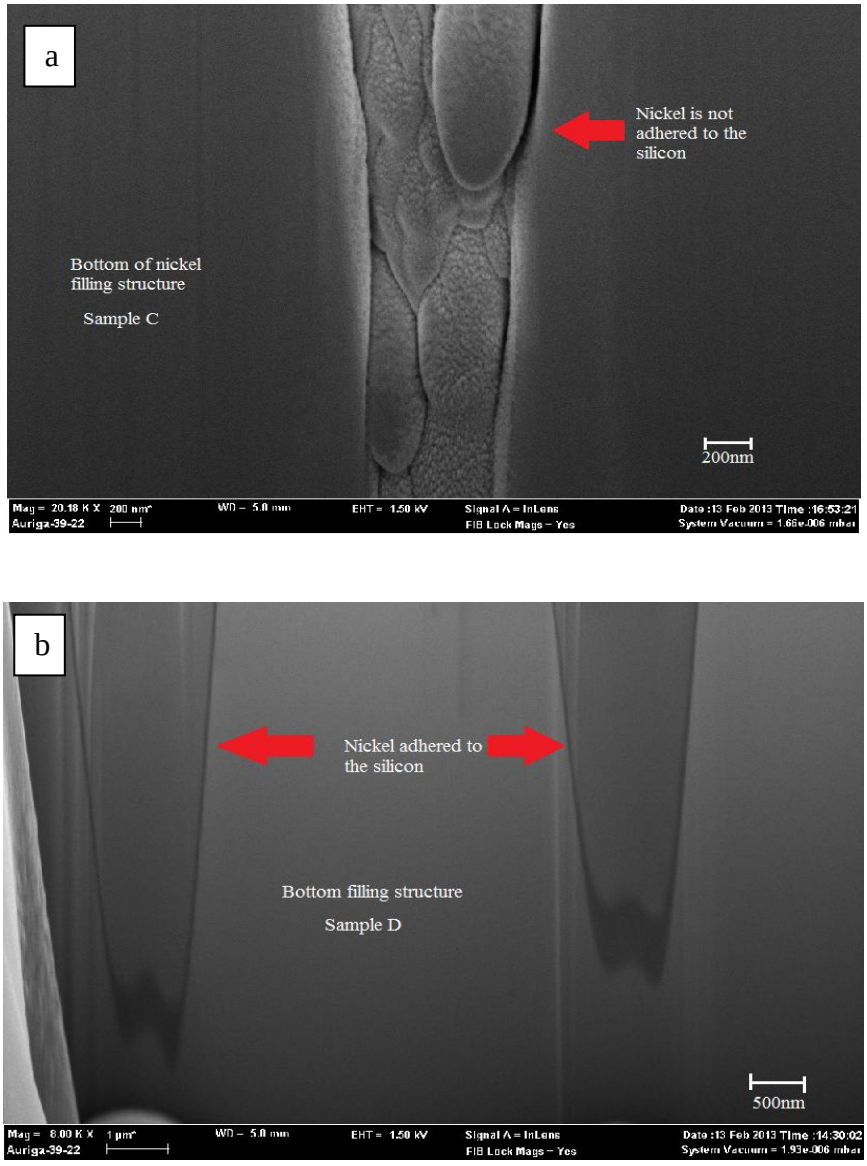

Fig. 4.20: The nickel filling structure at the bottom of hole (a) did not totally adhere to the Si sidewall after annealing at 500°C (sample C), (b) completely adhered to the Si sidewall after annealing at 900°C (sample D).

4.3.4 X-Ray Diffraction (XRD) Analysis on Ni-Si Phase Transformations

X-ray diffraction (XRD) analysis was performed to analyse nickel phases present and determine Ni/Si phase transformations on the nickel filling structure. XRD

analysis was done on the cross section of the filled structure after annealing at 500°C (Sample C) and 900°C (Sample D), as shown in Fig. 4.21(a) and (b).

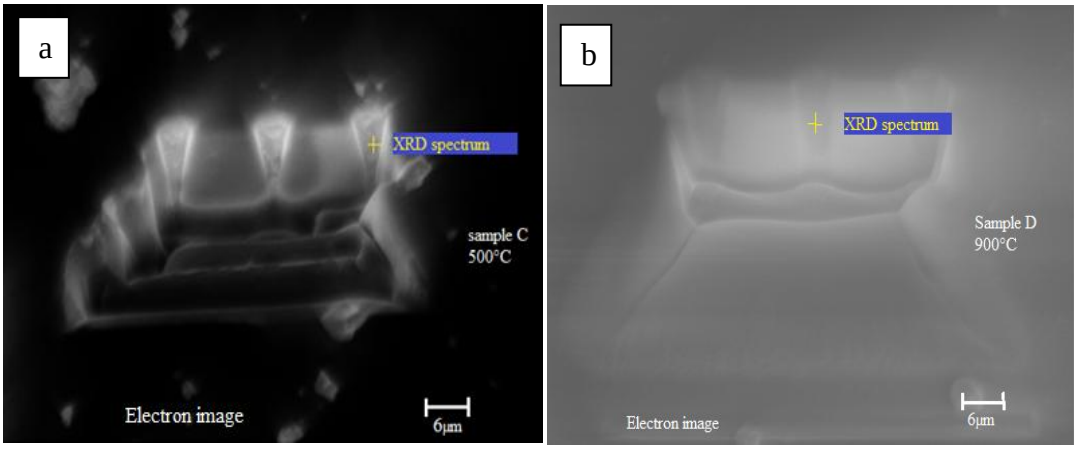

Fig. 4.21: The cross sectional SEM images of the filled structure after annealing at (a)500°C (Sample C) and (b)900°C (Sample D).

The XRD pattern in Fig. 4.22 corresponds to the formation of nickel silicide at temperatures of 500°C and 900°C and annealing time of 30 mins. There are three peaks which appeared at temperature of 500°C, whilst seven peaks appeared at 900°C. The crystalline orientations displayed are: Si (200) with $2\boldsymbol{\theta} \cong 33°$, NiSi (102) with $2\boldsymbol{\theta} \cong 37.2°$, NiSi (112) with $2\boldsymbol{\theta} \cong 43.2°$, NiSi (020) with $2\boldsymbol{\theta} \cong 61.8°$, $NiSi_2$ (400) with $2\boldsymbol{\theta} \cong 66°$, Si (400) with $2\boldsymbol{\theta} \cong 70°$, and NiSi (222) with $2\boldsymbol{\theta} \cong 76.8°$ (dos Santos, et al., 2008). All these peaks corresponded to the strongest reflections in the orthorhombic structures of the nickel silicide phases (NiSi and $NiSi_2$) for both samples, C and D.

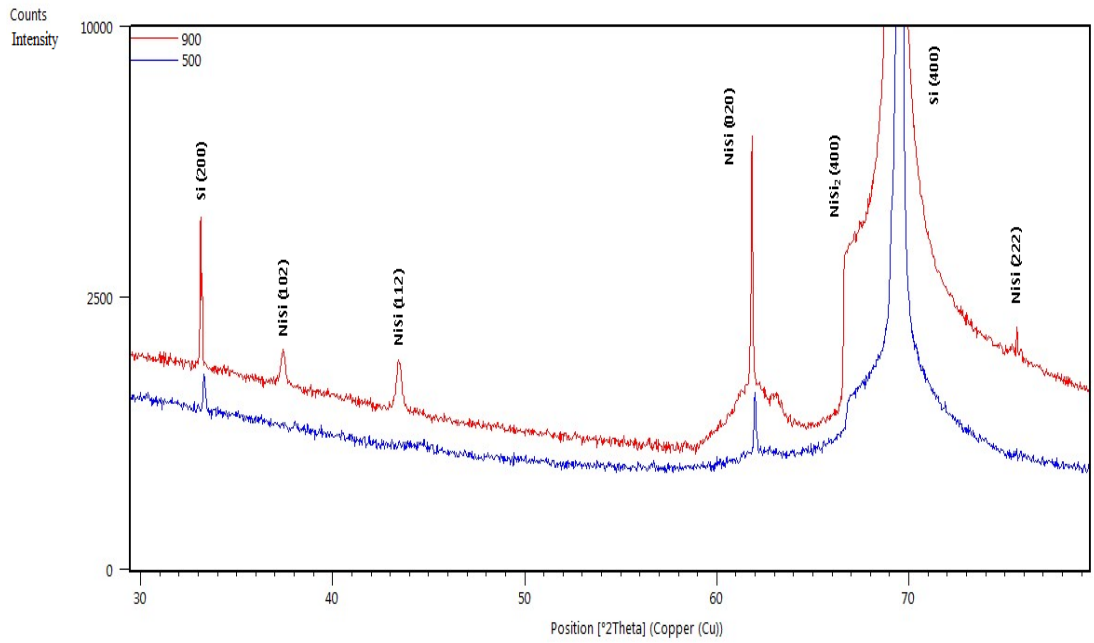

Fig. 4.22: The XRD pattern of Ni-Si phase transformation

At 500°C, only three peaks occurred; Si (200), NiSi (020) and Si (400). The first NiSi crystalline orientation was formed at the position between 40° and 50°. The depicted silicide layer in filling structure exhibited no $NiSi_2$ orientation, only the intensity change with the temperature. There were seven peaks which formed at 900°C; Si (200), NiSi (102), NiSi (112), NiSi (020), NiSi2 (400), Si (400) and NiSi (222). The intensity of NiSi (102) and NiSi (112) increased with increasing temperature. The first $NiSi_2$ crystalline orientation was observed at position 60° and 70° and this silicide layer only formed on the sample D at 900°C.

The first NiSi orientation formed at 500°C (sample C) shows that the NiSi phase is present in sample C. This means that the pure crystalline structure of nickel monosilicide (NiSi) was created in the form of large agglomerations. This also occurred during the formation of the first $NiSi_2$ orientation on sample D at 900°C. The formation of the nickel disilicide ($NiSi_2$) crystalline structure was confirmed by the intensity of $NiSi_2$, agglomeration occurred and the thickness was enhanced after annealing at 900°C.

Moreover, several NiSi intensities occurred at 900°C and these have shown that the NiSi phase is in a stable state. The XRD analysis has proved that nickel silicide phases were formed due to the annealing process, where the bonding of Ni-Si has been achieved successfully.

4.3.5 Elemental Analysis by Energy Dispersive X-Ray Spectroscopy (EDX)

The chemical composition at the sidewall of holes on Sample C (500°C) and Sample D (900°C) were analysed using the EDX measurement. The EDX spectra results are shown in Fig. 4.23 and Fig. 4.24 for annealing temperature of 500°C and 900°C. Both figures revealed that the sidewalls of micro holes are composed of Si and Ni, although the peaks of Ni are small. The small Ni peaks are attributed to the comparatively bigger electron scattering range in the sample, due to higher primary electron energy. The spectra are taken with 5keV primary electron energy to maintain the scattering volume as low as possible (Weber, et al., 2006).

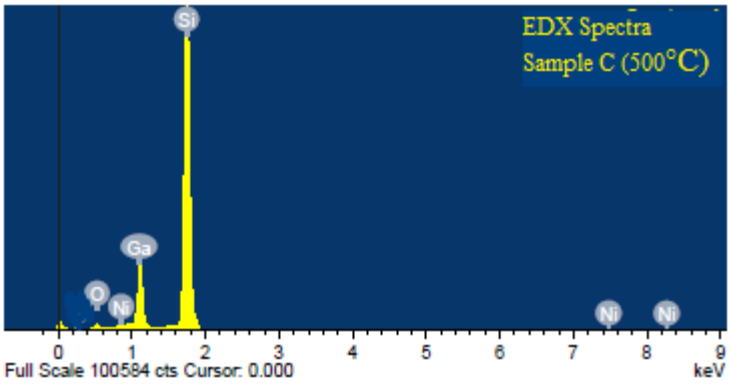

Fig. 4.23: The EDX spectra of nickel filling structure annealed at 500°C (Sample C).

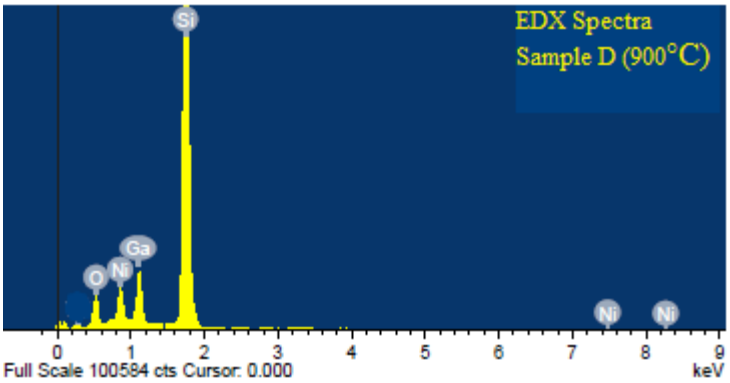

Fig. 4.24: The EDX spectra of nickel filling structure annealed at 900°C (Sample D).

Furthermore, the existence of gallium (Ga) in both figures is indicated by results from the FIB cross section method. During cross section process by FIB, the Ga^+ ions are implanted on the target surface. This means that the sidewall of the holes is coated with a thin gallium layer. Since no oxygen source was supplied to the high temperature furnace during annealing process, it is suggested that oxygen atoms came from the oxidised nickel nanopowder during sample preparation and contributed to the filling of nickel silicide as shown in Fig. 4.2.

Table 4.3: The weight and atomic percent of elements at temperature of 500°C

Element	Weight (%)	Atomic (%)
OK	1.47	2.76
SiK	75.45	80.80
NiL	4.36	8.36
GaL	18.72	8.08
Total	100.00	100.00

Table 4.4: The weight and atomic percent of elements at temperature of 900°C

Element	Weight (%)	Atomic (%)
OK	6.62	11.88
SiK	68.01	69.52
NiL	14.78	14.24
GaL	10.59	4.36
Total	100.00	100.00

From the EDX quantitative analysis, the weight percent and the atomic percent of each element was measured for both temperatures (500°C and 900°C), as shown in Table 4.3 and Table 4.4. In both samples, the composition of nickel was low. For sample C (500°C), the composition of nickel and silicon were 4.36% and 75.45%. However, the composition of nickel was increased after annealing at 900°C for sample D. The composition of nickel was 14.78%, which is only 5 times less than silicon (68.01%). The composition percentage of nickel was low due to the formation of thin layer of nickel silicide. Non-reacted nickel nanopowder was not diffused into silicon during annealing process (Jang, et al., 1998). Thus, the nanopowder has been removed in the cleaning process.

Comparing the composition of nickel in both samples, nickel has higher percentage after annealing at 900°C rather than 500°C. This is due to the formation of two NiSi phases; nickel monosilicide (NiSi) and nickel disilicide ($NiSi_2$). The thickness of filling structure annealed at 900°C was also high, with average thickness of 526.1nm compared to the filling structure of 500°C, which is 208.8nm. At higher temperatures, a thicker filling structure was formed which contained a greater percentage of nickel composition (Nath & Premnath, 2005). Thus, the optimal nickel filled structure with no

voids and contained a high percentage of nickel was achieved at an annealing temperature of 900°C.

\

CHAPTER 5 CONCLUSION

5.1 Conclusion

Nickel nanopowder was used as a metal filling for high aspect ratio micro holes. The focused ion beam (FIB) direct milling method was introduced to fabricate micro holes with aspect ratios of more than 5. Two different filling techniques, magnetic assembly and ultrasonic dispersion were used to fill high aspect ratio micro holes with nickel nanopowder. The quality of micro holes and filling structure were investigated using Scanning Electron Microscopy (SEM) for morphology, X-Ray Diffraction spectroscopy (XRD) for the existence of Ni-Si bonding/ phase transformations and Energy Dispersion X-ray Spectroscopy (EDX) for nickel and silicon composition in filling structures.

Microholes with a maximum aspect ratio 8 were achieved by the FIB direct milling technique. The parameters used to obtain this aspect ratio were 500pA for beam current and 100µm for initial milling depth, D_i. Milling at a beam current of 500pA formed the most precise hole structure with low milling time and aspect ratio close to 1 compared to the other holes. In addition, the re-deposition effect was minimised. The milling time is 42.1s per hole with dimensions of upper and bottom widths which are close to 2µm in the original design.

The aspect ratio of microholes increased with increase of the initial milling depth, D_i. The actual depth, D_f gained was 17.5µm at D_i = 100µm, which is five times less than initial milling depth. However the maximum aspect ratio achieved is more than 5 as expected, without gas injection system (GIS) for depth enhancement. A maximum aspect ratio of 15 can be achieved only if assisted-GIS is applied (Jamaludin, et al., 2013). Although FIB milling is less useful in mass production, it is an excellent

choice for producing highly precise microholes, with the effects of amorphisation and re-deposition as main limitations.

For depth enhancement, 25% TMAH solution has eliminated most of the re-deposited Si in the microholes after immersion for 10 mins at 85°C. The depth of microholes was increased almost twice of the original depth milled by FIB. Ga^+ ion implantation from FIB the milling process acted as a mask during TMAH etching. However, the structure of holes was affected due to the formation of small egg-like structure of silicic acid at the sidewall. Pyramidal hillock cavities were also formed at the non-Ga^+ ion implanted region on Si surface. These challenges need to be addressed for further etching by TMAH.

For filling process, two different methods were used; magnetic assembly and ultrasonic dispersion and annealing at 500°C. The nickel was not completely filled the holes using both methods. However, magnetic assembly technique has more nickel filling compared to ultrasonic dispersion method by the occurrence of agglomeration at the entire sidewall. This is due to the magnetic force that has attracted ferromagnetic nickel into the holes. There were also some voids which occurred because of reduced adherence between nickel and silicon.

The annealing temperatures are compared between 500°C and 900°C after nickel filling by the magnetic assembly method. SEM morphology analysis shows that the filling structure formed after annealed at 900°C has higher quality than the filling structure formed at 500°C. Only small agglomerations formed at the entire sidewall, no voids occurred and higher average thickness of filling structure, 526nm, was achieved.

The existence of Ni-Si bonding has been confirmed by the formation of the nickel silicide layer based on XRD analysis. At temperature of 900°C, there two nickel

silicide phases were formed, nickel monosilicide (NiSi) and nickel disilicide ($NiSi_2$). However, only nickel monosilicide (NiSi) phase occurred at 500°C due to less diffusion of nickel into silicon during annealing process at lower temperature. The elemental analysis of filling structure using EDS resulted that the composition of nickel was higher at 900°C rather than 500°C. This means that more nickel nanopowder has diffused into silicon and formed two phases of nickel silicide layer.

This concludes that high aspect ratio microfilling using nickel nanopowder was achieved with maximum aspect ratio 8 by FIB direct milling. Although the filling structure was not completely filled using magnetic assembly, the Ni-Si bonding existed with the formation of nickel silicide layer at the entire sidewall. Only small agglomerations and no voids occurred at 900°C. Thus, from this research nickel nanopowder is potentially, a highly viable candidate material as the metal filling component of HARMS in MEMS applications.

5.2 RECOMMENDATIONS

For future work related to this research, a few points are suggested for further exploration. The first suggestion is with regards to the FIB as a milling method for fabrication of high aspect ratio micro holes. The gas injection system (GIS) is recommended to be used together with FIB during milling process to avoid re-deposition effect and increase the aspect ratio of holes. For depth enhancement using TMAH solution, the Ga^+ ion need to be implant on a large area of silicon surface for better etching and avoid the formation of pyramidal hillocks structure.

The filling method using magnetic assembly is the second suggestion. An auto controllable magnetic workstation is recommended to fill nickel nanopowder into the holes consistently. Nano holes can be milled using FIB so that a large quantity of nickel

nanopowder can easily diffuse into silicon. The whole process of this research needs to be done in clean room to avoid contamination and the formation of oxide layer on filling structure. Although the microfilling using nickel nanopowder is not completely filled, nickel can be the most potential candidate as filling material in high aspect ratio microstructures (HARMS) for MEMS applications. Thus, more investigations are recommended to explore the electrical characteristics of nickel filling structure for electrical purposes in MEMS.

REFERENCES

Adams, D.P., Vasile, M.J., Mayer, T.M. & Hodges, V.C. (2003). Focused ion beam milling of diamond: Effects of H2O on yield, surface morphology and microstructure. *J Vac Sci Technol B* **21**(6), 2334-2343.

Ali, M.Y., Hung, W. & Fu, Y.Q. (2010). A Review of Focused Ion Beam Sputtering. *Int J Precis Eng Man* **11**(1), 157-170.

Allongue, P., Costa-Kieling, V., & Gerischer, H. (1993). Etching of Silicon in NaOH Solutions I. In Situ Scanning Tunneling Microscopic Investigation of n-Si (111). *Journal of The Electrochemical Society*, ***140***(4), 1009-1018.

Atiqah, N., Jaafar, I., Ali, M.Y. & Asfana, B. (2012). Application of Focused Ion Beam Micromachining: A Review. *Advanced Materials Research* **576**, 507-510.

Baloglu, B. (2011). *Finite Element Modeling of High Current Density Effects & Power Handling Capability of RF MEMS Capacitive Switches*. Lehigh University.

Bassett, W. A., & Brown Jr, G. E. (1990). Synchrotron radiation-Applications in the earth sciences. *Annual Review of Earth and Planetary Sciences*, ***18***, 387-447.

Benawra, J., Donald, A. & Shannon, M. (2008). Developing dual beam methods for the study of polymers. In *Journal of Physics Conference Series*, pp. 2079

Bleris, L.G., & Kothara, M.V. (2005). Real-time Implementation of Model Predictive Control. In *Proceedings of IEEE American Control Conference, June 2005*, pp. 4166-4171.

Bressers, P. M. M. C., Pagano, S. A. S. P., & Kelly, J. J. (1995). Ferricyanide reduction as a probe for the surface chemistry of silicon in aqueous alkaline solutions. *Journal of Electroanalytical Chemistry*, ***391***(1), 159-168.

Bushby, A.J., P'ng, K.M., Young, R.D., Pinali, C., Knupp, C. & Quantock, A.J. (2011). Imaging three-dimensional tissue architectures by focused ion beam scanning electron microscopy. *Nature Protocols* **6**(6), 845-858.

Cao, D. M., Guidry, D., Meng, W. J., & Kelly, K. W. (2003). Molding of Pb and Zn with microscale mold inserts. *Microsystem technologies*, **9**(8), 559-566.

Chiu, K. C., Chang, S. L., Huang, C. Y., & Guan, H. W. (2011, May). Design and fabrication of substrates with microstructures for bio-applications through the modified optical disc process. In *SPIE Microtechnologies, International Society for Optics and Photonics.* pp. 80680F-80680F.

Davis, J. R. (Eds.). (2001). *Copper and copper alloys*. ASM international.

dos Santos, R. E., Doi, I., Diniz, J. A., Swart, J. W., & dos Santos Filho, S. G. (2008). Investigation of Ni silicides formation on (100) Si by X-ray diffraction (XRD). *Revista Brasileira de Aplicações de Vácuo*, ***23***(1), 32-35.

Defforge, T., Coudron, L., Gautier, G., Kouassi, S., Vervisch, W., Tran Van, F., & Ventura, L. (2011). Effect Of Low Temperature And Concentration KOH

Etching On High Aspect Ratio Silicon Structures. *Physica Status Solidi (C)*, ***8***(6), 1815-1819.

Drobne, D., Milani, M., Zrimec, A., Leser, V. & Berden Zrimec, M. (2005). Electron and ion imaging of gland cells using the FIB/SEM system. *J Microsc-Oxford* **219**, 29-35.

Du, T., Vijayakumar, A., Sundaram, K. B., & Desai, V. (2004). Chemical mechanical polishing of nickel for applications in MEMS devices.*Microelectronic engineering*, ***75***(2), 234-241.

Einsle, J. F., Bouillard, J. S., Dickson, W., & Zayats, A. V. (2011). Hybrid FIB milling strategy for the fabrication of plasmonic nanostructures on semiconductor substrates. *Nanoscale research letters*, *6*(1), 1-5.

Elwenspoek, M., Lindberg, U., Kok, H., & Smith, L. (1994). Wet chemical etching mechanism of silicon. In *Micro Electro Mechanical Systems, 1994, MEMS'94, Proceedings, IEEE Workshop*. pp. 223-228.

Fischer, A.C., Bleiker, S.J., Haraldsson, T., Roxhed, N., Stemme, G. & Niklaus, F. (2012). Very High Aspect Ratio Through-Silicon Vias (TSVs) Fabricated using Automated Magnetic Assembly of Nickel Wires. *J Micromech Microeng* **22**(10), 105001.

Fu, G., Tor, S., Loh, N., Tay, B. & Hardt, D.E. (2007). A Micro Powder Injection Molding Apparatus For High Aspect Ratio Metal Micro-Structure Production. *J Micromech Microeng* **17**(9), 1803-1809.

Fu, G., Loh, N., Tor, S., Tay, B., Murakoshi, Y. & Maeda, R. (2005). Injection molding, debinding and sintering of 316L stainless steel microstructures. *Applied Physics A: Materials Science & Processing* **81**(3), 495-500.

Fu, Y., & Ngoi, K. A. B. (2005). Investigation of aspect ratio of hole drilling from micro to nanoscale via focused ion beam fine milling.

Fu, Y.Q. & Ngoi, B.K.A. (2001). Investigation of diffractive-refractive microlens array fabricated by focused ion beam technology. *Opt Eng* **40**(4), 511-516.

Fu, Y.Q. & Bryan, N.K.A. (2005). Investigation of aspect ratio of hole drilling from micro to nanoscale via focused ion beam fine milling. *Innovation in Manufacturing Systems and Technology (IMST);* (01).

Fu, Y. Q., Bryan, N. K. A., Shing, O. N., & Hung, N. P. (2000). Influence of the redeposition effect for focused ion beam 3D micromachining in silicon. *The International Journal of Advanced Manufacturing Technology*, *16*(12), 877-880.

Fu, Y., & Wang, L. (2010). Focused Ion Beam Machining and Deposition. In *Ion Beams in Nanoscience and Technology*. pp. 265-290. Springer Berlin Heidelberg.

Geissler, M., Wolf, H., Stutz, R., Delamarche, E., Grummt, U. W., Michel, B., & Bietsch, A. (2003). Fabrication of metal nanowires using microcontact printing. *Langmuir*, ***19***(15), 6301-6311.

Han, L. (2012). Improvement of Silicon Oxide Quality Using Heat Treatment.

Hwang, D.J., Chimmalgi, A. & Grigoropoulos, C.P. (2006). Ablation of thin metal films by short-pulsed lasers coupled through near-field scanning optical microscopy probes. *J Appl Phys* **99**(4), 044905-044905-044911.

Hruby, J. (2001). LIGA technologies and applications. *MRS bulletin*, **26**(04), 337-340.

Hung, S. Y. (2009). Optimization on hardness and internal stress of micro-electroformed NiCo/nano-Al2O3 composites with the constraint of low surface roughness. *Journal of Micromechanics and Microengineering*, ***19***(1), 015009.

Hutchison, D.N., Morrill, N.B., Aten, Q., Turner, B.W., Jensen, B.D., Howell, L.L., Vanfleet, R.R. & Davis, R.C. (2010). Carbon Nanotubes as a Framework for High-Aspect-Ratio MEMS Fabrication. *Journal of Microelectromechanical Systems* ***19***(1), 75-82.

Inoue, F., Shimizu, T., Yokoyama, T., Miyake, H., Kondo, K., Saito, T., ... & Shingubara, S. (2011). Formation of electroless barrier and seed layers in a high aspect ratio through-Si vias using Au nanoparticle catalyst for all-wet Cu filling technology. *Electrochimica Acta*, ***56***(17), 6245-6250.

Jamaludin, F.S. & Mohd Sabri, M.F. (2013). Investigation on Fabricating High Aspect Ratio Microholes on Silicon by FIB/SEM Milling. *Advanced Materials Research* **626**, 436-439

Jamaludin, F. S., Sabri, M. F. M., & Said, S. M. (2013). Controlling parameters of focused ion beam (FIB) on high aspect ratio micro holes milling. *Microsystem technologies*, ***19***(12), 1873-1888.

Jang, J., Oh, J. Y., Kim, S. K., Choi, Y. J., Yoon, S. Y., & Kim, C. O. (1998). Electric-field-enhanced crystallization of amorphous silicon. *Nature*, *395*(6701), 481-483.

Kang, S. K., Buchwalter, S. L., LaBianca, N. C., Gelorme, J., Purushothaman, S., Papathomas, K., & Poliks, M. (2001). Development of conductive adhesive materials for via fill applications. *Components and Packaging Technologies, IEEE Transactions*, ***24***(3), 431-435.

Khasanov, O. L., & Dvilis, E. S. (2008). Net Shaping Nanopowders with Powerful Ultrasonic Action and Methods of Density Distribution Control. *Advances in Applied Ceramics*, **107**(3), 135-141.

Kibria, G., Doloi, B., & Bhattacharyya, B. (2010). Experimental analysis on Nd: YAG laser micro-turning of alumina ceramic. *The International Journal of Advanced Manufacturing Technology*, *50*(5-8), 643-650.

Kim, C.S., Ahn, S.H. & Jang, D.Y. (2012). Review: Developments in micro/nanoscale fabrication by focused ion beams. *Vacuum* **86**(8), 1014-1035

Kim, J.H., Boo, J.H. & Kim, Y.J. (2008). Effect of stage control parameters on the FIB milling process. *Thin Solid Films* **516**(19), 6710-6714.

Kim, K., Park, S., Lee, J.B., Manohara, H., Desta, Y., Murphy, M. & Ahn, C.H. (2002). Rapid replication of polymeric and metallic high aspect ratio microstructures using PDMS and LIGA technology. *Microsystem Technologies* **9**(1), 5-10.

Krueger, R. (1999). Dual-column (FIB-SEM) wafer applications. *Micron* **30**(3), 221-226.

Langford, R. M., & Petford-Long, A. K. (2001). Preparation of transmission electron microscopy cross-section specimens using focused ion beam milling.*Journal of Vacuum Science & Technology A*, **19**(5), 2186-2193.

Langford, R. M., Nellen, P. M., Gierak, J., & Fu, Y. (2007). Focused ion beam micro-and nanoengineering. *MRS bulletin*, *32*(05), 417-423.

Larsen, K. P., Ravnkilde, J. T., Ginnerup, M., & Hansen, O. (2002). Devices for fatigue testing of electroplated nickel (MEMS). In *Micro Electro Mechanical Systems, Jan 2002. The Fifteenth IEEE International Conference.* pp. 443-446.

Latif, A. (2000). Nanofabrication using focused ion beam. (Doctor of Philosophy, University of Cambridge).

Lee, K. S., Mo, Y. H., Nahm, K. S., Shim, H. W., Suh, E. K., Kim, J. R., & Kim, J. J. (2004). Anomalous growth and characterization of carbon-coated nickel silicide nanowires. *Chemical physics letters*, ***384***(4), 215-218.

Li, X., Abe, T., Liu, Y., & Esashi, M. (2002). Fabrication Of High-Density Electrical Feed-Throughs By Deep-Reactive-Ion Etching of Pyrex Glass. *Microelectromechanical Systems, Journal of*, ***11***(6), 625-630.

Liao, Y.S., Chen, S.T., Lin, C.S. & Chuang, T.J. (2005). Fabrication of High Aspect Ratio Microstructure Arrays by Micro Reverse Wire-EDM. *J Micromech Microeng* **15**(8), 1547.

Lindquist, N.C., Nagpal, P., McPeak, K.M., Norris, D.J. & Oh, S.-H. (2012). Engineering metallic nanostructures for plasmonics and nanophotonics. *Rep Prog Phys* **75**(3), 036501.

Liu, J., Huang, B., Li, X., Li, P., & Zeng, X. (2010). Magnetic Silver-Coated Ferrite Nanoparticles and Their Application in Thick Films. *Journal of electronic materials*, *39*(12), 2702-2710.

Lohmann, C., Bertz, A., Küchler, M., & Gessner, T. (2003). A Novel High Aspect Ratio Technology for MEMS Fabrication Using Standard Silicon Wafers. In *Advanced Microsystems for Automotive Applications 2003*, pp. 59-66.

Lü, C., Yin, X., & Wang, M. (2007). Fabrication of High Aspect Ratio Metallic Microstructures on ITO Glass Substrate using Reverse-Side Exposure of SU-8. *Sensors and Actuators A: Physical*, **136**(1), 412-416.

Lühn, O., Van Hoof, C., Ruythooren, W. & Celis, J.P. (2009). Filling of microvia with an aspect ratio of 5 by copper electrodeposition. *Electrochim Acta* **54**(9), 2504-2508.

Malek, C.K., Hartley, F.T. & Neogi, J. (2003). Fast prototyping of high-aspect ratio, high-resolution X-ray masks by gas-assisted focused ion beam. *Microsyst Technol* **9**(6-7), 409-412.

Manu, R., Jayakrishnan, S.S. & Boopathi, S. (2011). Effect of sonication on via filling behavior for copper metallization in electronics packaging. In *Meeting Abstracts*, pp. 1602-1602. The Electrochemical Society.

Marques, C., Desta, Y.M., Rogers, J., Murphy, M.C. & Kelly, K. (1997). Fabrication of high-aspect-ratio microstructures on planar and nonplanar surfaces using a modified LIGA process. *Microelectromechanical Systems, Journal of* **6**(4), 329-336.

Mastrangeli, M., Abbasi, S., Varel, C., Van Hoof, C., Celis, J.P. & Böhringer, K.F. (2009). Self-assembly from milli-to nanoscales: methods and applications. *J Micromech Microeng* **19**(8), 083001.

McPhail, D. S., Chater, R. J., & Li, L. (2008). Applications of focused ion beam SIMS in materials science. *Microchimica Acta*, ***161***(3-4), 387-397.

Mei, F. (2009). *Fabrication, Bonding, Assembly, and Testing of Metal-based Microchannel Devices* (Doctoral dissertation, Louisiana State University).

Miney, P. G., & Cunnane, V. J. (2003). A study of the chemical breakdown of the anodic oxide formed on (100) oriented silicon in tetramethylammonium hydroxide (TMAH) solutions. *Electrochimica acta*, ***48***(11), 1475-1482.

Monajemi, P. & Ayazi, F. (2005). Thick Single-Crystal Silicon MEMS With High-Aspect-Ratio Vertical Air Gaps. In *MOEMS-MEMS Micro & Nanofabrication*, pp. 138-147. International Society for Optics and Photonics.

Morales, A.L. (2006). *Electrodeposited Metal Matrix Nanocomposites as Thin Films and High Aspect Ratio Microstructures for MEMS*. (Doctor of Philosophy, Universidad de Sonora, Mexico).

Murakami, T., Froment, B., Ouaknine, M., & Yoo, W. S. (2003). Nickel Silicide Formation Using A Stacked Hotplate-Based Low Temperature Annealing System. In *Proc. 203rd Electrochem. Soc. Meeting May 2003*. p. 347.

Nakahata, T., Sugihara, K., Abe, Y., & Ozeki, T. (2004). Low thermal budget selective epitaxial growth for formation of elevated source/drain MOS transistors. *Journal of crystal growth*, ***264***(1), 79-85.

Nath, R., & Premnath, O. (2005). Direct Observations of Nickel Silicide Formation on (100) Si And Si0. 75Ge0. 25 Substrates Using In-Situ Transmission Electron Microscopy.

Orloff, J. (Eds.). (2008). *Handbook of Charged Particle Optics*. CRC press.

Park, S. J., Lee, S. W., Jeong, S., Lee, J. H., Park, H. H., Choi, D. G., & Choi, J. H. (2010). Nanosilver Colloids-Filled Photonic Crystal Arrays for Photoluminescence Enhancement. *Nanoscale research letters*, ***5***(10), 1590-1595.

Pecht, M., Agarwal, R., McCluskey, F. P., Dishongh, T. J., Javadpour, S., & Mahajan, R. (1998). *Electronic packaging materials and their properties* (Vol. 4). CRC press.

Prime Faraday Technology Watch. (2002). An Introduction to MEMS (Micro-electromechanical Systems). *Prime Faraday Partnership*. Loughborough University, Loughborough, Leics LE11 3TU. 6.

Raffa, V., Vittorio, O., Pensabene, V., Menciassi, A., & Dario, P. (2008). FIB-nanostructured surfaces and investigation of bio/nonbio interactions at the nanoscale. *NanoBioscience, IEEE Transactions on*, **7**(1), 1-10.

Raffa, V., Castrataro, P., Menciassi, A. & Dario, P. (2006). Focused Ion Beam as a Scanning Probe: Methods and Applications. In *Applied Scanning Probe Methods II*, Bhushan, B. and Fuchs, H. (Eds.), pp. 361-412. Springer Berlin Heidelberg.

Rajsiri, S., Kempshall, B., Schwarz, S. & Giannuzzi, L. (2002). FIB Damage in Silicon: Amorphization or Redeposition? *Microsc Microanal* **8**(S02), 50-51

Ramm, P., Wolf, M. J., Klumpp, A., Wieland, R., Wunderle, B., Michel, B., & Reichl, H. (2008, May). Through Silicon Via Technology—Processes And Reliability For Wafer-Level 3D System Integration. In *Electronic Components and Technology Conference, 2008. ECTC 2008. 58th*. pp. 841-846.

Reyntjens, S. & Puers, R. (2001). A review of focused ion beam applications in microsystem technology. *J Micromech Microeng* **11**(4), 287-300

Semak, V., Campbell, B. & Thomas, J. (2006). On the possible effect of pedestal pulse on material removal by ultrahigh intensity laser pulses. *Journal of Physics D: Applied Physics* **39**(15), 3440.

Sievilä, P., Chekurov, N., & Tittonen, I. (2010). The fabrication of silicon nanostructures by focused-ion-beam implantation and TMAH wet etching.*Nanotechnology*, ***21***(14), 145301.

Stevie, F. A., Griffis, D. P., & Russell, P. E. (2005). Focused Ion Beam Gases for Deposition and Enhanced Etch. *Introduction to Focused Ion Beams*, 53-72.

Sunami, H., Furukawa, T., & Masuda, T. (2004). A three-dimensional MOS transistor formation technique with crystallographic orientation-dependent TMAH etchant. *Sensors and Actuators A: Physical*, **111**(2), 310-316.

Tanase, M., Silevitch, D. M., Hultgren, A., Bauer, L. A., Searson, P. C., Meyer, G. J., & Reich, D. H. (2002). Magnetic trapping and self-assembly of multicomponent nanowires. *Journal of applied physics*, ***91***(10), 8549-8551.

Tseng, A.A. (2004). Recent developments in micromilling using focused ion beam technology. *J Micromech Microeng* **14**(4), R15-R34.

Tseng, A.A., Insua, I.A., Park, J.S. & Chen, C.D. (2005). Milling yield estimation in focused ion beam milling of two-layer substrates. *J Micromech Microeng* **15**(1), 20-28

Urbánek, M., Uhlíř, V., Bábor, P., Kolíbalová, E., Hrnčíř, T., Spousta, J., & Šikola, T. (2010). Focused ion beam fabrication of spintronic nanostructures: an optimization of the milling process. *Nanotechnology*, **21**(14), 145304.

van Heeren, H. & Salomon, P. (2007). Recent Developments, Future Directions.

Van Tendeloo, G., Van Dyck, D., & Pennycook, S. J. (Eds.). (2012). *Handbook of Nanoscopy: Vol. 1*. John Wiley & Sons.

Weber, W. M., Geelhaar, L., Graham, A. P., Unger, E., Duesberg, G. S., Liebau, M., ... & Kreupl, F. (2006). Silicon-nanowire transistors with intruded nickel-silicide contacts. *Nano letters*, *6*(12), 2660-2666.

Wei, Z., Yan, P., Feng, W., Dai, J., Wang, Q., & Xia, T. (2006). Microstructural characterization of Ni nanoparticles prepared by anodic arc plasma. *Materials characterization*, ***57***(3), 176-181.

Yan, Y., Li, L., Sezer, K., Whitehead, D., Ji, L., Bao, Y. & Jiang, Y. (2012). Nano-second pulsed DPSS Nd:YAG laser striation-free cutting of alumina sheets. *International Journal of Machine Tools and Manufacture* **53**(1), 15-26.

Yao, N. (2005). Focused Ion Beam System—a Multifunctional Tool for Nanotechnology. *Handbook of Microscopy for Nanotechnology*, 247-286.

Yao, N. Fundamentals of the Focused Ion Beam System. *Handbook of Nanoscopy, Volume 1&2*, 645-671.

Yinghong, X., Xin, W., Xujie, Y., & Lude, L. (2003). Nanometre-Sized Tio2 As Applied To The Modification Of Unsaturated Polyester Resin. *Materials Chemistry and Physics*, ***77***(2), 609-611.

Youn, S.W., Okuyama, C., Takahashi, M. & Maeda, R. (2008). A Study on Fabrication of Silicon Mold for Polymer Hot-Embossing using Focused Ion Beam Milling. *J Mater Process Tech* **201**(1-3), 548-553.

Youn, S. W., Takahashi, M., Goto, H., & Maeda, R. (2007). Fabrication of micro-mold for glass embossing using focused ion beam, femto-second laser, eximer laser and dicing techniques. *Journal of Materials processing technology*,*187*, 326-330.

Youn, S.W., Takahashi, M., Goto, H. & Maeda, R. (2006). A Study on Focused Ion Beam Milling of Glassy Carbon Molds for The Thermal Imprinting of Quartz and Borosilicate Glasses. *J Micromech Microeng* **16**(12), 2576-2584.

Yu, Z. Y., Zhang, Y., Li, J., Luan, J., Zhao, F., & Guo, D. (2009). High aspect ratio micro-hole drilling aided with ultrasonic vibration and planetary movement of electrode by micro-EDM. *CIRP Annals-Manufacturing Technology*, ***58***(1), 213-216.

Zubel, I., & Kramkowska, M. (2001). The effect of isopropyl alcohol on etching rate and roughness of (1 0 0) Si surface etched in KOH and TMAH solutions.*Sensors and Actuators A: Physical*, *93*(2), 138-147.

Appendix A. PUBLICATIONS

ISI Papers:

1. **Fatin Syazana Jamaludin** & Mohd Faizul Mohd Sabri. (2013). Investigation on Fabricating High Aspect Ratio Microholes on Silicon by FIB/SEM Milling. *Advanced Materials Research, 626,* 436-439.
2. **Fatin Syazana Jamaludin**, Mohd Faizul Mohd Sabri, Suhana Mohd Said. (2013). Controlling Parameters of Focused Ion Beam (FIB) on High Aspect Ratio Micro Holes Milling. *Microsystem Technologies, **19***(12) 1873-1888.

Patent:

1. Ultrasonic Hot Plate Apparatus, 13 April 2012, PI 2012700190, Malaysia